Advanced Turbine Technology

ATTAP

Applications Project

DOE/NASA 0336-1
NASA CR-185133
EDR 14232

1988 Annual Report

Allison
Gas Turbine Division
General Motors Corporation
P.O. Box 420
Indianapolis, Indiana 46206-0420

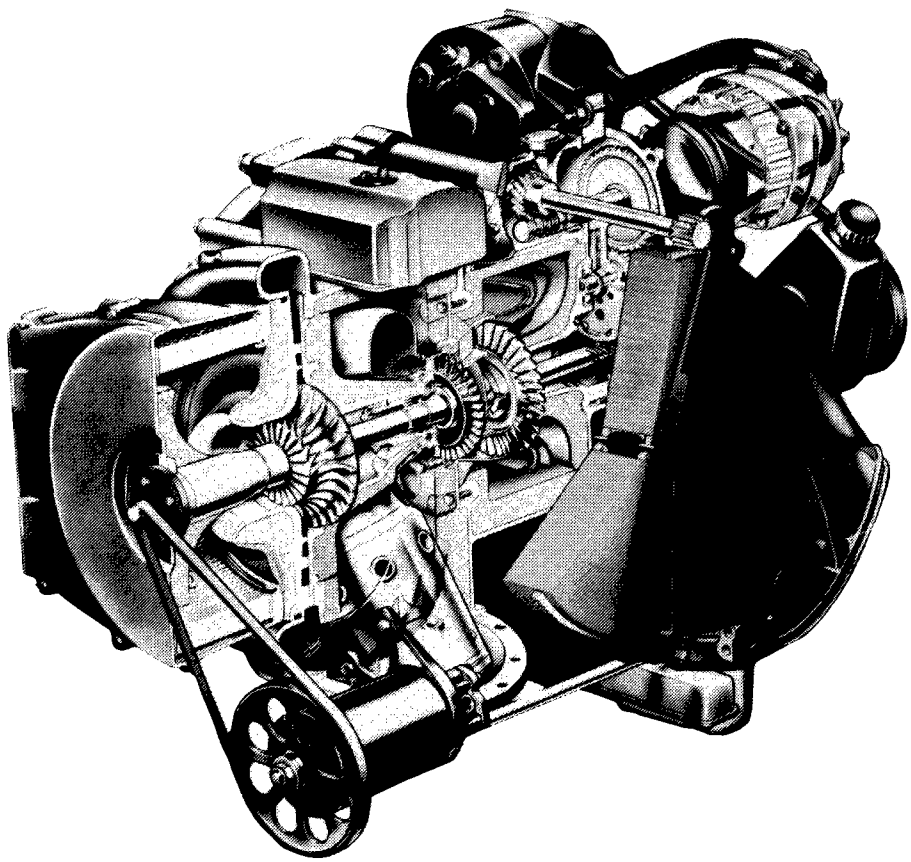

1 June 1989

Final

Prepared for
National Aeronautics
and Space Administration
Lewis Research Center
Cleveland, Ohio 44135
Contract DEN 3-336

For U.S. Department of Energy
Conservation and Renewable Energy
Office of Transportation Systems

NOTICE

DOE/NASA 0336-1
NASA CR-185133
EDR 14232

Advanced Turbine Technology
ATTAP
Applications Project

1988 Annual Report

Allison
Gas Turbine Division
General Motors Corporation
P.O. Box 420
Indianapolis, Indiana 46206-0420

1 June 1989

Final

Prepared for
National Aeronautics
and Space Administration
Lewis Research Center
Cleveland, Ohio 44135
Contract DEN 3-336

For U.S. Department of Energy
Conservation and Renewable Energy
Office of Transportation Systems

FOREWORD

This report presents a technical summary of work accomplished on the Advanced Turbine Technology Applications Project (ATTAP) under NASA Contract DEN3-336, from contract inception (October 1987) through the calendar year 1988. This technology project is funded by the U.S. Department of Energy, Office of Conservation and Renewable Energy, Transportation Systems, Heat Engine Propulsion Division. Project management and technical direction are provided by the NASA Lewis Research Center (LeRC), Aeronautics Directorate, Propulsion Systems Division, Terrestrial Propulsion Office.

The overall intent of the ATTAP is to bring the automotive gas turbine engine to a technology state at which industry can make commercialization decisions. Key to this goal is the development and demonstration of structural ceramic component technology as the critical high risk/high payoff element in this type engine. Such ceramic technology is the prime ATTAP focus. Automotive gas turbine attractions include the following potential advantages:

- o significantly increased fuel economy
- o ability to meet federal emission standards with untreated exhaust
- o ability to operate on a wide range of alternate fuels
- o inherently smooth, low-vibration operation

General Motors (GM) is addressing the ATTAP with a team which draws on:

- o the extensive ceramic design, analysis, and materials database and expertise in place at Allison Gas Turbine
- o the substantial experience, design and test capabilities, automotive gas turbine technology and hardware, and test vehicle resources that were developed under GM funding as background to this project and are in place at GM's Advanced Engineering Staff (AES)
- o the infrastructure of expertise and resources in place in the American ceramics industry and the working relationships between that industry and GM
- o the unique capabilities and resources existing at universities and at national laboratories, such as the High Temperature Materials Laboratory at Oak Ridge

In this arrangement, Allison serves as prime contractor. Major ceramic industry development subcontractors to date are: The Carborundum Company; GTE Laboratories Inc.; Corning Glass Works; Manville Corp; and the Garrett Ceramic Components Division of Allied-Signal Aerospace Company. Exploratory technology efforts were initiated at Ceramics Process Systems.

TABLE OF CONTENTS

TABLE OF CONTENTS (cont)

LIST OF ILLUSTRATIONS

LIST OF ILLUSTRATIONS (cont)

LIST OF ILLUSTRATIONS (cont)

LIST OF TABLES

SUMMARY

ATTAP activities during the past year were highlighted by an extensive materials assessment, execution of a reference powertrain design, test-bed engine design and development, ceramic component design, materials and component characterization, ceramic component process development and fabrication, component rig design and fabrication, test-bed engine fabrication, and hot gasifier rig and engine testing. Although significant technical challenges remain, all areas experienced progress.

Materials assessment activities entailed engine environment evaluation of domestically supplied radial gasifier turbine rotors that were available at the conclusion of the Advanced Gas Turbine (AGT) Technology Development Project as well as an extensive survey of both domestic and foreign ceramic suppliers and Government laboratories performing ceramic materials research applicable to advanced heat engines. A Carborundum alpha-SiC thickened airfoil radial rotor was engine tested for a total of 23:43 hr in three separate engine builds. The rotor was successfully tested through three low temperature cycles (899°C [1650°F]), followed by three thermal cycles to 1080°C (1976°F) with a steady-state dwell time of 9.5 hr on the final cycle. A total of 38 candidate ceramic suppliers were identified and surveyed. Based on this survey, the current state of the technology was assessed and the initial ATTAP major ceramic development subcontractors were selected.

A reference powertrain design was executed to reflect the selection of the AGT-5 as the ceramic component test-bed engine for the ATTAP. The RPD describes an advanced automotive gas turbine powertrain system installed in a 1988 Pontiac Grand Am vehicle. While fulfilling the same vehicle mission as the baseline 1988 2.5 ℓ 4-cylinder Grand Am, the RPD vehicle demonstrated the feasibility for a 57% improvement in composite fuel economy (35% improvement on an energy basis).

Test-bed engine development activity included mechanical design, power turbine flow path design, and engine system integration aimed at upgrading the AGT-5 from a 1038°C (1900°F) metal engine to a durable 1371°C (2500°F) structural ceramic component test-bed engine. A preliminary gearbox redesign was completed to meet the increased power output requirements of the ceramic engine. The gasifier module bearing system was redesigned for increased durability. A preliminary design of the seal platform was completed for use with a ceramic regenerator. An aerodynamic power turbine flow path was selected and a detailed aerodynamic design was initiated. The power turbine first-stage vane and both rotors were determined to be ceramic. Control software for durability schedule running was developed and implemented. The engine control software was modified for hot gasifier rig control. Fuel system testing was performed to determine the requirements of the ceramic engine at the 1371°C (2500°F) RPD conditions. Combustion system design/development activities were initiated to reduce carbon formation as a source of FOD and to reduce gaseous emissions.

Ceramic component design activities included the combustor, gasifier turbine static structure, and gasifier turbine rotor. A ceramitized standard diffusion flame AGT-5 combustor was configured and a thermal analysis of the assembly was initiated. Design guidelines were established for the gasifier turbine static structure components at the RPD conditions and a 2-D axisymmetric model was created. Steady-state heat transfer and stress analyses were completed. The scroll design is a two-piece configuration to accommodate manufacturing requirements and concerns. A gasifier turbine rotor shroud design was completed for utilization in ceramic rotor test evaluations at an intermediate turbine inlet temperature of 1204°C (2200°F). The shroud design meets probability of survival (POS) goals for both SiC and Si_3N_4 materials. The design of an Si_3N_4 20-bladed rotor meeting RPD POS goals was completed. The SiC 20-bladed rotor design does not meet POS goals. Plans for 1989 include redesign of the SiC 20-bladed rotor. Interference fit shaft attachment designs for both SiC and Si_3N_4 rotors meet RPD design goals.

The materials and component characterization efforts have included the testing and evaluation of several candidate ceramic materials and components being developed for use in the ATTAP. Material characterization activities have focused on microstructural, density, fracture toughness, and fast fracture strength examinations. Fracture surface analysis was also used to determine the nature and location of the strength-controlling defects. In addition, the time-dependent strength characteristics and oxidation resistance were evaluated for selected materials.

Ceramic component process development and fabrication activities were initiated for the gasifier tur-

bine rotor, gasifier turbine vanes, gasifier turbine scroll, extruded regenerator disks, and thermal insulation. Major ceramic industry development subcontractors are The Carborundum Company; GTE Laboratories Inc; Corning Glass Works; Manville Corp; and Garrett Ceramic Components Division of Allied-Signal Aerospace Company. Exploratory technology efforts were initiated at Ceramics Process Systems. Plans for 1989 include delivery of gasifier turbine rotors, vanes and scrolls, injection moldable thermal insulation, and extruded regenerator matrix samples.

Component rig development activities included combustor, hot gasifier and regenerator rigs. A preliminary design upgrade of an existing combustor rig for the increased temperature requirements of the RPD was completed. A hot gasifier rig design, based on the AGT-5 engine with the power turbine removed, was completed. Rig hardware was procured and fabrication completed. Overhaul of the regenerator cyclic temperature sample rig was initiated for adaptation to the AGT-5 engine cycles.

Test-bed engine fabrication activities consisted of the fabrication of an all-new AGT-5 durability test-bed engine and support of all engine test activities through instrumentation/build/repair. Test-bed engines were instrumented for regenerator spike and soak-back temperature testing. The new durability test-bed engine was reinsulated with Manville's injection moldable material via a hand lay-up process.

Hot gasifier rig and test-bed engine testing activities were performed.

Sixty-four hours of ceramic rotor test time were accumulated on an existing (GM-owned, AGT-5 family member) hot gasifier rig providing valuable information for the design of the AGT-5 hot gasifier rig. Initial shakedown testing of the AGT-5 hot gasifier rig and the new durability test-bed engine was successfully completed. Additional test-bed engine activities included soak-back temperature testing, regenerator inlet temperature spike testing, and initial engine testing of a ceramic gasifier rotor. The Kyocera rotor (background data to ATTAP) successfully accumulated 322 hr of engine operation. Maximum operating conditions attained were 78% design speed and 1028°C (1882°F) turbine inlet temperature.

INTRODUCTION

This is the first of a series of annual reports documenting work performed on the Advanced Turbine Technology Applications Project (ATTAP). This work is being conducted by a team directed by General Motors (GM), with significant activities underway at GM's Allison Gas Turbine Division (which serves as prime contractor), at GM's Advanced Engineering Staff (AES) location at the General Motors Technical Center, and at the several domestic ceramic suppliers who are under development subcontracts. The U.S. Department of Energy sponsors this work, which is managed and technically directed by NASA under contract DEN3-336.

GOAL AND OBJECTIVES

ATTAP is intended to advance the technological readiness of an automotive ceramic gas turbine engine based on efforts begun in the Automotive Gas Turbine (AGT) Project, a DOE/NASA program executed between 1979 and 1987. This AGT Project successfully demonstrated the feasibility of structural ceramic hot-section components in automotive-sized gas turbine engines. Specifically, ATTAP aims to develop and demonstrate the technology of structural ceramics that have the potential for competitive automotive engine life cycle cost and for operating for 3500 hr (automotive engine life) in a turbine engine environment at temperatures up to 1371 °C (2500 °F). Project objectives are the following:

- o to enhance the development of analytical tools for ceramic component design using the evolving ceramic properties data base
- o to establish improved processes for fabricating advanced ceramic components
- o to develop improved procedures for testing ceramic components
- o to evaluate ceramic component reliability and durability in an engine environment

PROGRAM SCHEDULE AND CONTENT

Figure 1 shows the scheduled activities in the 61-month program. Materials assessment occurred at the initiation of ATTAP and resulted in the targeting of

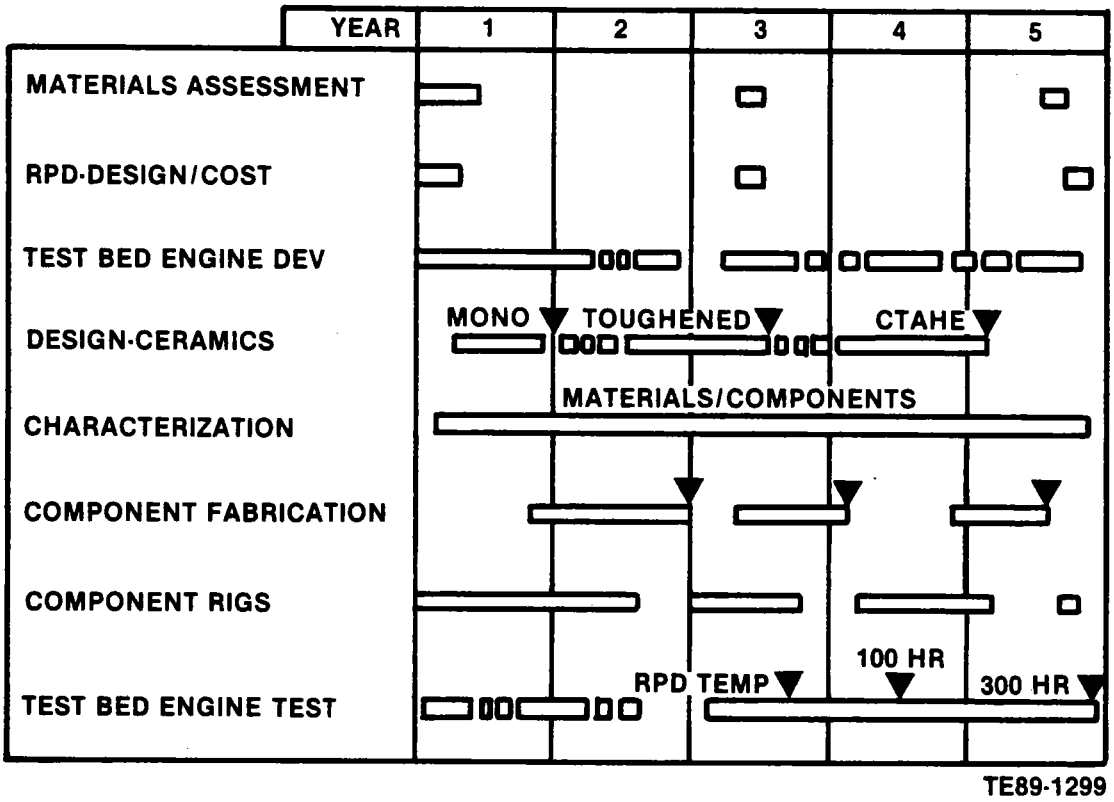

Figure 1. ATTAP schedule.

ceramic component technology goals and the identification of materials, processes, and manufacturers to address those goals. Materials assessment activities are also scheduled during Years 3 and 5, at which times the state of the art will be reassessed for each component and required technology improvements will be redefined. The identification and evaluation of materials, processes, and manufacturers are ongoing, continuous activities in ATTAP, and promising candidates are integrated into the program as merited. Similarly, those technologies and/or ceramic component suppliers which do not productively evolve to address program goals are truncated from ATTAP.

Reference powertrain design (RPD) activities include the preliminary design of a powertrain system which could meet performance, cost, and reliability design goals. Such a design was executed at the beginning of ATTAP using a high temperature derivative of the AGT-5 automotive gas turbine engine. The RPD is updated in Year 3 to reflect current ceramic component technology and goals, and again in Year 5 to provide a cost estimate of such a powertrain in production.

Test-bed engine development, shown in Figure 1 as an intermittent activity, includes those efforts aimed at ensuring the availability and functionality of the AGT-5 gas turbine engine as the test-bed for the high temperature ceramic components. Although engine development is not a primary focus of ATTAP, these activities recognize the need for continuing evolution of the engine to handle the power and thermal loads, as well as design changes resulting from the integration of a high temperature flow path.

Central to the logic of Allison's ATTAP approach is an iterative component development cycle. Three such cycles are shown in Figure 1 and include the design/fabrication/characterization/rigs/engine test sequences of activities. The design activity, shown with a milestone at the end of Year 1, features monolithic ceramic technology in the design of the gasifier turbine stage of the AGT-5 engine for 1371°C (2500°F) turbine inlet temperature (TIT) plus other required hot flow-path pieces. The second and third design phases feature toughened (monolithic and/or composite) and advanced (e.g., from Oak Ridge's Ceramic Technology for Advanced Heat Engines [CTAHE] project) materials, respectively, used in the same gasifier stage components. Component fabrication includes those process development activities executed by ceramic suppliers that result in the fabrication of engine-usable components. Characterization involves those laboratory activities both at suppliers and at Allison which measure and define the various properties and qualities of both ceramic materials in test bar form and those materials in components. Examples are microstructural evaluation and measurements of density, strength, oxidation resistance, toughness, etc. Included are the development and application of nondestructive evaluation (NDE) techniques.

Component rig activity includes the development of rigs for component verification and testing (e.g., a hot gasifier turbine rig) as well as the actual testing activities. Test-bed engine test includes those testing activities associated with test-bed engine development plus the verification and development testing of the ceramic components. Note that each of the three component development cycles begins with design, followed by component fabrication, characterization, then rig testing, and finally engine testing. This rigorous development process, shown in Figure 2, is iterative between the users and the ceramic supplier community and assures developing an understanding of the behavior of components in service and the continuous identification of areas for improvement.

TEST-BED ENGINE AND RPD

Figure 3 shows the automotive gas turbine engine being used as the ceramic component development test-bed for ATTAP. This GM-developed engine, the AGT-5, is a two-shaft, regenerative configuration with axial-flow gasifier and power turbines. The engine produces approximately 110 hp at its original full-power TIT of 1038°C (1900°F).

An RPD was completed at the outset of ATTAP in order to ensure that the AGT-5-type power plant has the potential to fulfill the overall fuel economy goals which underlie the DOE's sponsorship of automotive gas turbine technologies. This RPD is a preliminary engineering design of a powertrain system that integrates with vehicle characteristics to provide a system with the potential for meeting not only performance, but also cost and reliability design goals. Specific performance goals are the following:

- 30% improvement in fuel economy over the reference 1988 Pontiac Grand Am equipped with a 2.5 ℓ, 4-cylinder, spark-ignition engine over the combined Federal Driving Cycle
- competitive vehicle drivability and performance with the reference 1988 Grand Am

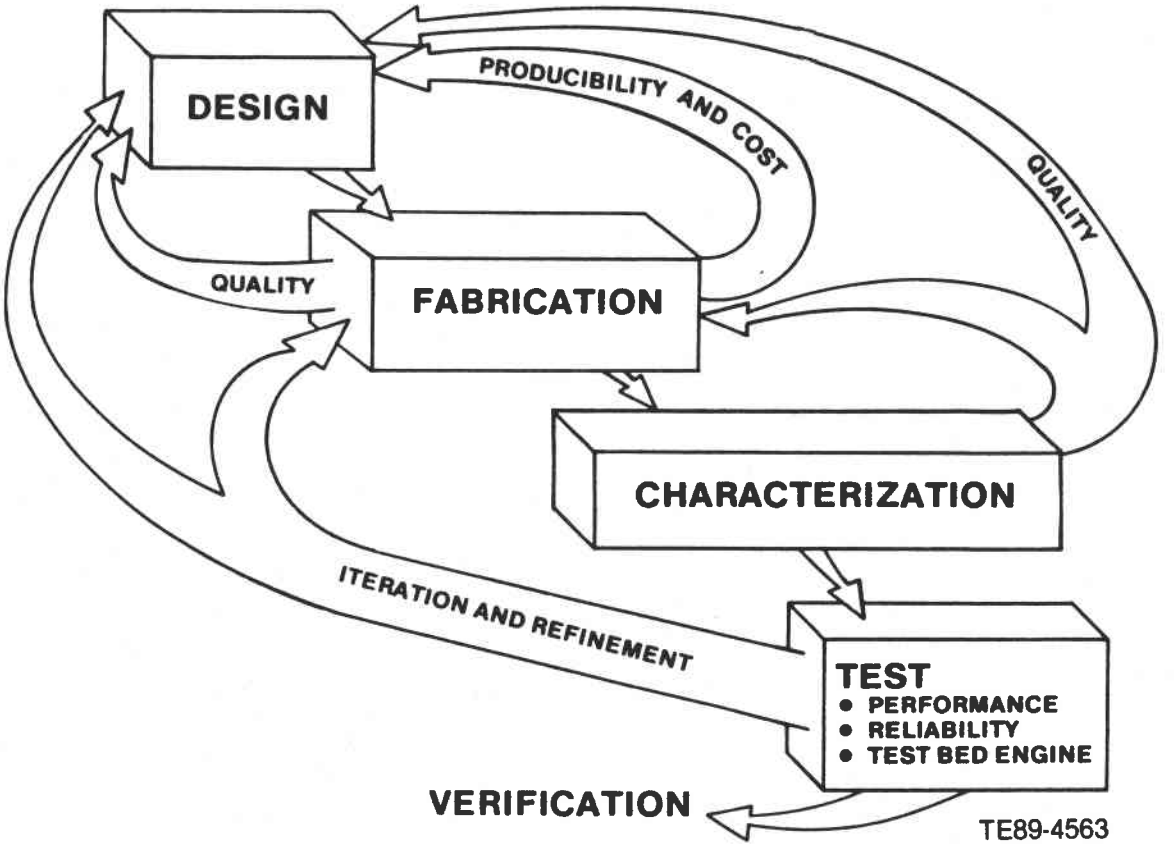

Figure 2. Ceramic component development cycle.

- o gaseous emissions and particulate levels less than the following (based on diesel fuel No. 2):

  NO_x = 0.249 gm/km (0.4 gm/mile), HC = 0.255 gm/km (0.41 gm/mile), CO = 2.11 gm/km (3.4 gm/mile), particulates = 0.129 gm/km (0.2 gm/mile)

- o ability to use a variety of alternate fuels

Table I shows the results of the RPD performance simulation, based on the AGT-5-type engine, versus the baseline reference vehicle.

Thus the RPD gas turbine equivalent vehicle outperforms the reference piston engine installation in critical fuel economy, performance, and drivability parameters.

The emissions and alternate fuels goals are considered achievable based on demonstrated GM experience. For example, the AGT100 AGT engine's combustion system has displayed steady-state emissions of NO_x, CO, and unburned hydrocarbons well within Federal Emission Standards using diesel fuel,

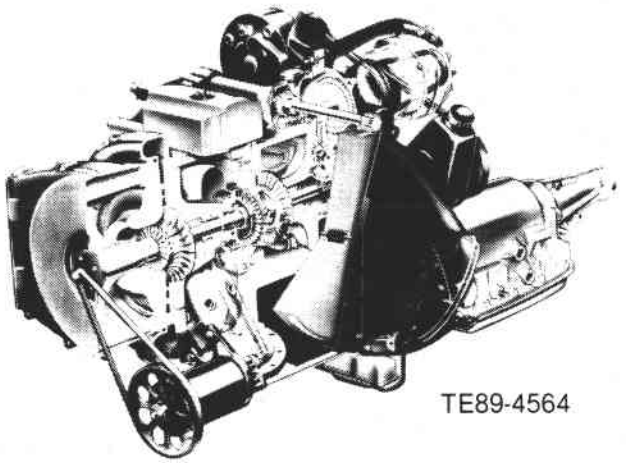

Figure 3. ATTAP test-bed engine-- AGT-5 (GM AES).

Table I.
Comparison of RPD vehicle performance to baseline Grand Am.

	Baseline--2.5ℓ spark-ignition	RPD-- turbine
0-96.5 kmph (60 mph) time--sec	13.5	13.1
Top gear gradability at 88.5 kmph (55 mph)--%	7.9	10.9
Composite fuel economy-- ℓ/100 km (miles/gal)	7.66 (30.7)	4.87 (48.3)

jet fuel, and methanol. The AGT-5 engine has successfully run on dry powdered coal. Although such systems have demonstrated the potential for low emission/alternate fuel gas turbine combustion, much work remains to achieve a fully-functional system suitable for automotive application. Such efforts are outside the scope of ATTAP. The definition of power plant cost and reliability goals, in addition to performance, is included in ATTAP.

CRITICAL COMPONENTS

Consistent with the strong ATTAP emphasis on ceramic component technology is the focus on specific gas turbine components as development/ demonstration targets. Four ceramic components and the engine insulation have been identified as critical development components because: (1) their functional success is critical to the viability of the ceramic automotive gas turbine engine, and (2) each requires some further technological development to be proven reliable and durable in the automotive engine environment. These critical elements, shown in Figure 4, are the following:

- o gasifier turbine rotor
- o gasifier turbine vanes
- o gasifier turbine scroll
- o regenerator disks
- o thermal insulation

For each component, specific areas and parameters requiring improvement have been identified and quantified where possible.

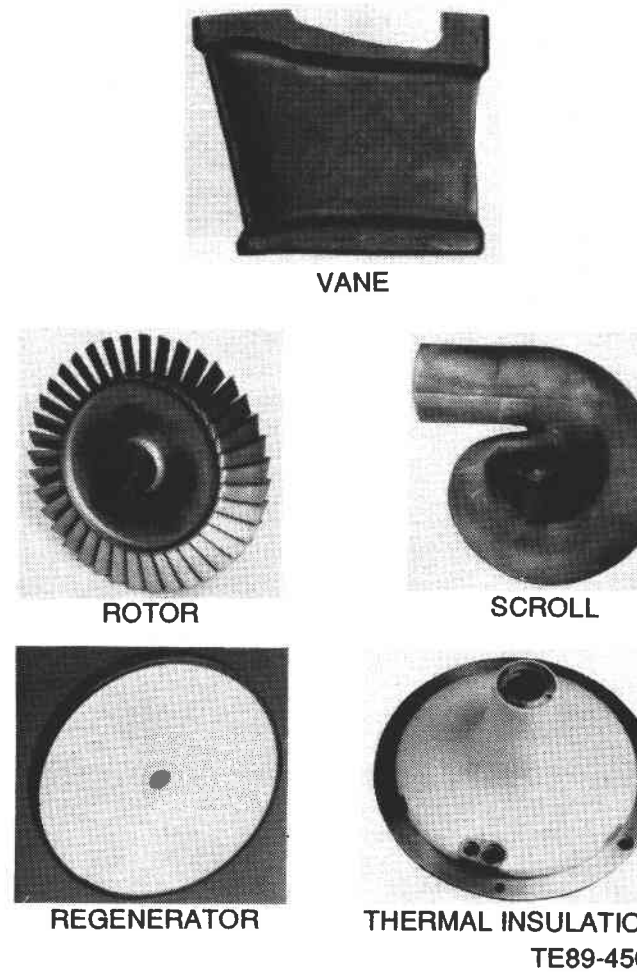

Figure 4. Ceramic components selected for development.

I. ENGINE/POWERTRAIN DESIGN, ANALYSIS, AND MATERIALS ASSESSMENT

1.1 MATERIALS ASSESSMENT

1.1.1 Current Generation Components Assessment in Engine Environment

Objective/Approach

The objective of this activity was to assist in the evaluation/establishment of the current ceramic material state of the technology and the validity assessment of the design methodology. Specifically, this entailed engine environment evaluation of domestically-supplied radial gasifier turbine rotors that were available at the conclusion of the Advanced Gas Turbine (AGT) Technology Development project. The rotor material systems (Carborundum's sintered alpha silicon carbide [SiC] and GTE Labs' PY6 sintered silicon nitride [Si_3N_4]) were potential prime candidates for initial gasifier rotor development work in the AT-TAP. Also of interest was the thickened airfoil geometry of the Carborundum (CBO) rotor, which was designed to reduce the rotor's foreign object damage (FOD) vulnerability. The approach was to engine test one rotor of each of the aforementioned material systems with a metal gasifier turbine static structure at a TIT of 1080°C (1976°F) for a total of ten hours. Following the endurance run, the rotor was to be tested at 100% design speed for approximately 30 min. The engine was then to be reconfigured with an all-ceramic gasifier static structure to allow a 10-hr endurance run at 1199°C (2100°F) to 1204°C (2200°F).

Accomplishments

The accomplishments of the engine environment assessment activity are as follows:

- o successfully ran CBO alpha-SiC thickened airfoil rotor through three low temperature cycles (899°C [1650°F]), followed by three thermal cycles to 1080°C (1976°F) with a steady-state dwell time of 9.5 hr on final cycle
- o CBO rotor engine-tested for a total time of 23:43 hr (20:57 hr burn time) in three separate engine builds (BUs)

AGT100 Engine S/N 2, BU20

The build was configured with a CBO hot isostatic pressed (HIP), sintered alpha-SiC gasifier rotor with thickened airfoils and a GTE-AY6 Si_3N_4 inner backplate and a metal gasifier static structure. The balance of the engine hardware was metal or proven ceramic components, such as the combustor assembly, thermal shim rings, regenerator disk, and bulkhead.

The rotor was exposed to three low temperature (899°C [1650°F] TIT) thermal cycles at 60% N_1 without incident. Three thermal cycles were then run to 1080°C (1976°F) and 70% N_1 with 15-min steady-state dwell times for the first and second cycles. The third cycle had a steady-state endurance dwell time of 9.5 hr. All attempts at running to 100% gasifier design speed following the endurance testing were unsuccessful due to fuel nozzle/system problems. A total of nine start attempts were made on three start nozzles with the result being either no ignition or an unstable flame when ignition was successful. Following the ninth start attempt, engine inspection revealed carbon accumulation in the pilot flame tube and in the combustor main body. To prevent possible rotor damage from FOD, the engine was removed from the test stand for disassembly and inspection.

Disassembly revealed a carbon soot buildup both inside and outside the combustor assembly. The gasifier rotor was intact and in excellent condition. The regenerator bulkhead cold-side compliant layer seal showed signs of coking, indicating a probable fire in the bulkhead region. The most likely causes of the bulkhead fire are oil leakage into the compressor discharge airflow causing puddling in the regenerator cavity or an accumulation of unburned fuel from either too high a fuel flow rate or a bad nozzle spray pattern. Only the compliant seal was damaged, and it was replaced.

Total running time for BU20 was 17:49 hr.
Motor time was 00:56 hr.
Burn time was 16:53 hr.

AGT100 Engine S/N 2, BU21

Following a fuel nozzle/system interrogation, in which the fuel control valve was cleaned and recalibrated, the engine was rebuilt with the all-American, all-ceramic gasifier section shown in Table II.

After initial running to 760°C (1400°F) TIT and 60% N_1, precautionary inspection revealed excessive soot in the combustor indicating off-spec combustion. Teardown inspection revealed no significant hardware defects. The burner variable geometry (BVG) actuation system was found to contain approximately

Table II.
S/N 2, BU21 ceramic components.

Gasifier inner backplate	GTE	Sintered Si_3N_4	AY6
Gasifier vanes	GTE	Sintered Si_3N_4	AY6
Gasifier scroll	Norton	Siliconized Si_3N_4	NC430
Gasifier rotor	CBO	SiC	Hexoloy SA
Gasifier outer backplate	CBO	SiC	Hexoloy SA
Combustor assembly	CBO	SiC	Hexoloy SA
Interturbine coupling and piston rings	Pure Carbon	Reaction-bonded (RB) SiC	Refel

2.54 mm (0.1 in.) of backlash. In addition, it was determined that the BVG set point, although consistent with previous builds, did not correlate to the set point used for the combustor test rig. Data review indicated that the burner inlet temperature (BIT) was 4°C (40°F) lower than past testing would predict after 90 sec of burn time at 649°C (1200°F) burner outlet temperature (BOT).

Total running time for BU21 was 0:48 hr.
Motor time was 0:16 hr.
Burn time was 0:32 hr.

AGT100 Engine S/N 2, BU22

Engine S/N 2 BU22 maintained the all-American all-ceramic gasifier turbine section defined for BU21. Hardware changes implemented subsequent to the teardown of BU21 were:

- o replacement of the regenerator disk and inboard seal with identical but new hardware to reduce regenerator leakage
- o rework of the BVG yoke to eliminate backlash in the BVG actuation system
- o reset of the BVG to correlate to combustor rig set points

Engine operation resulted in carbon accumulation consistent with that seen on BU20 and BU21. Further investigation into the fuel system showed that the start assist air biasing regulator was not operating correctly. Manual adjustment of the regulator during running was then implemented, and subsequent testing indicated carbon formation was reduced but was not eliminated. A trial run to 871°C (1600°F) BOT was conducted to determine if the carbon would be eliminated at higher temperatures (previous testing was conducted at 649°C [1200°F] TIT). Inspection of the fuel nozzle following a trial run to 871°C (1600°F) BOT indicated that the carbon was being eliminated at higher temperatures. It was then decided to proceed with the first thermal cycle to 982°C (1800°F). This cycle was completed per schedule. During this cycle, oil mist was emitted from the inner gearbox-to-outer combustor chamber (OCC) cavity, similar to that seen during BU19. Borescope inspection following engine shutdown indicated that all hardware was in good condition.

The second and third 982°C (1800°F) TIT cycles were then completed. During the coast down from the third cycle after fuel flow was stopped, an audible change in engine operation was noted. In addition, the engine was observed to have moved or "jumped." The engine was then stopped and subsequent removal of the main combustor nozzle revealed that the gasifier rotor and scroll, as well as other hardware, had failed. The main combustor nozzle had carbon accumulation as shown in Figure 5. This accumulation was approximately 1.27 cm x 1.27 cm x 0.254 cm (0.5 in. x 0.5 in. x 0.1 in.).

Tear down inspection (Figure 6) revealed that the following ceramic hardware had failed: rotor, scroll, vanes, and inner and outer backplates. The combustor body, lower dilution band, combustor dome, and flame tube had small nicks at various locations. The power turbine blades and vanes (metal) sustained extensive damage. The No. 1 seal housing had slight oil leak indications; however, this did not appear to be the cause of the mist which was emitted since the insulation ring on the bearing support was not oil-soaked. The inner gearbox-to-OCC insulation was oil-soaked consistent with the oil mist which was emitted during running.

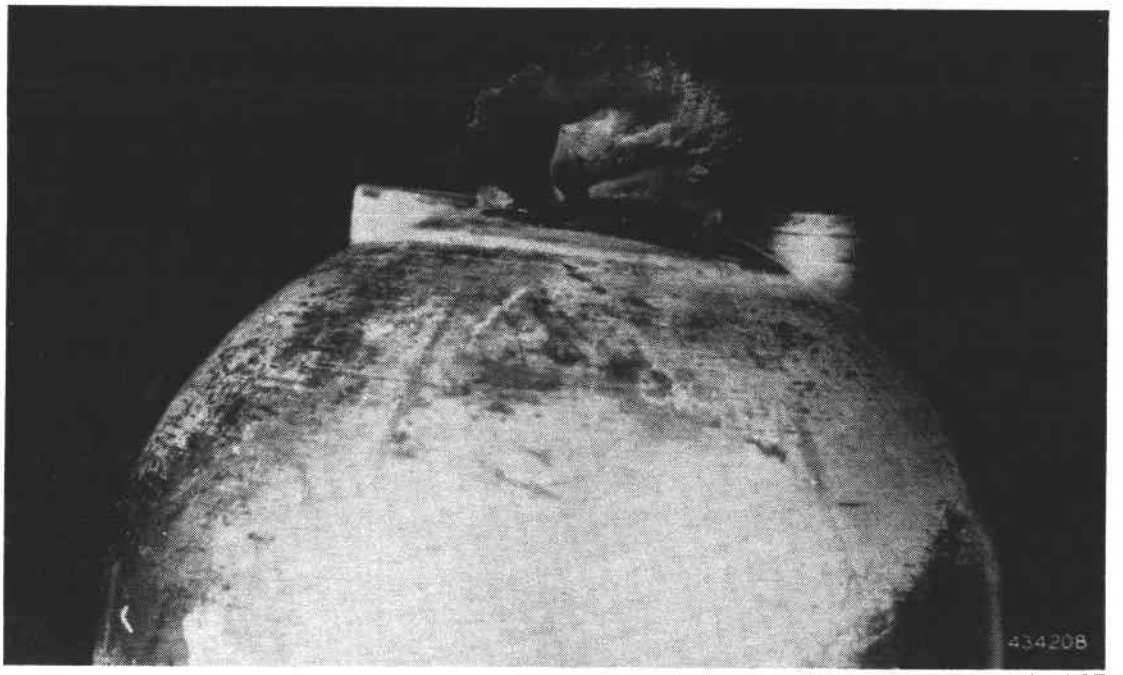

TE89-4567

Figure 5. Carbon accumulation on S/N2, TD22 main combustor nozzle.

Total running time for BU22 was 5:06 hr.
Motor time was 1:34 hr.
Burn time was 3:32 hr.

Post-test examination of the engine data records revealed simultaneous response of all vibration and whip signals. No abnormalities were noted prior to the sudden increase in vibration and whip. Fractographic analysis (reference subsection 3.1.3) supports the scenario that the rotor was the initial ceramic component to fail in the chain of events. What triggered the rotor failure is less clear although FOD and particularly carbon debris must be considered.

Two potential rotor failure modes are envisioned. These are:

1. Inducer airfoil fracture typical of radial machinery "ping-pong" action of debris trapped between the inducer airfoils and the vane row. The thickened airfoil fracture progresses through the rotor hub and shaft.

This contrasts with the observed failure mode for the thin airfoil rotors. The inducer area of the airfoil is simply "cobbed off" by FOD impact and the rotor hub remains intact.

2. Similar to the above except the debris impact created torque spikes which fractured the rotor stub shaft in a shock manner. Concurrent with fracture of the shaft was fracture of the hub into relatively large pieces which subsequently impacted the shroud and shattered. This scenario is favored by the fractographic analysis.

Thus, the exact failure mode of the rotor has not been defined although it is very likely that the rotor was the initial ceramic component which failed.

The rotor had been carefully screened and qualified for the test. The various steps in this process are briefly summarized below.

- o Processing
  1986, final group, shaft end injection, thickened airfoil and HIP processed at ASEA. Rotor density was 97.8% of theoretical density.
- o Inspection
  Cleared radiographic and visual. Minor surface fluorescent penetrant inspection (FPI) indications were successfully blended.
- o Proof spin
  The casting was successfully spin-proof-tested to 86,500 rpm (approximately 100% N_1) with a 30-sec dwell at speed.
- o Machining
  Machined by Atlas Tool and Die Co. to RPD open geometry. The machined dimensions conformed to the drawing.

TE89-4568

Figure 6. S/N2, TD22 with regenerator seal platform removed.

- Qualification
  The machined edge of the airfoils was carefully rounded by hand blending. The rotor successfully cleared FPI. The ceramic rotor/metal gasifier shaft joint was successfully proof-tested to twice design load. The joint passed FPI following the flexural test. The first three natural frequencies were experimentally measured for every airfoil (12 airfoils total). The speed range for the failure event was identified to be remote from any vane passage potential response.
- Engine build
  The critical airfoil/shroud clearances all met the desired tolerances. Other build dimensions also conformed.

The key points relative to the fracture of the SiC gasifier rotor in engine S/N 2 BU22 are summarized as follows:

- The rotor was carefully screened and fully qualified for engine test.
- There was evidence of missing carbon debris from the combustor region.
- The rotor was likely the initial ceramic component to fail in the ceramic gasifier section.
- The stress conditions at engine failure (677°C [1250°F]) RIT and 62% N_1) were less severe than prior exposure (1080°C [1976°F] and 70% N_1).
- The failure event was remote from vane passage interference.

- The ceramic rotor stub shaft fracture mirror indicated relatively low stress (14 MPa [20 ksi]) suggesting a shock load fracture mechanism.
- Concurrent with fracture of the shaft was fracture of the hub into relatively large pieces which subsequently impacted the shroud and shattered.

Detailed failure analysis discussion is presented in subsection 3.1.3.

1.1.2 Materials Assessment

Objective/Approach

The objective of this effort was to conduct an extensive survey of both domestic and foreign ceramic suppliers and Government laboratories performing ceramic materials research applicable to advanced heat engines. Each of the candidate companies was assessed and information was generated pertaining to the following qualifications and capabilities:

- corporate affiliation
- products
- ceramic material systems of interest
- fabrication capabilities
- size of effort/corporate commitment
- attractions/strengths/deficiencies/Allison experience base
- overall evaluation for ATTAP
- contact

Accomplishments

The accomplishments of the materials assessment activity are as follows:

- completed materials assessment survey and presented information to NASA LeRC in January 1988
- compiled an initial work plan for 1988 with the ceramic suppliers, components, and material systems

A total of 38 candidate ceramic suppliers were identified and surveyed; these suppliers are listed below.

- AC Spark Plug
- Alcoa Advanced Ceramics
- ARCO Chemical
- Asahi Glass
- ASEA Cerama AB
- Atlantic Research Corporation (ARC)
- Textron Specialty Materials
- Babcock & Wilcox
- Boride Products
- British Nuclear Fuels Limited (BNFL)
- Carbon-Carbon Advanced Technologies (C-CAT)
- Carborundum (CBO)
- Ceradyne
- Ceramics Process Systems (CPS)
- Coors Porcelain
- Corning Glass Works
- Dow Corning Advanced Ceramics
- DuPont Advanced Composites
- Duramic Products
- ESK Engineered Ceramics
- Feldmuhle
- Garrett Ceramic Components Division (GCCD)
- General Electric (GE) Corporate R&D Center
- GTE Laboratories
- Hitachi Metals America
- Howmet
- Hughes Aircraft
- Kaiser Aerotech
- Kennametal
- Kyocera International
- Lanxide
- Manville Sales Corporation Technical Center
- NGK-Locke
- NGK Spark Plugs U.S.A.
- Norton/TRW Ceramics
- Refractory Composites
- Société Européenne de Propulsion (SEP)
- 3M New Products Department

Based on this survey, Allison assessed the current state of the technology and projected the expected state of development at the end of this contract for each of the ceramic components in the ATTAP RPD. In addition, the candidate ceramic suppliers were separated into three categories:

- major ceramic development subcontractors who have demonstrated viable material properties and relevant shape-making capabilities
- emerging ceramic development subcontractors who have demonstrated a material, process, or technology of interest
- ceramic parts buy sources with demonstrated material/component fabrication capabilities who will be used on a cost-per-part basis

At the conclusion of the materials assessment, a list was prepared identifying the ceramic suppliers that Allison proposed to use for initial development efforts to address each of the critical ceramic components in

the ATTAP AGT-5 engine. This initial work plan for 1988, with the ceramic suppliers, components, and material systems, is summarized in Table III. In addition, selected ceramic components will be procured on a "parts-buy" basis with no development efforts. These parts-buy components will be obtained as required to support engine test characterization and evaluation of the developmental ceramic components.

Allison will update the materials assessment at 30 months and 56 months. Written results will be presented to the NASA project manager for concurrence.

1.2 REFERENCE POWERTRAIN DESIGN (RPD)

Objective/Approach

The RPD was updated to reflect the selection of the AGT-5 as the ceramic component test-bed engine for the ATTAP. Engine model performance characteristics were integrated with vehicle characteristics to provide a system that has the best potential for meeting performance, cost, and reliability design goals. Current state-of-the-art and evolving technologies were used to the extent that they could reasonably be developed in the same time frame as the target ceramic component technologies. The RPD describes an advanced automotive gas turbine powertrain system which, when installed in a 1988 Pontiac Grand Am vehicle (or equivalent four-door, 3000-lb mission vehicle) meets the following objectives:

- o 30% improvement in fuel economy (S.L., 16°C [60°F] day) over reference 1988 Pontiac Grand Am equipped with 2.5 ℓ, four-cylinder, spark-ignition engine over the combined Federal Driving Cycle (automatic transmission and DF-2 fuel will be used). The target vehicle drivability and performance shall be competitive with the reference 1988 spark-ignition engine-powered Pontiac Grand Am.
- o gaseous emissions and particulate levels less than the following (based on diesel fuel No. 2 as basis for design):
  NO_x = 0.249 gm/km (0.4 gm/mile),
  HC = 0.255 gm/km (0.41 gm/mile),
  CO = 2.11 gm/km (3.4 gm/mile),
  particulates = 0.129 gm/km (0.2 gm/mile)
- o ability to use a variety of alternate fuels
- o make minimum use of strategic materials
- o reliability and life comparable with powertrains currently on the market
- o a competitive initial cost and a life cycle cost no greater than that of a comparable conventionally powered automobile
- o drivability suitable for safety and consumer considerations
- o noise and safety characteristics that meet currently legislated Federal standards

Accomplishments

While fulfilling the same vehicle mission as the baseline 1988 2.5 ℓ, four-cylinder Grand Am, the RPD vehicle demonstrated the feasibility for a 57% improvement in composite fuel economy (35% improvement on an energy basis). Table IV presents a summary of the ATTAP RPD simulation results.

Table III.
1988 workplan for ceramic component development activities.

Component:	Scroll	GG vanes	GG rotor	Regen disk	Insulation
Supplier					
CBO	SA SiC	SA SiC	SA SiC		
GTE Labs		Si_3N_4, PY6	Si_3N_4, PY6		
Corning				Ext AS	
GCCD			Si_3N_4, GN-10		
Manville					Alumina silica chromia
CPS			Si_3N_4		

Table IV.
Summary of ATTAP RPD simulation results.

Baseline vehicle--1988 Grand Am with 2.5 ℓ, 4-cylinder engine

1304.1 kg (2875 lb) IWC (1299.6 kg [2865 lb] test wt)
0-96.5 kmph (60 mph) in 13.5 sec
9.41 ℓ/100 km (25.5 mpg) city/5.78 ℓ/100 km (40.7 mpg) highway--
7.66 ℓ/100 km (30.7 mpg) composite

RPD vehicle--fulfills same mission

0-9.65 kmph (60 mph) in 13.1 sec
4.87 ℓ/100 km (48.3 mpg) composite (DF-2)--57% improvement
(35% improvement on energy basis)

Component Performance Levels

Individual component performance levels used in the engine characterization were assigned based primarily on: (1) Allison's extensive database with small engine components including that derived from the AGT100 program, and (2) recent GM development work (background data to ATTAP) on the AGT-5 family of engines, one of which is within 10% of the RPD engine size. The degradation effects due to scaling were based on these internal databases on engines and components in the 0.23 kg/sec (0.51 lbm/sec) to 0.64 kg/sec (1.41 lbm/sec) range and on open literature data.

Compressor

General Motors' test data for a radial-bladed centrifugal compressor, used in a 1038°C (1900°F) 76 kW (101.9 hp) design point engine, demonstrate that efficiency levels above 80% are achievable. Recent data from a much smaller machine demonstrated an adiabatic efficiency of 79% at design point pressure ratio.

The RPD compressor performance levels were assigned using the extensive AGT-5 test performance level database and an efficiency level degradation due to the Reynold's No. and size effects of scaling. Data compiled by Pampreen[1] for various centrifugal compressors, from 0.23 kg/sec (0.51 lbm/sec) to 1.59 kg/sec (3.51 lbm/sec) size, indicate an efficiency degradation of approximately 1% can be expected due to the Reynold's No. effect scaling from the AGT-5 to the RPD (see Figure 7). Larkin[2] indicates that

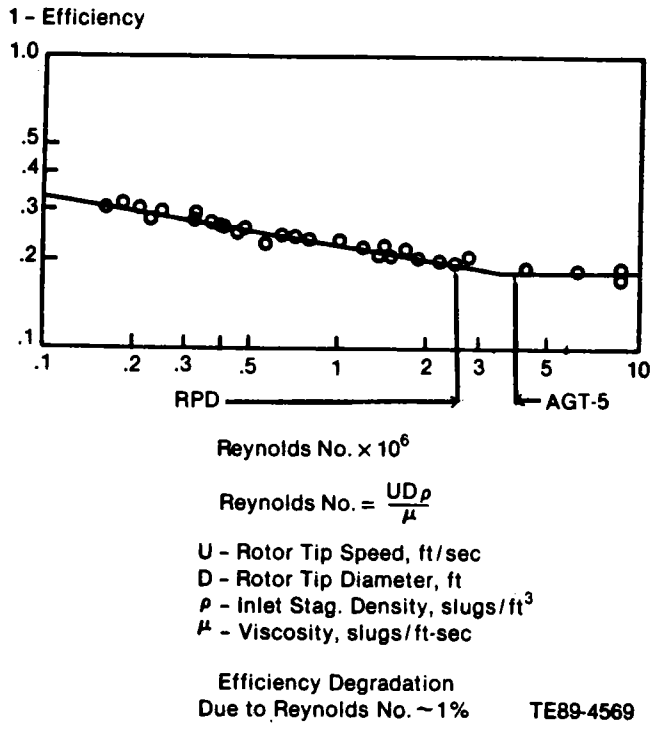

Figure 7. Compressor efficiency loss due to Reynolds No.

when the size effects due to scaling from the AGT-5 to the RPD are also considered, a polytropic efficiency degradation of approximately 1.5% can be expected (see Figure 8). This translates to approximately a 1.7% adiabatic efficiency degradation for compressors with a pressure ratio of 5:1. GM's direct scaling experience with the AGT family of engines suggests that a one-point loss from the AGT-5 to the RPD is

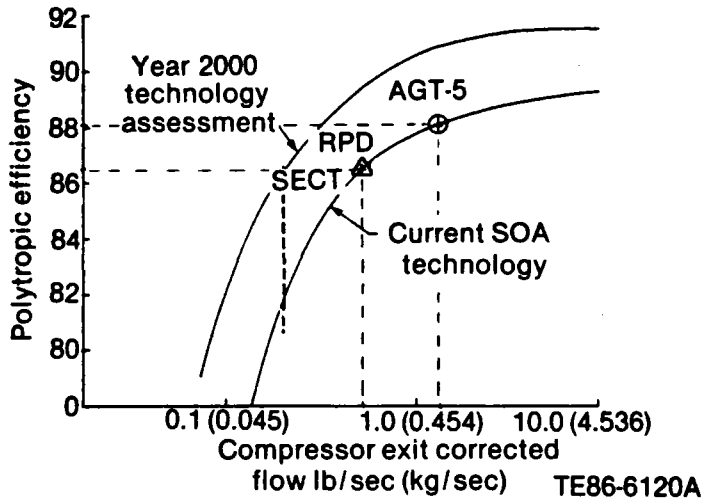

Figure 8. Compressor efficiency loss due to scaling.

reasonable. However, to be conservative, a much larger degradation was applied yielding a maximum power compressor total-to-static efficiency of 77.9%.

Turbine Stages

Measured maximum power match point total-to-total gasifier turbine efficiency for the AGT-5 is in the mid 80% range. Internal research suggests that an approximate degradation of 1.3% from the AGT-5 performance level could be expected for the RPD due to reduced Reynold's number. Therefore, a degradation value of 1.3% was assigned to the RPD gasifier turbine.

The RPD power turbine total-to-static efficiency of 76.1% is based directly on measured performance data for an engine of similar size. Because the power turbine from this engine has received a relatively small amount of development time, it is felt that the scaling degradation can be sufficiently recouped through an improved interstage diffuser and two-stage power turbine design.

Regenerator

Early experience on small axial-flow GM regenerative gas turbine engines resulted in used seal leakage from 4.5% to 6.8% of compressor discharge flow rate. Recent development indicates that used seal performance is steadily approaching that of new seal performance. Therefore, an RPD design point level of leakage of 4.93% has been selected. The study to define the regenerator core specification was performed at a gasifier speed of 70% since maximum fuel usage occurs between 70% and 80% during the Federal Test Procedure (see Figure 9). In sizing the regenerator cores, the following constraints were considered:

- o minimum wall thickness of 0.01 cm (0.004 in.)
- o maximum extrudable diameter of 25.4 cm (10 in.)
- o gas side pressure drop < 8.27 kPa (1.2 psi)
- o effect of core size on overall engine dimensions

RPD Engine Model

Using the aforementioned component performance levels, an engine model performance characterization was developed. The mechanical losses and the heat rejection rates were based on engine and rig tests.

RPD Vehicle Model

A computer model of the "N body" vehicle platform (which the Pontiac Grand Am is based on) was obtained from GM's Buick, Oldsmobile, Cadillac (BOC) engineering group. Accessory loads, tire characteristics, final drive losses, drive line inertias, aerodynamic drag, and static rolling resistance coefficients from this model were used for the RPD vehicle. Several other aspects of the vehicle model were modified to account for differences between the RPD engine and the baseline piston engine. Finally, various vehicle parameters were optimized to obtain the best fuel economy and drivability.

RPD Vehicle Optimization

After a suitably modified vehicle model had been combined with a computer model of the RPD engine performance, a series of studies were carried out to optimize the vehicle performance and fuel economy. This is similar to the process that takes place whenever a new engine is matched to a given vehicle. It should be noted that the fuel economy and performance of the two-shaft gas turbine engine is actually much less sensitive to drivetrain matching than a piston engine. Nonetheless, it was felt that it would be inappropriate to judge the RPD vehicle with a drivetrain that was optimized for a piston engine. No attempt was made to determine at what level of production it would be cost-effective to make a given change (for example, using a torque convertor with a different stall speed).

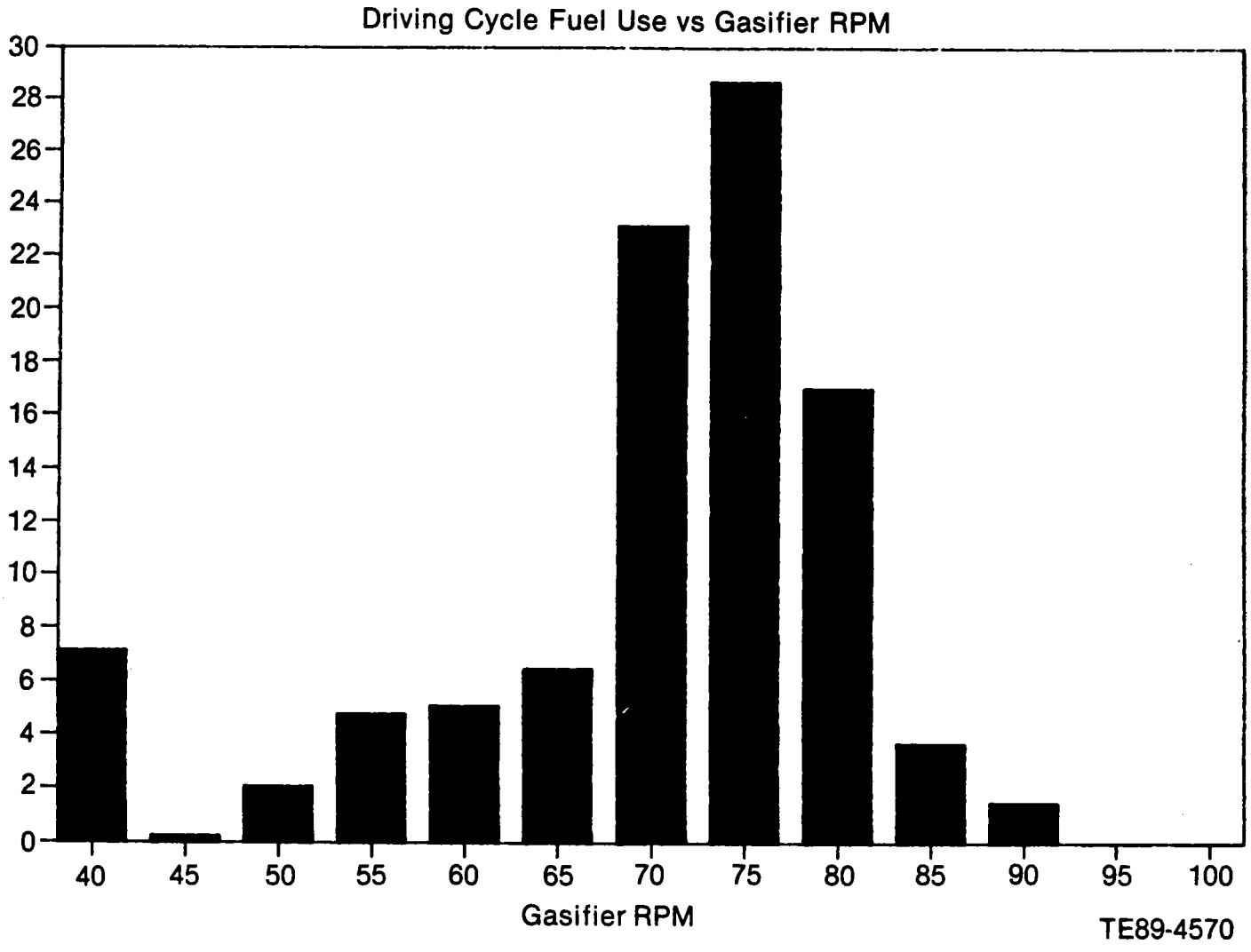

Figure 9. RPD fuel use.

The most significant difference in the behavior of the RPD gas turbine and the piston engine is the constant slope of the gas turbine torque curve with peak torque occurring at minimum rpm. One consequence of this is that the torque convertor is actually detrimental to the performance of the vehicle under most circumstances. This can be remedied quite readily by extending the lock-up torque convertor feature to include second gear in addition to third gear. It might be beneficial to lock-up the torque convertor in first gear sometimes as well, but it is difficult to develop a stable lock-up algorithm in first gear that demonstrates any improvement in performance or fuel economy.

The approach selected for the RPD vehicle was to leave the torque convertor clutch disengaged in first gear, and optimize the torque convertor for the torque characteristic of the gas turbine engine. This was accomplished by scaling the torque convertor diameter in the simulation program. The program then creates a new torque convertor model based on hydrodynamic scaling laws with the same stall torque ratio and efficiency curve but a different stall speed. In this study (Table V), a torque convertor with a diameter of 279 mm (10.98 in.) versus 245 mm (9.65 in.) for the baseline was found to give the best overall results, with the emphasis on improving initial wide open throttle (WOT) acceleration.

Another consequence of the broad power curve of the RPD gas turbine is that the optimum transmission ratios are more widely spaced than the production

Table V.
Comparison of RPD and production torque convertors.

	Production	RPD
Diameter--mm (in.)	245 (9.65)	279 (10.98)
Stall torque ratio*	2.35	2.35
"K" factor**	177	127
Peak efficiency in convertor range	88%	88%
Gears in which lock-up clutch engages	3rd	2nd and 3rd

* at 135.58 N-m (100 ft-lb)
** K factor is defined as $K = \frac{N_{\text{input shaft}}}{\sqrt{T_{\text{input shaft}}}}$ where

N = stall speed in rpm with 135.58 N-m input torque

T = 135.58 N-m

ratios. A study was conducted (iteratively with the optimization of shift pattern and final drive ratio) to determine the transmission ratios which produced the best combination of initial acceleration, WOT 0-96.5 kmph (60 mph) performance, and composite fuel economy with consideration given to practical limitations based on energy dissipation during shifting. The resulting RPD selected transmission concept has 27% more overall ratio than the baseline transmission. Table VI compares the RPD and baseline ratios.

Selection of the final drive ratio was based on optimization of composite fuel economy. It is characteristic of two-shaft automotive gas turbines that the final drive can be selected to place the top gear road-load operating line in the region of minimum brake specific fuel consumption (BSFC) without sacrifice of performance. This is in contrast to the situation with a piston engine, where best fuel economy always occurs at a top gear overall ratio too low for good performance. The selected RPD final drive ratio is 2.3:1, for an overall top gear ratio of 2.576:1. The excellent top gear gradeability of the RPD vehicle demonstrates that this does not involve a loss in performance.

The last vehicle parameter that was modified for the RPD definition is the transmission shift pattern. The shift pattern was optimized for fuel economy and performance (no trade-offs were necessary just as for final drive ratio) based initially on simplified calculations of the idealized engine-vehicle system, but the final shaping of the shift control was performed by trial-and-error with the simulation program.

It should be noted that the modification of the shift schedule is unavoidable because the production shift schedule has shift points exceeding the RPD engine governed maximum speed (3750 rpm), but the other driveline-related changes discussed above are not strictly necessary for the application of the RPD engine to an automobile. In fact, in consideration of the small gains realized, some or all of these changes

Table VI.
Comparison of RPD and production transmissions.

	RPD	THM125C
Transfer chain ratio	1.12	1.12
First gear ratio	3.60	2.84
2nd gear ratio	1.85	1.60
3rd gear ratio	1.00	1.00
Final drive ratio	2.3	2.84
Overall ratio in 1st gear	9.27	9.03
Overall ratio in 2nd gear	4.77	5.09
Overall ratio in 3rd gear	2.58	3.18

might be deemed as not cost-effective in an initial production scenario. The computer simulation indicates that the torque convertor, final drive, and transmission ratio changes described above result in a fuel economy gain of only 3.3% and a 4.4% decrease in the 0-96.5 kmph (60 mph) time. However, other considerations (such as top speed and noise at cruise) exhibit greater improvements as a result of the driveline optimization (see Table VII).

Table VII shows the results for the RPD vehicle simulation with production drivetrain (designed as production transmission and final drive ratios, torque convertor, and lock-up clutch but with a modified shift schedule) compared to the optimized drivetrain.

Table VIII summarizes the ATTAP RPD vehicle performance.

1.4 TEST-BED ENGINE DESIGN AND DEVELOPMENT

The overall objective of this task is to perform the necessary preliminary and detail design activities to ensure that the test-bed engine(s) can accept the improved ceramic components and can operate at the higher temperatures of the improved ceramics. Design activities will be based on the RPD. Specifically, efforts will be concentrated in four areas:

- o mechanical
- o combustion systems
- o alternate flow paths
- o engine system integration

1.4.1 Mechanical

Objective/Approach

The objective of the mechanical design and development activity is to upgrade the AGT-5 from a 1038°C (1900°F) metal engine to a durable 1371°C (2500°F) structural ceramic component test-bed engine. Activity focused on the following areas: gearbox, gasifier module, regenerator seal platform, and computer graphics detailed drawings.

Accomplishments

Accomplishments for the test-bed engine design and development activity are listed below.

- o completed preliminary gearbox redesign and initiated design layout
- o completed gasifier module bearing system design update
- o completed preliminary design of regenerator seal platform
- o converted 262 hand drawings to the computer graphics system

Table VII.
Results of drivetrain optimization.

	Production drivetrain	Optimized drivetrain	% difference
Composite fuel economy--ℓ/100 km (mpg)	5.04 (46.7)	4.87 (48.3)	+ 3.3%
0-96.5 kmph (60 mph) time--sec	13.7	13.1	- 4.4%
(Below are some of the other considerations)			
Top speed*--kmph (mph)	134.7 (83.7)	154.5 (96)	+ 15%
Engine rpm at 88.5 kmph (55 mph)**	2446	2000	- 19%

*Top speed is limited by maximum engine speed with the production drivetrain but it is only limited by power for the optimized drivetrain.
**Higher engine speed during cruise increases engine noise levels.

Table VIII.
ATTAP RPD vehicle performance.

* Time to 96.5 kmph (60 mph) from standing idle = 13.1 sec

* Time to distance from standing idle

Time--sec	1	2	3	4
Distance--m (ft)	1.83 (6)	8.53 (28)	18.29 (60)	31.09 (102)

* Top speed = 154.5 kmph (96 mph)

* Top gear gradeability at 88.5 kmph (55 mph) = 10.9%

(All performance for 15°C [59°F] sea level conditions)

Gearbox

The gearbox redesign is aimed at increasing the load carrying capacity of the power turbine's speed reduction (16.94:1) pinion/gear and chain system (see Figure 10) due to the increased power output of 1371°C (2500°F) RPD. Allison's gear analysis program (AL13) was employed to evaluate tooth bending and contact stresses for gear and pinion variations. The preliminary gear design, along with horsepower and torque levels, was given to Borg-Warner (manufacturer of the Morse Hy-Vo chain) for chain evaluation/redesign. A preliminary design layout of the upgrade gearbox was initiated to incorporate the new pinion/gear and chain envelope. A modular gearbox approach is also being investigated with the potential of minimizing the front gearbox casting revisions by incorporating a new gearbox cover.

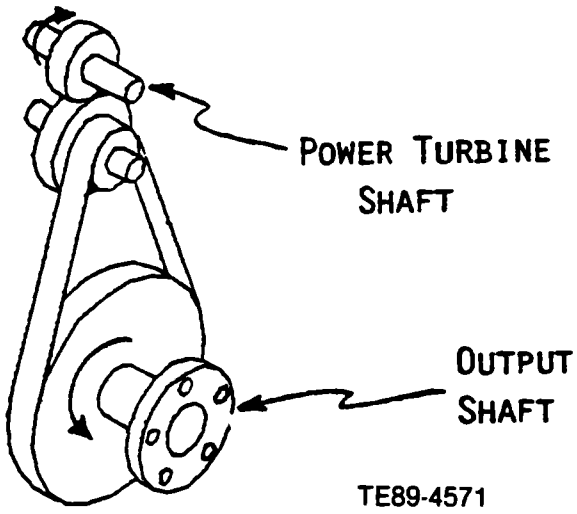

Figure 10. Power turbine speed reduction system.

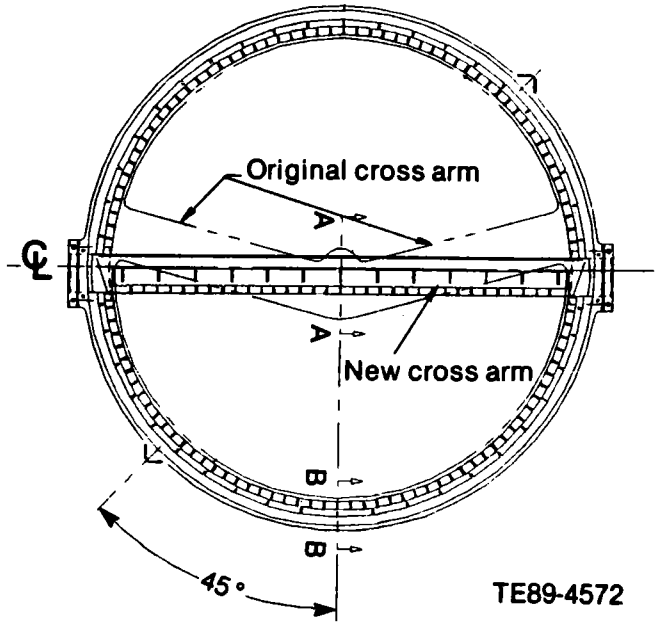

Figure 11. AGT-5 straight crossarm ceramic regenerator seal platform.

Gasifier Module

Prior to ATTAP, axial-flow automotive gas turbine work at General Motors was focused on a newer, less mature, developmental engine than the AGT-5. One of the most noteworthy pieces of technology developed during this activity was the redesign of the gasifier module bearing system for increased durability. The bearing retention and mounting technique, developed by GM as background data to the ATTAP and considered GM proprietary, was transferred to the AGT-5. Design activity is complete and castings have been procured. Four upgraded gasifier housings have been machined and inspected and await assembly.

Regenerator Seal Platform

The regenerators of the metal AGT-5 engine are limited to approximately 1149°C (2100°F) TIT. In order to meet the operating requirements of a 1371°C (2500°F) TIT RPD, a regenerator system capable of intermittent inlet temperatures approaching 1093°C (2000°F) will be required. Steady-state standard day maximum regenerator inlet temperature would be approximately 960°C (1760°F). One solution under way is the design of a ceramic regenerator system. The merits of a straight crossarm ceramic regenerator seal platform versus that of the original elbowed crossarm (Figure 11) have been evaluated. The simplified design would allow the gas- and air-side rim seals to be identical while allowing symmetrical thermal growth. The constant height seal leaf of the ceramic design and the removal of the mitered leaf joints of the elbow design would effectively reduce the leakage by approximately 1% across the operating range of the engine. The effectiveness of the regenerator would be reduced slightly at peak power due to the reduction of gas-side exposure area with the straight arm. This penalty is considered acceptable when the payoffs of a reduced leakage simplified design are considered. Two seal leaf systems were also evaluated. In the first system, the seal leaf is housed in the engine block. The second system attaches the leaf to the crossarm wear face. The first system eliminates the thermal fight between the seal leaf and the wear face.

Computer Graphics Detailed Drawings

As stated previously, GM's activity pursuant to the development of axial flow automotive gas turbines was focused on a newer developmental engine prior to ATTAP. Therefore, only a random handful of AGT-5 drawings were done on the new computer graphics system. In order to expedite the upgrade of the AGT-5 engine and the design of ceramic components, hand drawings will be converted to the computer graphics system on an as-needed basis. To date, 262 drawings have been converted.

1.4.2 Combustion Systems

Objective/Approach

The objective of this effort is to reduce carbon formation, a source of FOD, in the combustion system.

Design/development of the combustion system is to be consistent with the contractual design specifications of meeting gaseous emissions plus satisfying the RPD reliability, life, and initial and life cycle cost goals of the integrated engine/powertrain.

The standard combustion system developed for the 1038°C (1900°F) TIT metal AGT-5 engine is a fixed geometry can-type diffusion flame burner. This diffusion flame burner does not meet the federal NO_x emission level, and most importantly, it has the tendency to form hard carbon in the region of fuel site delivery. Fortunately, both of these shortcomings can be addressed by leaning out the primary zone combustion process. A leaner reaction zone will reduce the likelihood of producing local fuel rich zones in the vicinity of the delivery site and thereby inhibit the formation of hard carbon. The resulting lower primary zone temperatures will also reduce the concentrations of NO_x.

Two design approaches to a lean, carbon-free combustion system are presently being pursued. These are listed below.

- o a passive thermally actuated variable geometry (TVG) mechanism as an add-on feature to the present diffusion flame burner
- o a new active variable geometry (AVG) two-stage air admission combustor design

Accomplishments

Accomplishments for the combustion systems activity are listed below.

- o performed successful TVG proof of concept engine test with an altered/modified standard diffusion flame burner
- o completed design modifications to fully incorporate the TVG into the standard diffusion flame burner
- o initiated design efforts for a new AVG two-stage air admission burner
- o cold-flow-tested "preliminary design" AVG combustor hardware

TVG

The TVG concept (Figure 12) uses a bimetallic strip to affect airflow distribution in the diffusion flame burner. Bimetallic strips of 440 SS and 310 SS were spot-welded together and tacked at one end to a flange surrounding the dome of the burner. Eight strips, equally spaced, cover and block enlarged dome swirl ports. When hot, the strips deflect away from the surface and allow air to be inducted into the primary zone. This simple form of variable geometry ensures a rich mixture for cold light-off conditions and a leaner primary zone during operation. This reduces carbon build-up, NO_x emissions, and thermal damage to the igniter and burner extremities. This modified burner was installed in an engine and tested on the vehicle rolls dynamometer. NO_x emissions were consistently 40% lower than the standard diffusion flame burner. Testing on 100% and 85% methanol was also performed. HC emissions increased on 100% methanol operation as expected. The standard diffusion flame burner (not specifically designed for methanol) combustion process is lean when run on methanol. TVG leans the process out even more thereby increasing the HC formation. Operation on an 85%/15% mixture of methanol/gasoline reduced HC formation but increased NO_x.

Design modifications were completed to fully incorporate the TVG into the standard diffusion flame burner. Procurement of the various combustor components was initiated. Rig and engine testing of the new TVG combustor is planned for final design concept evaluation. Once completely finalized, these combustors will begin to replace the standard burners in all rigs and test-bed engines. While it is recognized that this design will not fully meet the emission requirement or completely eliminate the formation of hard carbon, usage will substantially impact rig and engine testing of ceramic components. The leaner warm engine primary zone combustion process (via a 30% increase in admission air) will reduce the thermal damage to the igniter and the burner extremities as well as reduce the likelihood of ceramic component FOD. The possibility of carbon formation during a cold start remains due to the thermal inertia of the engine. The resulting lag in TVG operation allows a rich primary zone for several minutes. The ability of the AVG design to begin leaning out the fuel/air mixture, immediately after light-off, should address this problem.

AVG

Design efforts were initiated for a new AVG two-stage air admission burner (Figure 13). Variable geometry is accomplished via a butterfly valve located at the inlet of the burner scroll (vortex). Actuation is proportioned to yield a variable airflow. A computer program which calculates steady-state global temperatures within the combustor for various operating conditions was used to iterate to the proper airflow split at a given gasifier speed to maintain primary zone temperatures be-

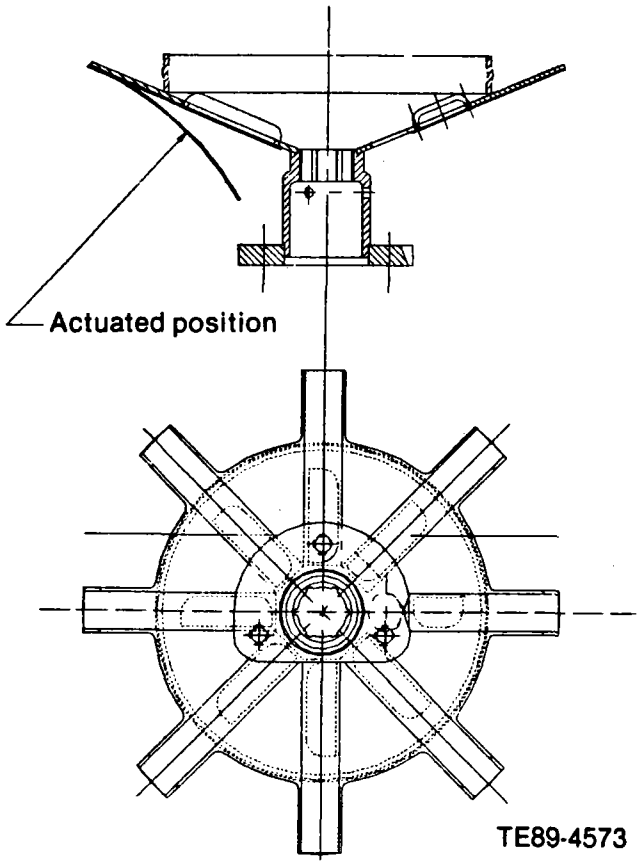

Figure 12. TVG combustor--bimetallic strips.

tween 1250°C (2282°F) and 1350°C (2462°F). Transient response analysis of the new geometry was initiated to evaluate airflow distribution, stoichiometry, and mechanical operation.

A set of "preliminary design" hardware was fabricated and cold-flow-tested. Testing revealed a maldistribution of flow through the vanes of the combustor dome. The flat vane angles were adjusted up to a maximum of ±10 deg to compensate for the asymmetric flow pattern created by the vortex/butterfly assembly. The modified vane setting angles will be employed during the first hot test.

The mechanical linkage used to operate the butterfly valve is under design considerations for both compressor discharge pressure actuation via a pressure diaphragm and accelerator cable actuation. Initial rig testing will use a standard dynamometer cell control cable for butterfly actuation. Transient testing will be via a joy stick that will actuate the fuel command and link directly to the butterfly valve control cable.

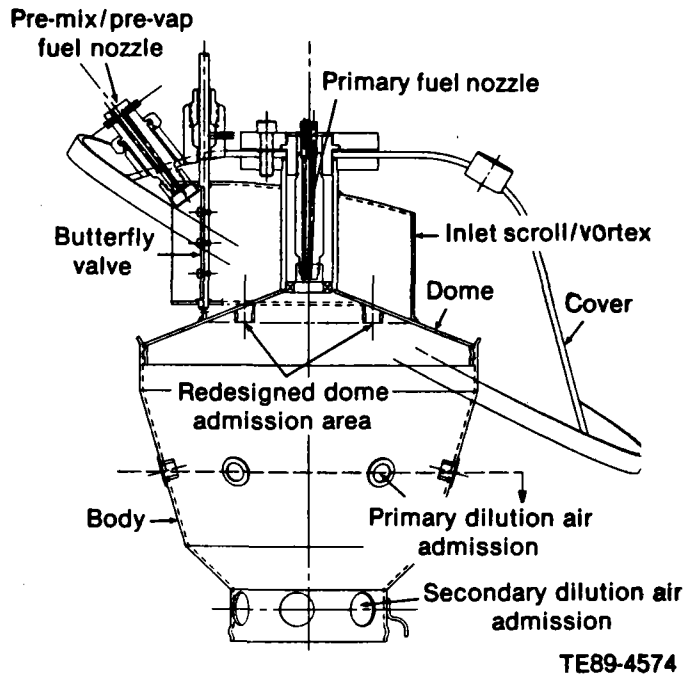

Figure 13. AVG combustor.

1.4.3 Alternate Flow Paths

Objective/Approach

The objective of this aerodynamic development effort is to upgrade the power turbine of the existing 1038°C (1900°F) metal AGT-5 engine to meet the requirements of the 1371°C (2500°F) RPD, specifically the increased temperature and total-to-static pressure ratio (from 2.1 to 2.42). Aerodynamic evaluations are performed using a free vortex performance program with the goal total-to-static stage efficiency being 77% and a preferred 1st stage/2nd stage work split of 46%/54%, respectively.

Accomplishments

Accomplishments for the alternate flow paths activity are listed below.

- o selected an aerodynamic power turbine configuration
- o preliminarily defined that the 1st stage vane and both rotors would be ceramic
- o initiated detailed aerodynamic design activities

Three different aerodynamic design configurations (see Figure 14) were evaluated for impact on overall

engine performance, integrity of mechanical design and packaging, as well as ceramitization feasibility.

Design No. 1 is the most radical departure from the existing power turbine design. This design takes advantage of the counterrotating gasifier and power turbine shafts and eliminates the 1st stage power turbine nozzle. From a mechanical design and packaging point of view, this was the most desirable flow path. Aerodynamically, however, this configuration had several shortcomings. The relative inlet angle for the 1st stage power turbine was inadequate resulting in a skewed work split between the 1st and 2nd stage power turbines of 38% and 62%, respectively. The steep outer wall angle of the 2nd stage power turbine nozzle and insufficient flow acceleration through the stage resulted in flow separation from the outer wall. Predicted total-to-static efficiency for this design was only 72%.

Design No. 2 incorporated an interstage duct into Design No. 1. The 1st stage power turbine rotor was slid back and a centerbody, which is held by three struts, was inserted between the gasifier turbine and the 1st power turbine. This design cleaned up the flow problem in the 2nd stage power turbine nozzle allowing flow to accelerate in the nozzle and allowing the nozzle to remain attached to the outer wall. The work split in the power turbine remained unchanged and the predicted total-to-static efficiency was 74%. Design No. 3 is very similar to the existing metal power turbine design. There is an interstage duct and a vaned 1st stage power turbine nozzle. The worksplit for the power turbine is 47%/53% with a predicted total-to-static stage efficiency of 76.5%.

Based on the above results, it was concluded that the power turbine design for the 1371°C (2500°F) RPD engine will have 1st and 2nd stage vanes and will be similar to Design No. 3. The poor aerodynamic features and efficiency losses of Designs No. 1 and No. 2 outweighed any mechanical design and/or packaging advantages.

Initially, we believed that the power turbine design goal could be met with a ceramic 1st stage power turbine rotor and a metal second stage power turbine rotor. From a mechanical design standpoint, it was desirable to keep the 2nd stage rotor metal. Preliminary stress calculations were performed on the proposed metal 2nd stage rotor at the RPD conditions, and it was found to have insufficient life. To meet the design goals, it was determined that both the 1st and 2nd stage power turbine rotors would have to be ceramic.

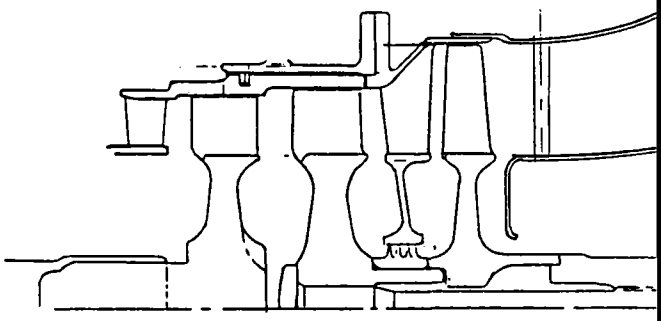

Design I

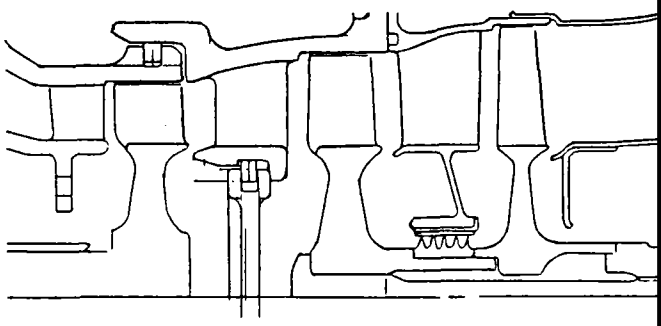

Design II

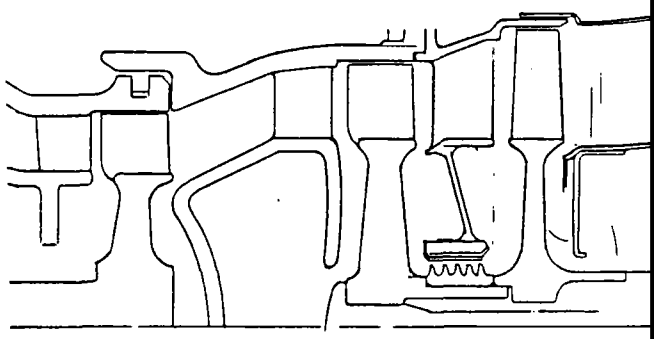

Design III

TE89-4575

Figure 14. Conceptual turbine aerodynamic design configurations.

A detail design effort was initiated for a power turbine with ceramic 1st stage vanes and all-ceramic rotors. Initially, to determine the design speed, a series of design trade-offs were evaluated. The velocity triangles at the hub, mean, and tip sections were determined at different rpm along with preliminary rotor stress numbers. A design speed of 62,000 rpm met both the aero and preliminary stress requirements.

Airfoil shapes were created for the hub, mean, and tip sections of the 2nd stage rotor. From these shapes, a detailed stress model was constructed. To keep the hub stress under 200 MPa (29 ksi), the short term shift point rpm would have to be limited to 115% over speed. Previous vehicle/engine simulation work determined that it is desirable to run the power turbine to 125% over speed before shifting the transmission. Presently, the power turbine design is being reworked to lower the design point speed.

1.4.4 Engine System Integration

Objective/Approach

The objective of the engine system integration activity is the modification of the current AGT-5 engine control and accessory systems to meet the requirements of the RPD. This includes engine and rig work necessary to perform specific tests as well as the routine maintenance, calibration, and testing to support normal test procedures.

Accomplishments

Accomplishments for the engine system integration activity are listed below.

- o developed and implemented control software for durability schedule running
- o modified the engine control software for hot gasifier rig control
- o performed fuel system testing to determine requirements for 1371°C (2500°F) RPD conditions

The AGT-5 engine is microprocessor-controlled using a GM function control module (FCM). The control program was modified to run an engine durability cycle automatically. The program controls gasifier and power turbine speeds versus a time schedule (see Figure 15) while continuing to provide safety monitoring. The use of a standard cycle will allow better comparison between engine builds and will provide an improved understanding of the benefits obtained through the use of ceramic component designs. The schedule algorithm and necessary shutdown routines were successfully coded, implemented, and tested.

Modifications were made to the engine control program for the hot gasifier rig to account for the following differences: no output shaft speed signal, no gasifier TIT signal, and different gasifier speed calculations due to air start hardware. These, as well as other minor changes, were successfully implemented and verified during rig operation. The fuel, oil, and coolant system requirements for the AGT-5 hot gasifier rig were determined and a system was designed and implemented to meet these requirements. A standard engine fuel system was used while coolant and external oil systems were developed.

Testing conducted on the engine's motor-driven fuel pump revealed that the system did not fully meet the idle flow requirements of the engine. Smaller capacity pumps solved this problem, but further testing revealed that this particular combination of pump and motor hardware did not have adequate capacity to meet the anticipated engine maximum fuel flow conditions at 1371°C (2500°F) TIT. New motors to meet these requirements were selected and ordered.

REFERENCES

1. Pampreen, R.C., "Small Turbomachinery Compressor and Fan Aerodynamics," ASME Paper No. 73-GT-6, May 1973.
2. Larkin, T.R., "Small Engine Component Technology (SECT) Study Final Report," NASA CR-175081, to be released March 1991.

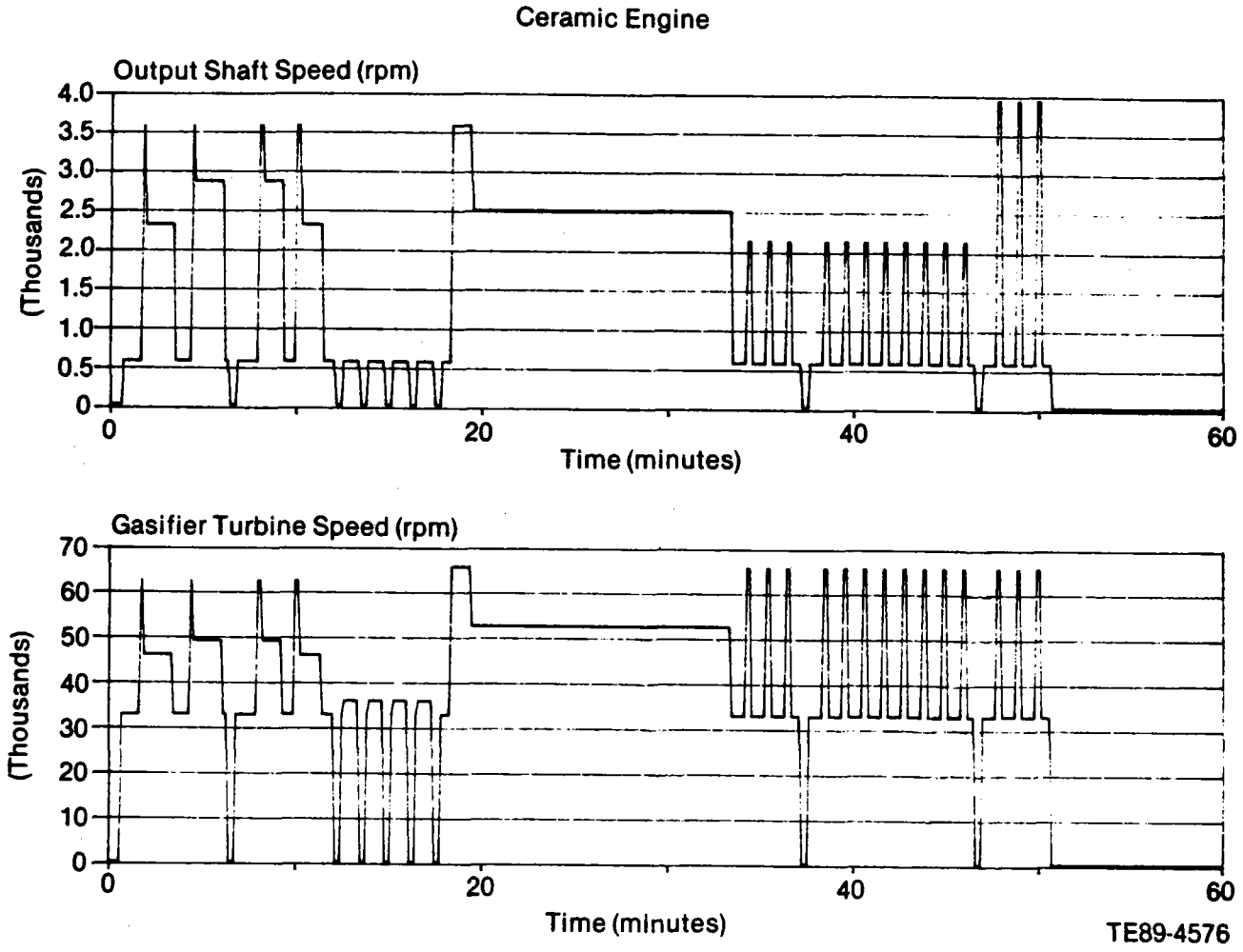

Figure 15. ATTAP durability schedule.

II. CERAMIC COMPONENT DESIGN

2.1 DESIGN ACTIVITIES

2.1.1 Combustor

Objective/Approach

The objective of this effort is to provide a combustor assembly design which will allow operation of the test-bed engine at RPD temperature levels. The goals of this design are as follows:

- o provide a combustor assembly capable of operating at 1371°C (2500°F) average outlet gas temperature at full power engine operating conditions
- o develop a reliable interface with ceramic gasifier turbine components and other associated engine components
- o calculate probability of survival (POS) of ceramic component(s) to be 0.9752 or greater under worst operating condition

The combustor design will be based on the successful design used in the AGT100 program with modifications to reflect the aerodynamic design parameters and the mechanical configuration of the AGT-5.

Accomplishments

The accomplishments for the combustor activity are listed below.

- o initial conceptual design configuration prepared including interface with associated components
- o original (metal with cooling) aerodesign of combustor modified to reflect ceramic combustor assembly without skin cooling
- o design configuration refined to reduce complexity of attachment hardware and ceramic component
- o thermal analysis of combustor assembly initiated
- o design of ceramic component reviewed with fabricating vendor

The intent of the initial combustor design activity was to use as much as practicable of the design and test experience gained from the ceramic combustor used in the AGT100 engine program. The AGT100 combustor assembly, a premix-prevaporization, variable geometry design included three ceramic components: body, dome, and pilot igniter tube. The ceramic components used in that assembly worked very satisfactorily when assembled and operated as designed. The AGT100 combustor components were stacked together (like blocks) and held in position against the gasifier turbine scroll with springs positioned at the combustor inlet. Difficulty was experienced during testing of the AGT100 engine in maintaining reasonable loads on the springs during all conditions of engine operation. If the spring load became too small, the combustor would not stay positioned properly against the scroll inlet. If the combustor was loaded against the scroll excessively, the turbine scroll would tilt and cause the rotor to rub or the cross key locating features on the scroll assembly would fracture resulting in engine failure. It was clear from test experience of all the static ceramic components that minimizing or eliminating redundant mechanical loads on the ceramic components should be a primary design objective.

Thus, two features of the initial combustor design concept for the ATTAP test-bed engine were different from those of the AGT100 design. One feature was to support the ceramic combustor assembly by attaching it to the engine case burner cover rather than spring loading it against the turbine scroll inlet. This will reduce the load on the scroll's ceramic cross keys as well as on the scroll/combustor interface. The other feature was to allow the combustor to swivel at its attachment point to prevent binding due to any relative lateral motion between the scroll inlet and engine case burner cover.

Concepts studied involved variations of a ball-and-socket-type joint for allowing the combustor to swivel. One promising concept (Figure 16) has two coaxial air-cooled coil springs enclosed in a metallic housing. The outer spring is used to keep the body and dome pressed together, while the inner spring loads the combustor assembly against the ball joint. The springs would be sized to provide enough preload to maintain contact of the combustor components throughout the gas pressure and vibratory shock load range they would encounter in service. The environment surrounding the attachment mechanism reaches approximately 899°C (1650°F) at maximum power conditions. To maintain a high yield strength in the springs, they would be cooled with compressor discharge air supplied inside the spring housing. The spring housing and ball joint are set back from the combustor and shielded by the dome to reduce the radiative heating from the combustion zone. A collar surrounds the combustor body and engages tabs at the end of the body to load it against the dome.

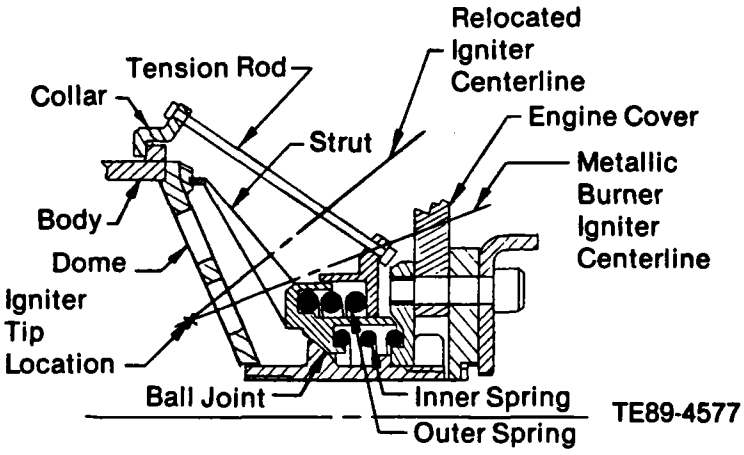

Figure 16. Ceramic combustor attachment mechanism (cross-section).

Tension rods transmit the spring load to the collar. The dome in turn is pushed against the body by struts attached to the spring housing. The mechanical loads on the dome are all applied near the outer edge to minimize bending moments on the dome.

The igniter attaches to the external combustor cover and passes through the combustor dome. Sufficient clearance must be provided by the hole in the dome and by the moving attachment mechanism to prevent contact with the igniter body through the range of movement of the combustor assembly. The angle of entry of the igniter for the concept shown would be altered from that of the current metallic combustor to maintain the same igniter tip location inside the burner.

This design, however, placed two metallic springs in a very high temperature environment. The design was revised to combine the ceramic combustor body and dome into one piece, thereby eliminating the requirement (and hardware) to hold the parts together. By deleting both coil springs, compressor discharge cooling air requirements were eliminated. The revised concept (see Figure 17) shows the combustor body and dome assembly held by a lip near the inner portion of the dome. While this is an added feature on the dome, the need for retaining tabs (on the combustor body outside diameter), outer collar, and tension rods is eliminated.

Design efforts primarily addressed the combustor attachment mechanism. While held in place, the combustor must be free to pivot as necessary to accommodate relative motion between the gasifier scroll inlet and the burner cover. A variety of joints including the following were considered: ball and socket, universals, and flexible fingers. The simplified, flexible metal fingers joint was selected and is thought to be adequate due to the small range of pivoting motion actually required.

The size and shape of the ceramic combustor body/dome is similar to the current AGT-5 metallic burner. The outer diameters of the two burners are the same; however, the ceramic burner is cylindrical rather than slightly tapered like the metallic burner to compensate for the thicker ceramic walls while keeping the internal volume nearly the same. The air inlet holes in the various regions of the burner have been sized to provide the same flow splits as in the metallic burner. Metallic burner design similarity has been incorporated into the ceramic burner design to help ensure its successful operation. These design modifications result in fewer parts, reduced part complexity, and reduced machining and assembly time. Reduction in the size of the attachment will also permit the igniter insertion angle of the metallic combustor to be used if so desired. Actual implementation of this design is dependent on achieving an acceptable survivability in the integral body/dome ceramic component and a sufficiently low stress level design for the flexible fingers.

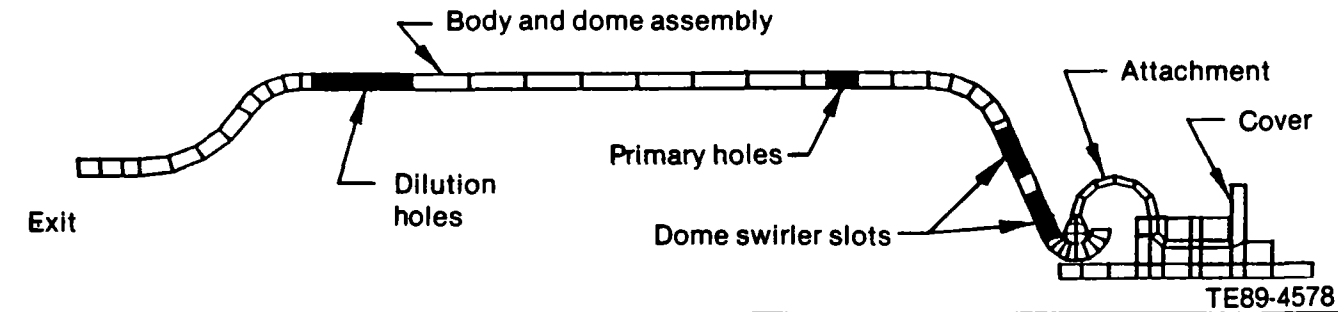

Figure 17. Ceramic combustor and assembly.

A two-dimensional (2-D) axisymmetric finite element method (FEM) model of the combustor assembly was created for analyzing temperature, stress, deflection, and probability of survival of the revised design. Steady-state and transient operating conditions will be analyzed. Work on applying the appropriate thermal boundary conditions for determining combustor assembly material temperatures was initiated.

Initial results indicated that the combustor body/dome and the metallic attachment temperatures would be much higher than anticipated. Calculated temperatures of the metallic attachment near its point of contact with the ceramic combustor body were unacceptably high. Design modifications were initiated to reduce the operating temperature of the metallic structure. These design modifications included lengthening the neck between the dome and the attachment, adding cooling holes in the neck region, and adding an insulating material between the neck and the metallic attachment. Each of these changes would reduce the amount of heat transfer to the attachment thereby lowering its operating temperature.

This design activity will continue during 1989. In anticipation that the one-piece ceramic combustor body/dome will meet the design probability of survival goal, a design review was held with a potential fabricating vendor to determine if the one-piece configuration could be fabricated. After study, a positive response was expressed by the vendor.

2.1.2 Gasifier Turbine Static Structure

Objective/Approach

The primary objective of this activity is to design the static structure components of an all-ceramic gasifier turbine capable of operating at the 1371°C (2500°F) RPD conditions. The secondary objective is to design a ceramic turbine shroud to be used in ceramic rotor test evaluations at an intermediate TIT of 1204°C (2200°F). A ceramic shroud will match the thermal growth of a ceramic rotor and will thereby allow rig/engine operation with the proper rotor tip clearances. Ceramic component design integrity will be verified analytically using the 2-D axisymmetric finite element method in conjunction with the Weibull statistical criteria to demonstrate an acceptable probability of survival. Stress levels and temperature limits will also be scrutinized on interfacing parts.

Accomplishments

The accomplishments for the gasifier turbine static structure activity are listed below.

- 1371°C (2500°F) components
  - established design guidelines
  - completed 2-D axisymmetric model of the gasifier turbine static structure
  - redesigned gasifier housing and ceramic component attachment features to alleviate excessive housing temperatures
  - changed scroll to a two-piece design
  - completed steady-state heat transfer and stress analyses
- ceramic gasifier shroud
  - completed shroud design as well as associated metal components
  - completed FEM analyses of steady-state and transient conditions for two shroud materials
  - achieved probability of survival design goals for both Si_3N_4 and SiC materials

1371°C (2500°F) Components

The following design guidelines were established to facilitate the ceramic design activity:

- minimize heat transfer from ceramic components to connecting (metal) engine structure (minimizes thermal stresses in ceramic components and reduces heat rejection)
- minimize constraints on ceramic components to allow free relative movement during engine operation
- maintain maximum control of shroud-to-rotor concentricity by minimizing number of stack dimensions between shroud and rotor bearing(s)
- minimize radial flanges in ceramic components which would be subject to radial thermal gradients
- establish assembly procedure (sequence) which minimizes exposure of ceramic components to accidental damage during engine assembly

These guidelines, along with general arrangement configuration studies and vendor input on fabrication techniques, were used in the ceramic component design process.

A 2-D axisymmetric model was constructed for Allison's STRATA FEM program. This model was used to determine deflections and to provide rationale necessary for the selection of materials and heat flow reducing schemes necessary to interface between ceramics and the metallic framework of the engine. Figure 18 presents a plot of this model. A 1371°C (2500°F) TIT, max power, steady-state, heat transfer analysis was run for the model. The resulting temperatures were then used to calculate stresses and probability of survival for the ceramic components. The probabilities of survival for the ceramic components were found to be nearly 100% for the steady-state temperatures. The analysis also indicated that some temperatures in the interface area between the ceramic parts and the bearing housing were higher than anticipated.

Test data was investigated to arrive at a correlation between inlet and housing temperatures to verify the existence of a high temperature problem in the housing. Studies were then made in an attempt to reduce the heat flow through the cross keys and ultimately to reduce the temperature into the bearing housing. A number of design alternatives were considered. Previous designs appeared to allow too much heat flow into the housing. Studies were directed toward the reduction of heat flow at the ceramic-to-metal interface area. The study resulted in a new cross-key scheme that greatly reduces the heat flow due to a much more difficult heat path.

The scroll configuration was reviewed with Carborundum. Concern was raised over the brazed joints' ability to provide the required strength as well as the fabrication difficulty of the cross keys under the vane. Carborundum recommended that the scroll be made in two pieces. Modifications to the design were made, changing the configuration enough that an entirely new FEM had to be defined for the scroll assembly including the attachment features. A plot of a cross section showing the two-piece scroll is presented in Figure 19. Steady-state temperature analyses were completed. Temperature plots are shown for the structural ceramic parts in Figure 20. Corresponding maximum principal stresses for these parts are presented in Figure 21. The material used for the ceramic structural components in this analysis was alpha-SiC.

Ceramic Gasifier Shroud

The ceramic gasifier turbine shroud (shown in Figure 22) has several characteristics similar to those used on previous ceramic projects. The shroud has a cross-key arrangement to form an interface between the ceramic and metallic components. By cross keying the dissimilar materials together, the metal pins may translate radially at a different rate than the ceramic shroud due to incompatible thermal growth coefficients but may still provide adequate positioning of the shroud. The cross-key components are formed by elongated slots (see Figure 23) in the ceramic shroud which rest on three metal pins.

Past experience has shown that a ceramic shroud with similar characteristics will have a very low probability of failure, and the largest magnitudes of stress are induced by thermal gradients. Due to this past structural history, the new ceramic shroud design was

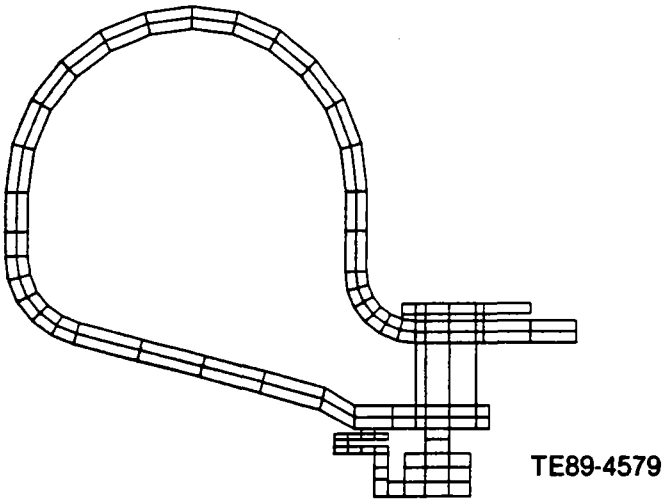

Figure 18. FEM model of gasifier turbine scroll assembly.

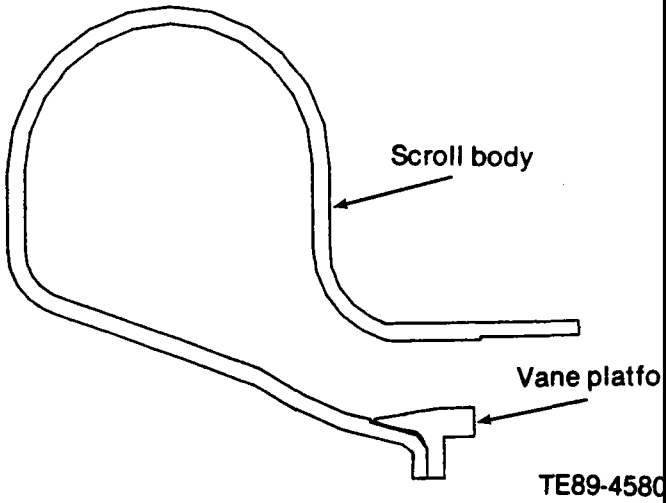

Figure 19. Two-piece scroll configuration for CBO.

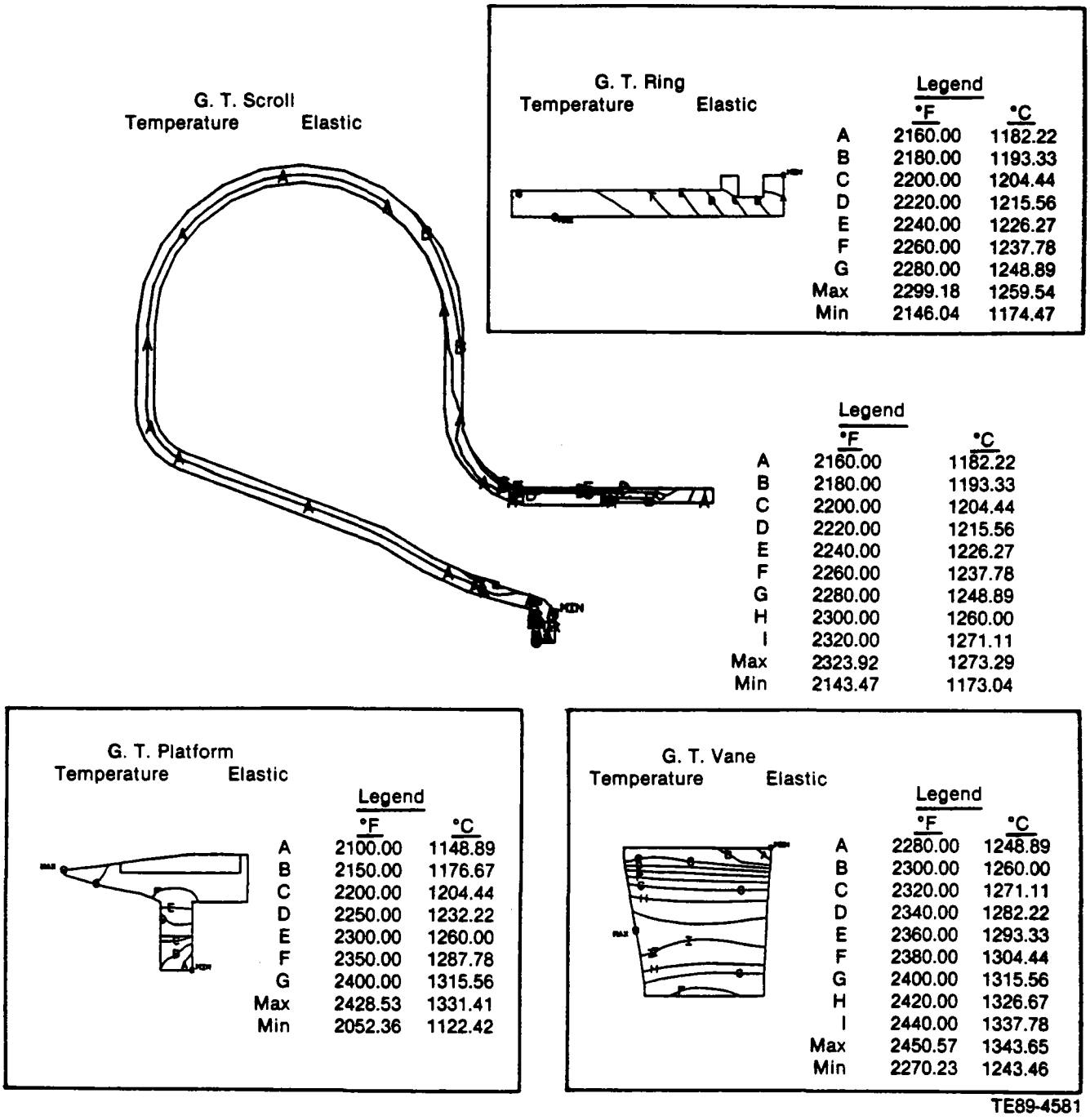

Figure 20. Scroll assembly components--temperature distributions at max power steady-state.

simulated using simple and inexpensive 2-D axisymmetric FEMs with emphasis placed on the transient conditions of the turbine cycle. Because of the regenerative design of the engine, the worst case transient was determined to be full acceleration from a cold start. Using the described design approach, the developed ceramic shroud design will have a high probability of survival.

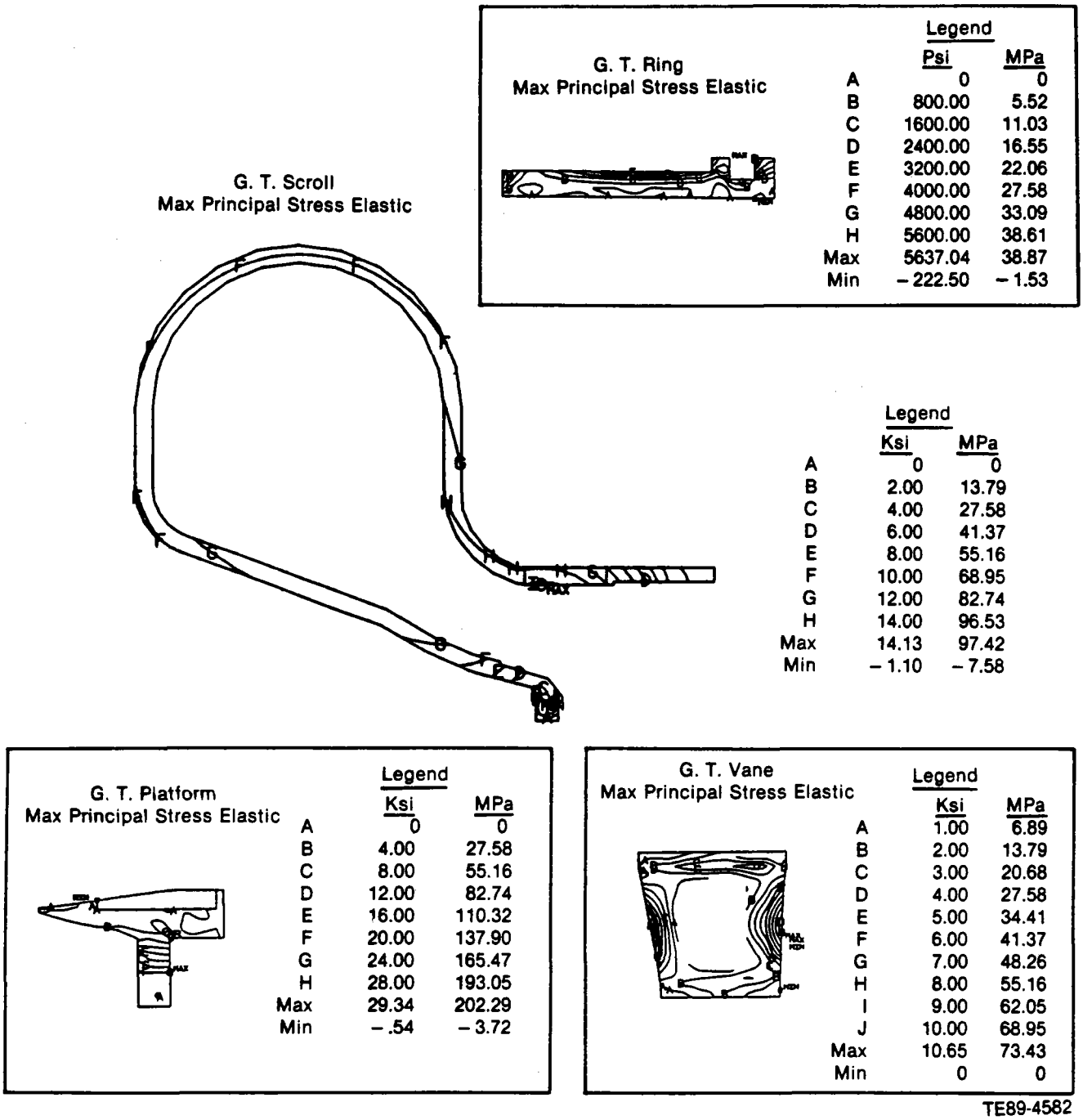

Figure 21. Scroll assembly components--maximum principal stress distributions at max power steady-state.

Table IX compares the results of the analyses of the alpha-SiC and Si_3N_4 shrouds for both steady-state and transient conditions. It is apparent that both shrouds exhibit very low levels of stress and high probabilities of survival. Figures 24 and 25 display both alpha-SiC and Si_3N_4 materials in steady-state operations.

Table IX.
Ceramic gasifier turbine shroud.

	Alpha-SiC	SN251 Si_3N_4
Steady-state conditions		
Max temp--°C (°F)	933 (1711)	936 (1717)
Max principal stress--MPa (ksi)	11.191 (1.623)	10.329 (1.498)
POS	1.0	1.0
Start-up transient conditions		
Time of max principal stress--sec	20	25
Max temp--°C (°F) (at max stress condition)	438 (820)	531 (988)
Max principal stress--MPa (ksi)	11.784 (1.709)	12.721 (1.845)
POS	1.0	1.0
POS goal	0.998	0.998

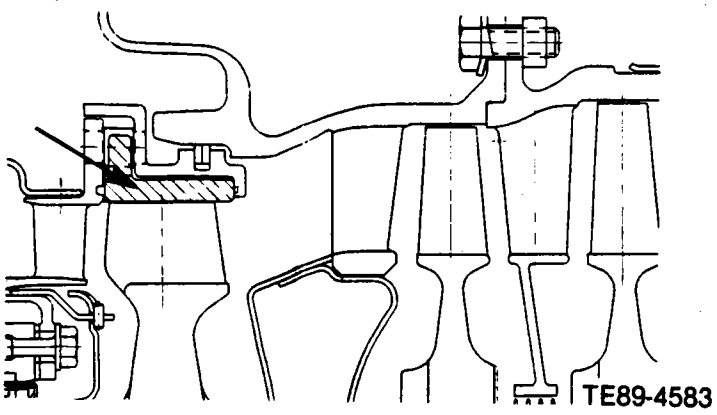

Figure 22. Ceramic gasifier turbine shroud--flow-path view.

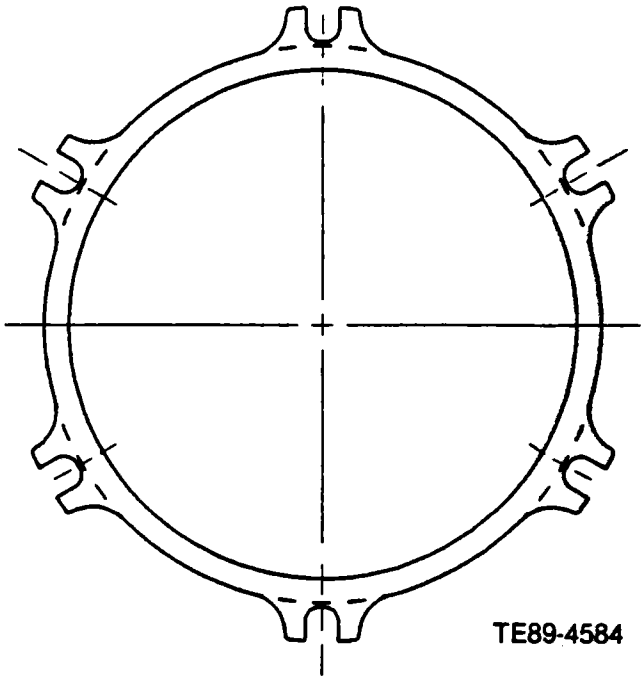

Figure 23. Ceramic gasifier turbine shroud.

2.1.3 Gasifier Turbine Rotor

Objective/Approach

The objective of this activity is to design a ceramic gasifier rotor capable of operating at the 1371°C (2500°F) RPD conditions. Design of the ceramic rotor is an iterative closed loop approach such that specific requirements for each of the following areas are met: aerothermo efficiency, gas path pullability, minimum trailing edge thickness, vibration stiffness, rotor/shaft attachment, and probability of survival.

Ceramic shroud temperature profile
T4 = 2200 °F S.S.
Carborundum αSiC

Shroud

*T_{max} = 1711.3 °F (932.9 °C)

T_{min} = 1661.3 °F (905.2 °C)

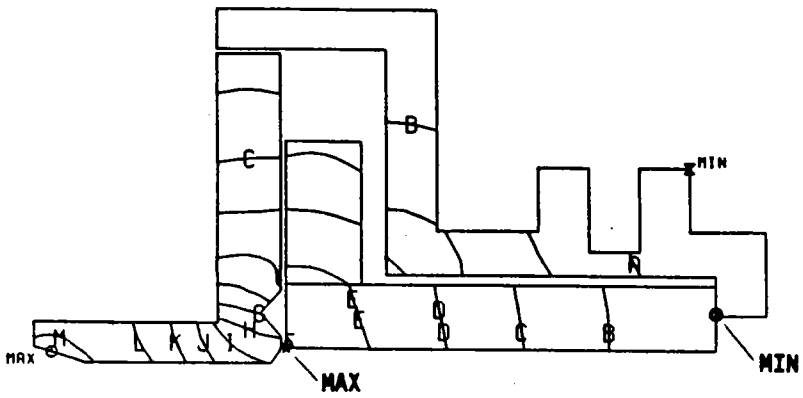

Legend	°F	°C
A	1660.00	904.4
B	1670.00	910.0
C	1680.00	915.6
D	1690.00	921.1
E	1700.00	926.7
F	1710.00	932.2
G	1720.00	937.8
H	1730.00	943.3
I	1740.00	948.9
J	1750.00	954.4
K	1760.00	960.0
L	1770.00	965.6
M	1780.00	971.1
Max	1781.93	972.2
Min	1651.15	899.5

Ceramic shroud principal stress profile
T4 = 2200 °F S.S.
Carborundum α SiC

Shroud

*Max tangential = 1623 psi (11.19 MPa)

POS = 1.0

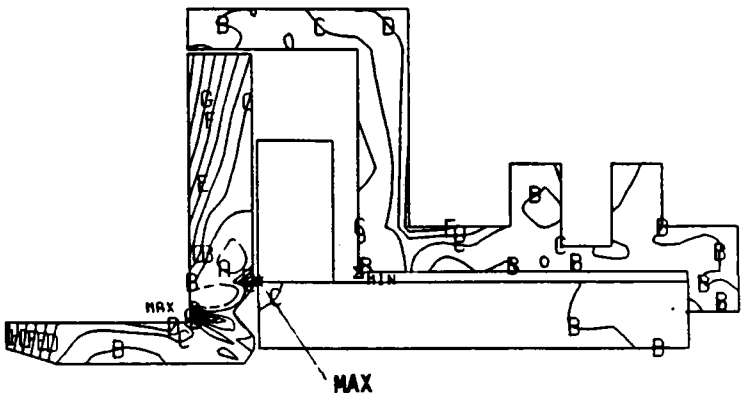

Legend	Ksi	MPa
A	−1.00	−6.90
B	0	0
C	1.00	6.90
D	2.00	13.79
E	3.00	20.69
F	4.00	27.58
G	5.00	34.48
H	6.00	41.37
I	7.00	48.27
J	8.00	55.16
Max	8.80	60.68
Min	−1.33	−9.17

TE89-4585

Figure 24. Alpha-SiC shroud design.

Ceramic Shroud Temperature Profile
T4 = 2200°F S.S.
Kyocera SN251

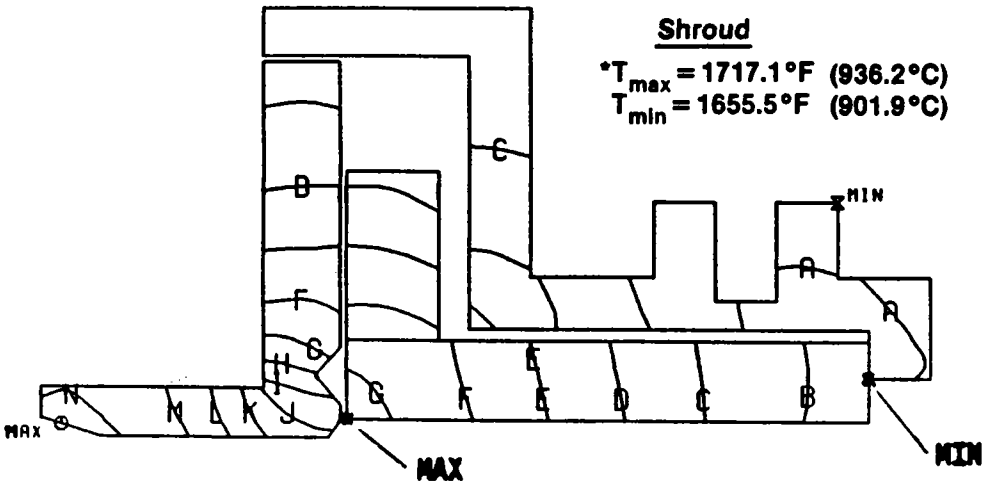

Legend	F	C
A	1650.00	898.9
B	1660.00	904.4
C	1670.00	910.0
D	1680.00	915.6
E	1690.00	921.1
F	1700.00	926.7
G	1710.00	932.2
H	1720.00	937.8
I	1730.00	943.3
J	1740.00	948.9
K	1750.00	954.4
L	1760.00	960.0
M	1770.00	965.6
N	1780.00	971.1
Max	1782.67	972.6
Min	1647.18	897.3

Ceramic Shroud Principal Stress Profile
T4 = 2200°F S.S.
Kyocera SN251

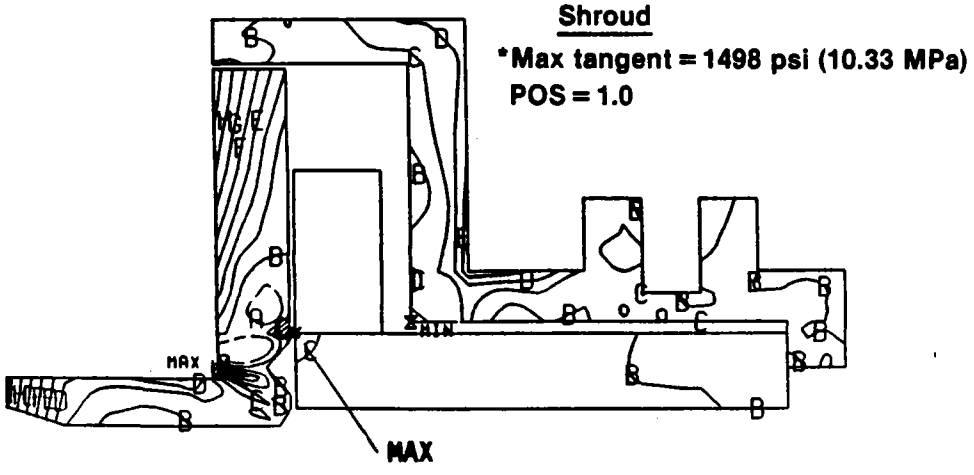

Legend	Ksi	MPa
A	−1.00	−6.90
B	0	0
C	1.00	6.90
D	2.00	13.79
E	3.00	20.69
F	4.00	27.58
G	5.00	34.48
H	6.00	41.37
I	7.00	48.27
J	8.00	55.16
K	9.00	62.06
Max	9.30	64.12
Min	−1.42	−9.79

TE89-4586

Figure 25. SN251 Si_3N_4 shroud design.

Accomplishments

Accomplishments for the gasifier turbine rotor activity are listed below.

- o completed design of a Si_3N_4 20-bladed rotor meeting the design probability of survival goal of 0.9797
- o achieved interference fit shaft attachment design goals for both SiC and Si_3N_4

The basic RPD design requirement for the ceramic gasifier rotor is operational capability at 1371°C (2500°F) TIT and 65,323 rpm with a design probability of survival of 0.9797. The ceramic airfoil must also satisfy aerothermo efficiency, gas path pullability and minimum trailing edge thickness in the 1 to 0.5 mm (0.040 to 0.020 in.) range. The airfoil hub diameter was fixed by the existing test bed engine. Multiple iterations were made of the airfoil geometry in an effort to satisfy the various requirements. The ceramic airfoil was assessed for impact survivability on an engineering judgement and test experience basis. Consideration of the various requirements resulted in 15 and 20 airfoil designs in SiC and Si_3N_4 materials. The matrix of gasifier rotor designs and vendors is shown in Table X. This matrix has been specifically constructed for engine test assessment of the various material systems and designs.

The 20-airfoil configuration was designed to the engine aerodynamic criteria and the 15-airfoil geometry was scaled by the ratio of 20/15. This scaling was applied to the axial chord and the airfoil thickness but not to the height. The height or span of the airfoil is fixed by the engine flow path. An example of the scaling is described for the trailing edge thickness as:

Trailing edge thickness, 20 airfoil = 0.71 mm (0.028 in.)
Trailing edge thickness, 15 airfoil = 0.94 mm (0.037 in.)

(0.71 mm) x 20/15 = 0.94 mm

Pullability of the gas passage between airfoils was assessed by layout of adjacent airfoil sections. Inspection indicated no overlapping or locking sections, so the airfoil geometry meets the pullability requirement.

Vibration stiffness is a design goal for the ceramic airfoil. This means sufficient stiffness to place the airfoil natural modes remote from vane passage interference (potential response) in the engine operating range. Shown in Figure 26 is the 3-D FEM of the 20-blade airfoil. Using this model, the airfoil natural frequencies and mode shapes were calculated for SiC and Si_3N_4 materials. The results are presented as frequency-speed (Campbell) diagrams in Figures 27 and 28.

Table X.
ATTAP axial gasifier rotor matrix.

Vendor	No. of airfoils	Trailing edge thickness --mm (in.)	Material	Molding process	Vendor proof spin	Part No.
GE *	20	0.71 (0.028)	beta-SiC	injection mold	No	5-67345
CBO	20	0.71 (0.028)	alpha-SiC	injection mold	No	5-80502
CBO	15	0.94 (0.037)	alpha-SiC	injection mold	No	5-80501
GTE	15	0.94 (0.037)	Si_3N_4(PY6)	injection mold	No	5-80503
Kyocera**	20	0.71 (0.028)	Si_3N_4(SN252)	slip cast	Yes 80k rpm	5-67200

*GM-funded, outside ATTAP
**Parts buy basis

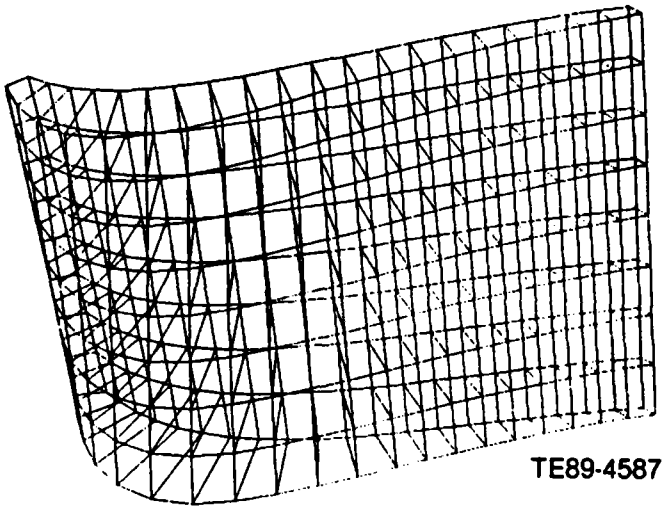

Figure 26. 3-D FEM of 20-blade ceramic gasifier airfoil.

There are no predicted interferences in the operating range for either case. However, note that the analyses considered 20 vanes for the SiC case (Figure 27) and 14 for the Si_3N_4. The existing metal nozzle consists of 20 vanes, and a 14-vane configuration was selected for the 1371°C (2500°F) ceramic nozzle. The 14-vane nozzle provides substantial margin of the first mode for both rotor materials. The 15-airfoil rotor provides an even greater margin of safety for potential interference response by virtue of shifting all modes to higher frequencies.

The previously developed (as background data to AT-TAP) AGT-5 interference fit rotor/shaft joining scheme has been successfully demonstrated to 1204°C (2200°F) rotor inlet temperature (RIT). Analyses support the application of the scheme at the RPD design point.

Structural analyses of the ceramic gasifier rotor were conducted. Two-dimensional body-of-revolution FEMs were developed for the 20- and 15-airfoil rotors. These are shown in Figures 29 and 30, respectively. The basic finite element is a 20-node, body-of-revolution element capable of modeling very sharp (rapid) strain gradients. The matrix of cases analyzed for temperature and stress gradients, probability of survival, and compressor shaft attachment integrity are shown in Figure 31.

The envelope of conditions analyzed on a fast fracture basis are:

- o cold proof spin, casting
- o rotor/metal shaft interference fit assembly
- o steady-state engine operation--rotor and shaft
  - o idle
  - o max power
- o transient--rotor and shaft
  - o cold start/snap accel
  - o decel
  - o shutdown and soak back

The following discussion pertains to the 20-airfoil design. The results for the Si_3N_4 material rotor are presented first, followed by the SiC material. The material unit strengths used in the analyses are listed in Table XI, and these values are for an oxidized condition (both materials).

The overall results can be briefly summarized as follows:

- o considering the fast fracture analysis basis
  - o PY6 grade Si_3N_4 rotor meets the design goal POS (0.9797)
  - o alpha-SiC rotor does not meet the design goal and structural redesign is required
  - o interference fit shaft attachment is satisfactory, both materials

Figures 32 through 36 present the finite element analysis for the various cases.

The results of the analysis for the interference fit clamp load study are shown in Table XII.

A summary of POS calculations is shown in Table XIII. Redesign of the alpha-SiC material gasifier rotor is planned for 1989.

Table XI.
Material unit strength spin test analyses.

Unit strength, oxidized surface

	Si_3N_4	SiC
σos--MPa/mm^2 (ksi/in.^{2})	1079.7* (82.0) 798.8** (60.0)	660.8 (53.0)
m_s	10.0	10.92
σov--MPa/mm^3 (ksi/in.^{3})	1000.8 (55.0)	686.5 (32.3)
m_v	10.0	8.62

Symbols

- σos Weibull unit characteristic strength, surface flaw strength distribution
- m_s Weibull modulus, surface flaw strength distribution
- σov Weibull unit characteristic strength, volume flaw strength distribution
- m_v Weibull modulus, volume flaw strength distribution

* machined surface
**as-cast surface

Table XII.
Analytic results, 2-D analyses.

G.T. ceramic rotor/metal compressor shaft

	Interference fit clamp load--kg (lb)	
Operating condition	alpha-SiC	PY6 Si_3N_4
Rotor/shaft assembly, cold	14,198 (31,300)	14,515 (32,000)
Max power, steady-state	6,713 (14,800)	8,301 (18,300)
Max transient	11,748 (25,900)	10,886 (24,000)

Table XIII.
Analytic results, POS, 2-D analyses, G.T. rotor.

Design goal POS = 0.9797

Engine operation point	POS/location alpha-SiC	PY6 Si_3N_4
Max power, steady-state	0.461/web	0.972/stub shaft fillet
Max transient	0.0/web	0.995/stub shaft fillet

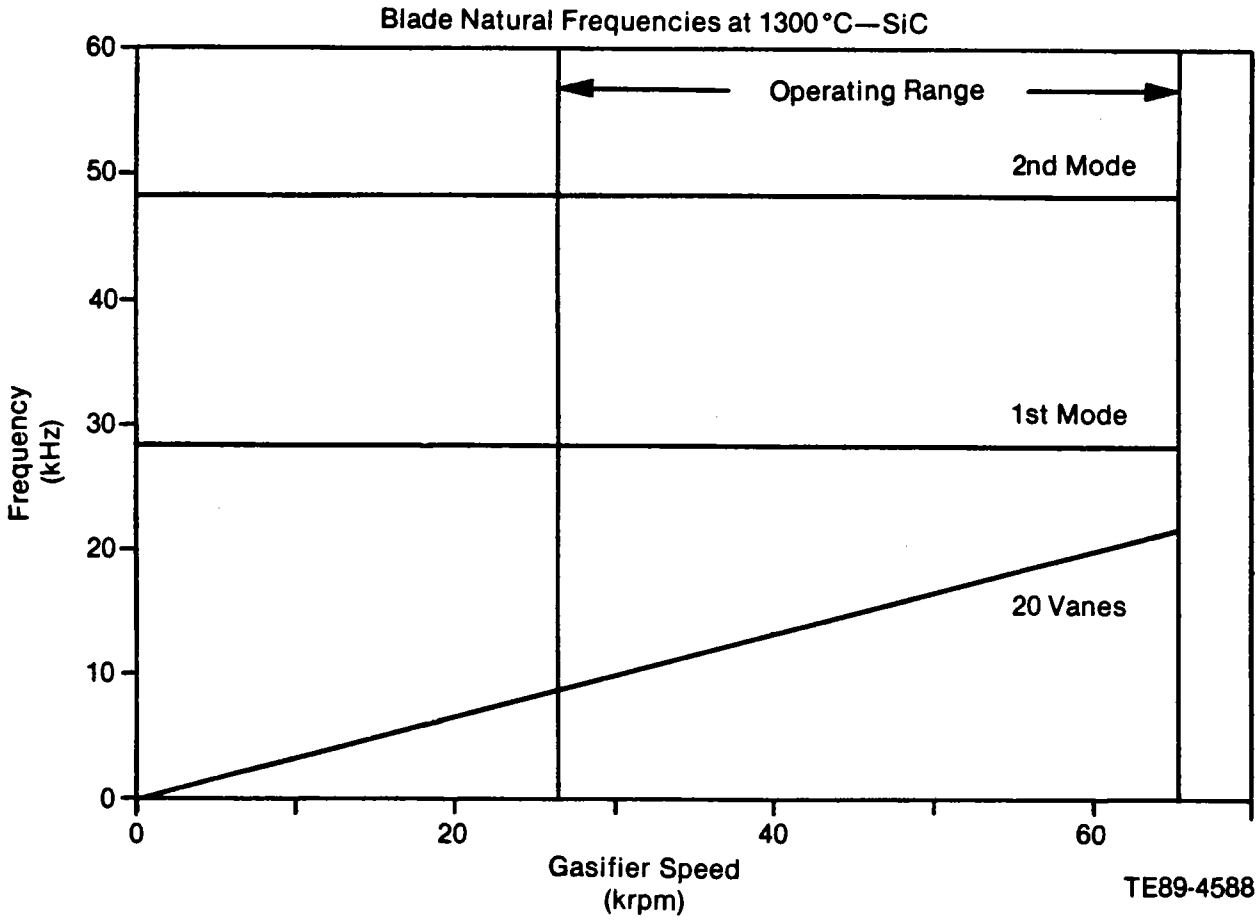

Figure 27. Frequency-speed interference diagram, 20-airfoil SiC gasifier rotor.

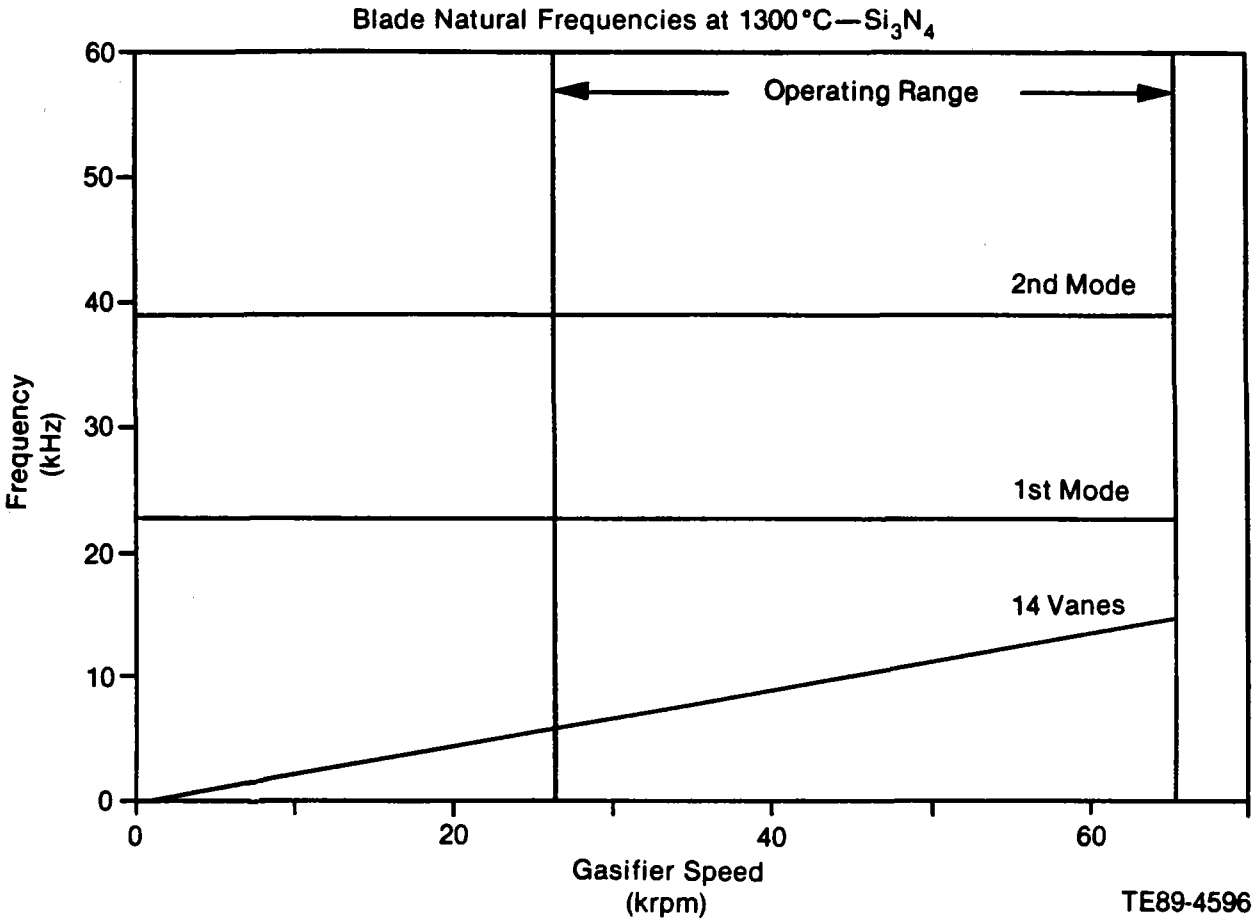

Figure 28. Frequency-speed interference diagram, 20-airfoil Si_3N_4 gasifier rotor.

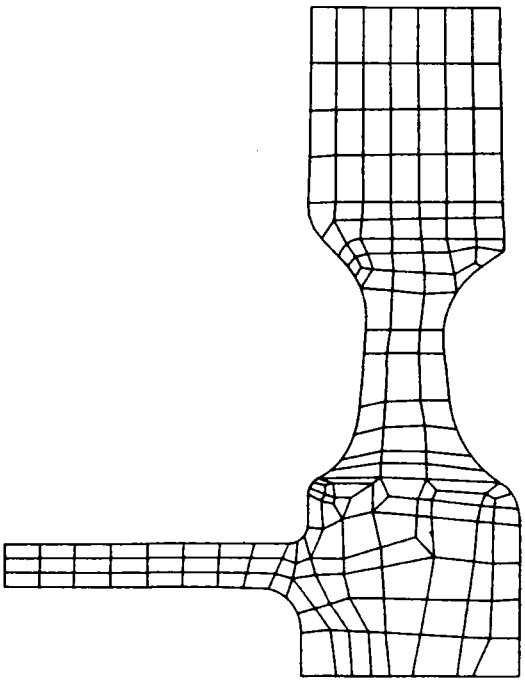

TE89-4597

Figure 29. FEM model of 20-airfoil ceramic gasifier rotor, as-cast configuration.

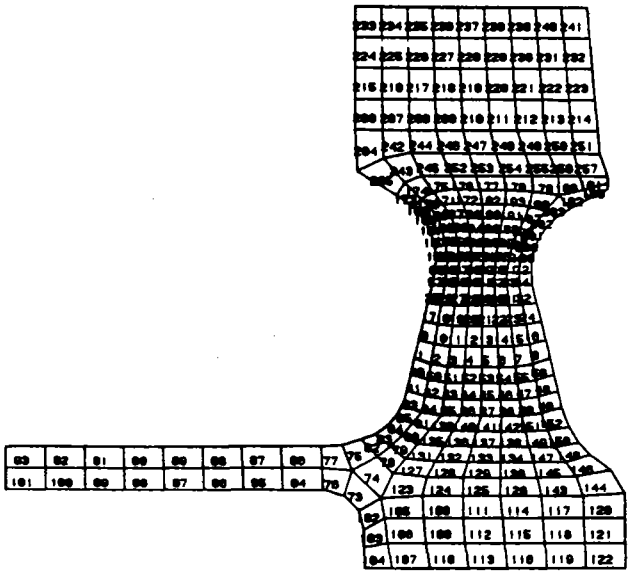

TE89-4598

Figure 30. FEM model of 15-airfoil ceramic gasifier rotor, as-cast configuration.

Material	SiC	Si_3N_4
No. airfoils	15 20	15 20

TE89-4676

Figure 31. Matrix of cases analyzed.

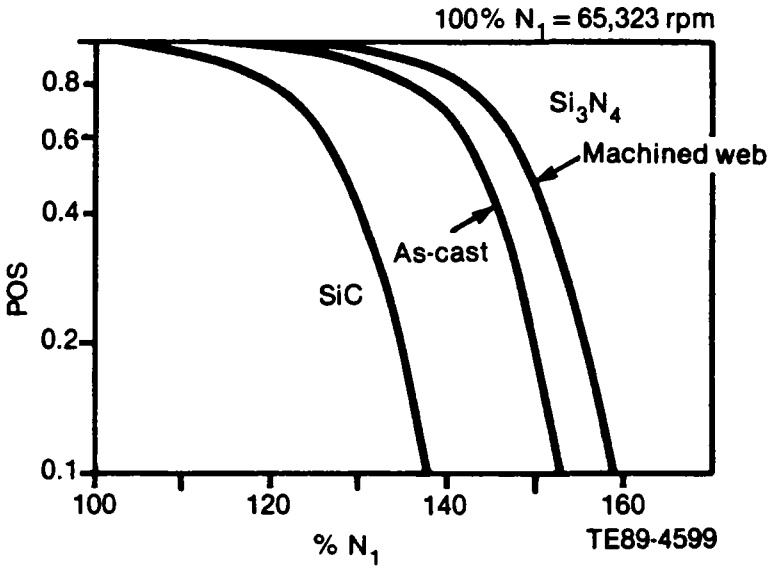

Figure 32. Room temperature spin test analyses, 20-airfoil gasifier rotor.

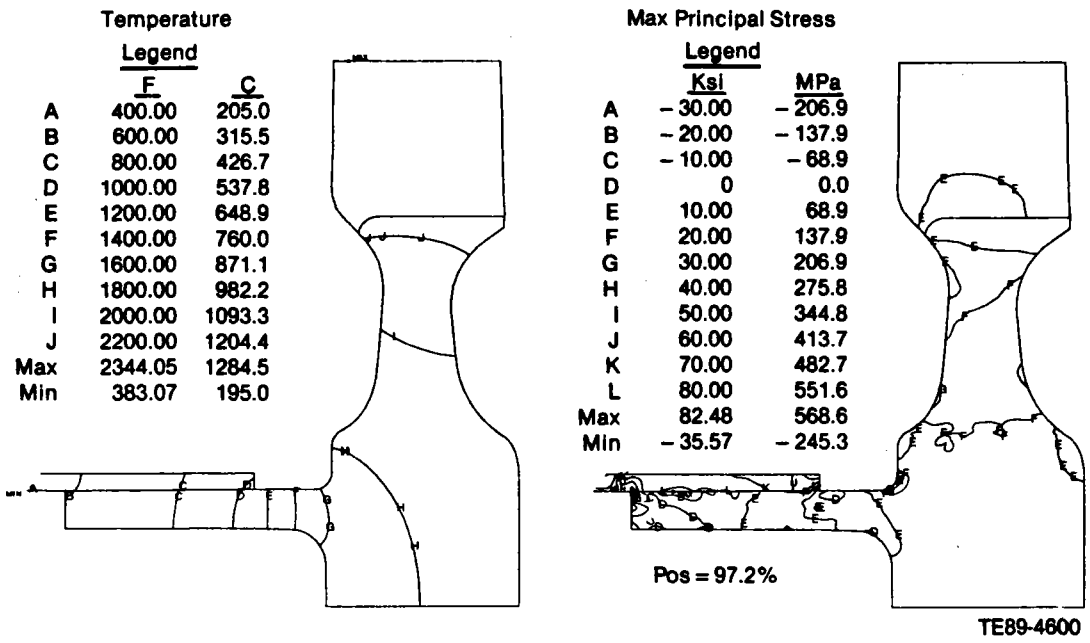

Figure 33. Max power, steady-state, 20-airfoil gasifier rotor, PY6 Si_3N_4.

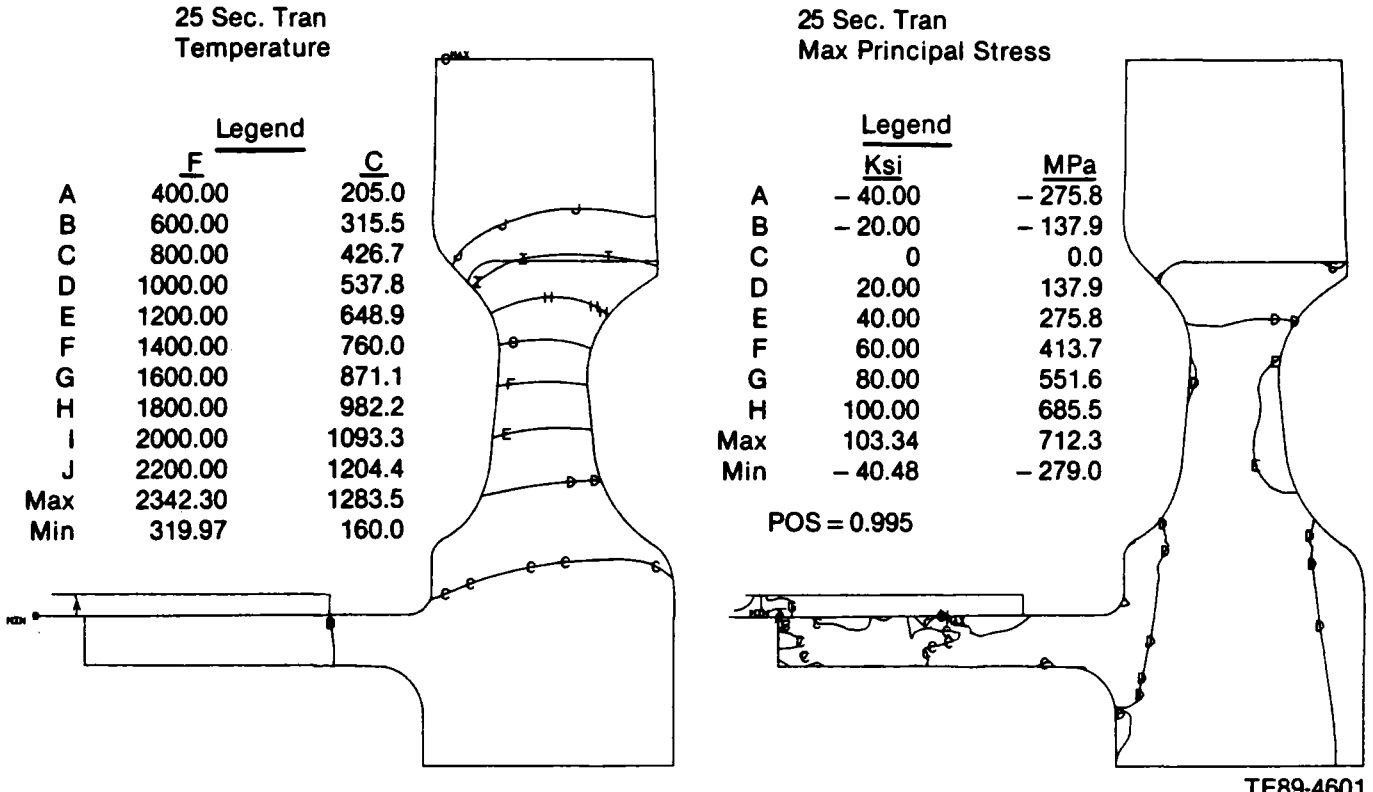

Figure 34. Max transient, 20-airfoil gasifier rotor, PY6 Si_3N_4.

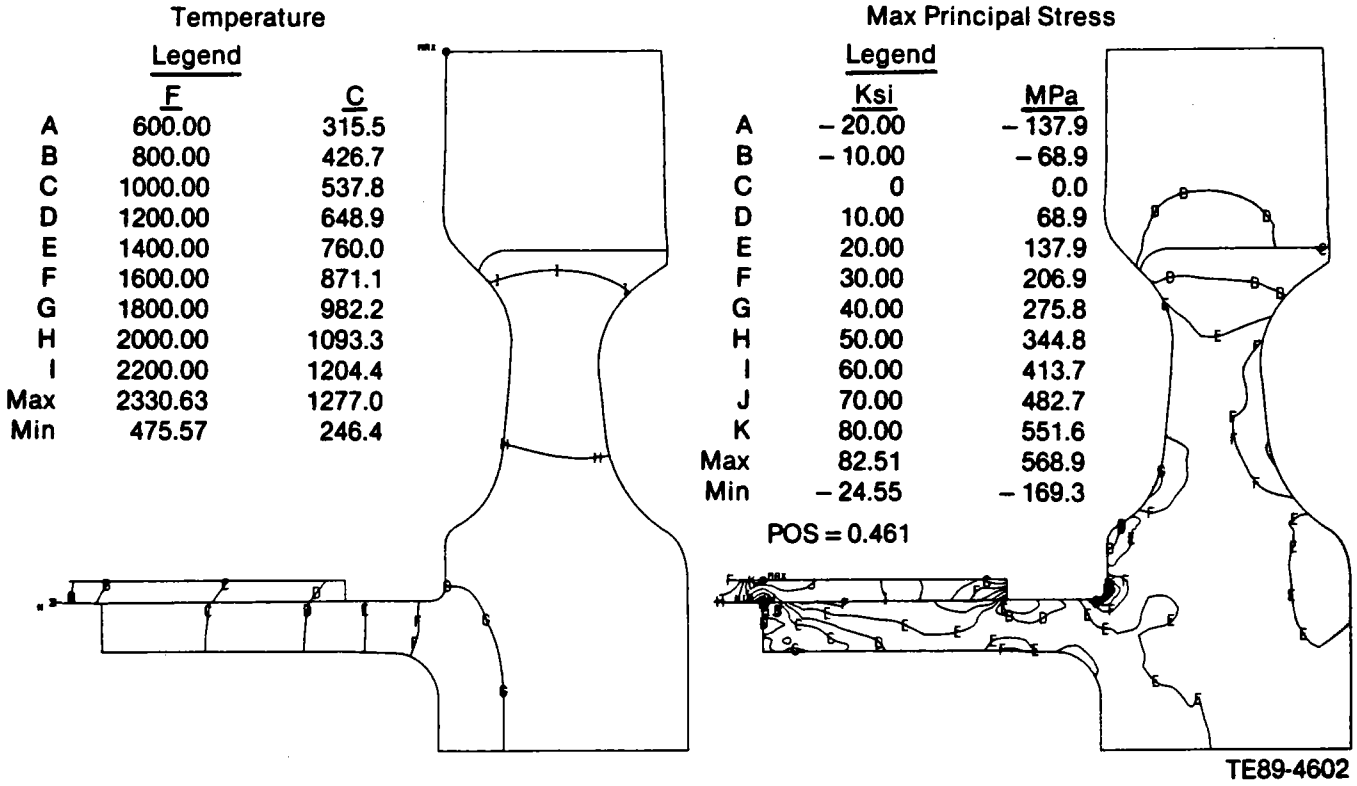

Figure 35. Max power, steady-state, 20-airfoil gasifier rotor, alpha-SiC.

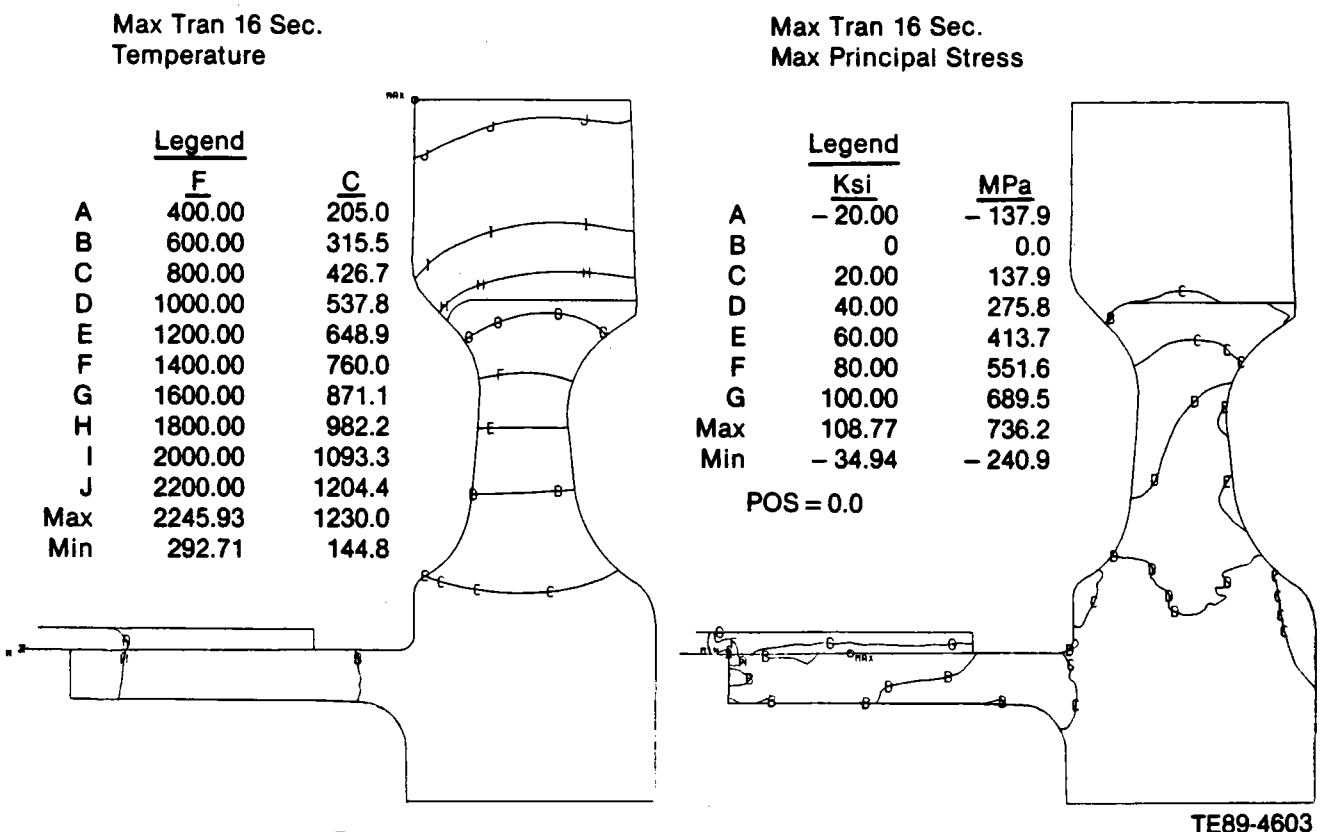

Figure 36. Max transient, 20-airfoil gasifier rotor, alpha-SiC.

III. MATERIALS CHARACTERIZATION AND CERAMIC COMPONENT FABRICATION

The materials characterization and ceramic component fabrication sections review the ongoing ceramic material and component characterization and development activities that are a focus of the ATTAP program. The ceramic materials subsection documents the results of characterization and qualification of candidate ceramic materials and components being developed for advanced gas turbine engines, including characterizations of material properties (fracture strength, microstructure, fracture toughness), results of failure analysis of rig/engine tested components, and nondestructive evaluation results. The ceramic component fabrication subsection reviews the ongoing ceramic component process development activities at the selected ceramic suppliers, including Carborundum, Manville, GTE Laboratories, Corning Glass Works, Garrett Ceramic Components Division, Ceramics Process Systems, Drexel University, and Textron Aerospace Development Center. Allison's approach to ceramic component development continues to be one of subcontracting process development to the domestic ceramic manufacturing community and working in an iterative development loop with those suppliers in areas of component design, characterization, and rig/engine data feedback. While basic ceramic materials development is not a part of the ATTAP program, the program integrates material developments from Oak Ridge programs, supplier in-house activities, and other sources as they become available for component fabrication efforts.

3.1 MATERIALS AND COMPONENT CHARACTERIZATION

3.1.1 Material Properties and Microstructure

Objective/Approach

The materials and component characterization efforts have focused on the testing and evaluation of candidate ceramic materials and components being developed for use in the ATTAP AGT-5 automotive gas turbine engine. The primary objective of this task is to establish appropriate material characteristics to support the design, development, and testing of hot section ceramic components. A secondary objective is to evaluate new candidate ceramic materials and suppliers and to assess which, if any, should be used in specific component development activities. The material characterization activities have focused on microstructural, density, fracture toughness, and fast fracture strength examinations of candidate ceramic materials. Fracture surface analysis was also used to determine the nature and location of the strength-controlling defects. In addition, the time-dependent strength characteristics and oxidation resistance were evaluated for selected materials.

Accomplishments

The ceramic materials that were characterized include the following:

- Alcoa sintered beta-SiC
- Garrett Ceramic Components Division GN-10 Si_3N_4
- GTE Laboratories AY6 Si_3N_4
- GTE Laboratories PY6 Si_3N_4
- Kyocera SC221 sintered beta-SiC
- Ceramics Process Systems JW-15 Si_3N_4 rotors
- Kyocera SN251 Si_3N_4 radial turbine rotors
- Kyocera SN252 Si_3N_4 axial turbine rotors

Alcoa Sintered Beta-Silicon Carbide. The Alcoa material consisted of sintered beta-SiC isostatically pressed at a pressure of 137.9 MPa (20 ksi). The SiC powder was produced by Alcoa using a plasma process with a powder surface area of 9.2 m^2/g. The average density of this material was 3.135 g/cm^3 (97.7% theoretical density).

The fast fracture strength characteristics of the Alcoa SiC material were evaluated at room temperature, 1250°C (2282°F), and 1371°C (2500°F). The results of this testing are summarized in Table XIV. All of the bars were tested with a machined tensile surface condition. The average room temperature flexural strength was 417.70 MPa (60.58 ksi) with a Weibull modulus of 10.0. The typical strength-controlling defects were observed to be small pores, as shown in Figure 37. The average strength measured 400.12 MPa (58.03 ksi) at 1250°C and 434.11 MPa (62.96 ksi) at 1371°C. Surface and internal porosity was observed as the primary fracture origin, as shown in Figure 38. The room temperature fracture toughness (K_{IC}) of the Alcoa sintered beta-SiC material measured 3.0 MPa-$m^{1/2}$, determined using the single edge notched beam (SENB) method.

Garrett Ceramic Components Division (GCCD). The GCCD material was GN-10 Si_3N_4, fabricated by cold isostatic pressing followed by hot isostatic pressing (HIP). The microstructure of this material, shown in Figure 39, consists of a mixture of

Table XIV.
Strength characteristics of Alcoa sintered beta-SiC.

Temperature--°C (°F)	Strength--MPa (ksi)
25 (77)	417.70 (60.58)
1250 (2282)	400.12 (58.03)
1371 (2500)	434.11 (62.96)

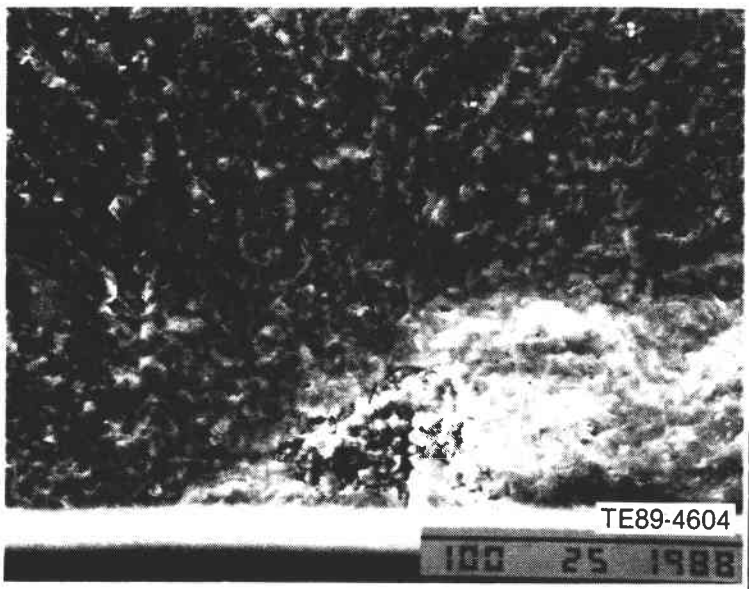

Figure 37. Typical fracture origin (surface pore) observed in Alcoa sintered beta-SiC bars tested at room temperature.

relatively large (5-10 micron) tabular Si_3N_4 grains in conjunction with small equiaxed submicron Si_3N_4 grains. Chemical analysis indicated that yttria (Y_2O_3) is the primary sintering additive. The average density of this material measured 3.31 g/cm^3 (99.5% theoretical).

Test bars were evaluated to determine the fast fracture material strength characteristics. All specimens were tested with a longitudinally ground tensile surface condition. The flexural strength test results are summarized in Table XV. The average room temperature strength was 753.62 MPa (109.30 ksi) with a Weibull modulus of 8.7. The primary fracture origins were small surface flaws and/or low density regions, as shown in Figure 40. The secondary fracture origins (see Figure 41) were identified as relatively large (50-100 micron diameter) metallic inclusions, composed primarily of iron with traces of chromium. The typical strength-controlling defects observed in the specimens tested at elevated temperature were similar to those found in the room temperature tests, i.e., surface flaws and metallic inclusions. The room tempera-

Table XV.
Strength characteristics of GCCD GN-10 Si_3N_4.

Temperature--°C (°F)	Strength--MPa (ksi)
25 (77)	753.62 (109.30)
1000 (1832)	703.22 (101.99)
1150 (2102)	670.13 (97.19)
1250 (2282)	629.79 (91.34)
1371 (2500)	599.18 (86.90)

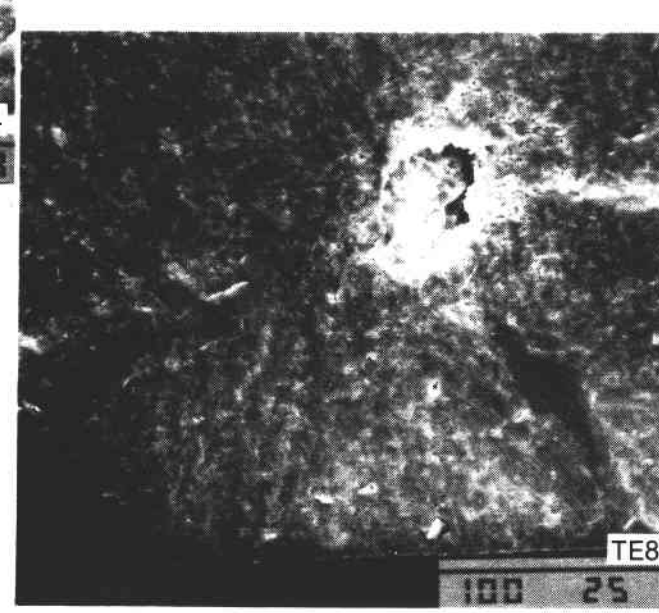

Figure 38. Typical fracture origin (internal pore) observed in Alcoa sintered beta-SiC tested at elevated temperature.

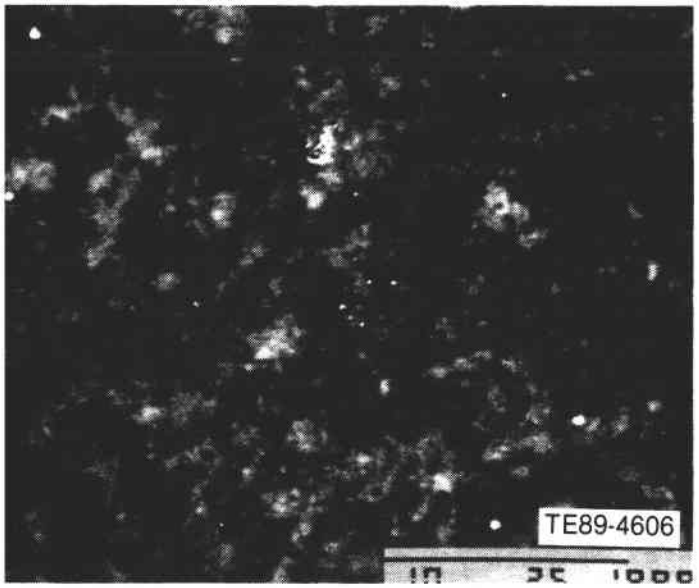

Figure 39. Microstructure of GCCD isopressed and HIP processed GN-10 Si_3N_4.

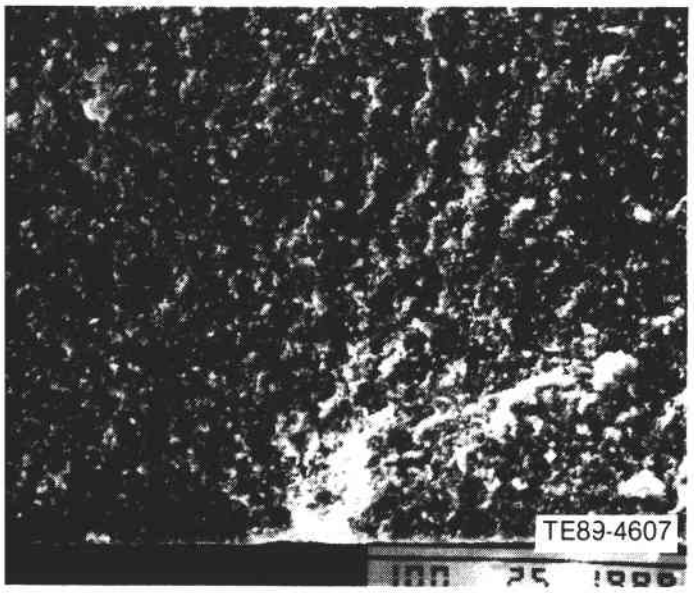

Figure 40. Typical fracture origin (surface low density region) observed in GCCD GN-10 Si_3N_4.

ture fracture toughness (K_{IC}) of the GCCD GN-10 Si_3N_4 material measured 5.9 MPa-$m^{1/2}$, determined using the SENB method.

GTE Laboratories AY6 Silicon Nitride. GTE's AY6 Si_3N_4, containing 6% Y_2O_3 and 2% Al_2O_3 as sintering additives, was produced using Ube Si_3N_4 powder and the new processing facilities at the GTE Labs Prototype Engineering Center. The test bars were fabricated by injection molding and hot isostatic pressing. All specimens were tested with a machined

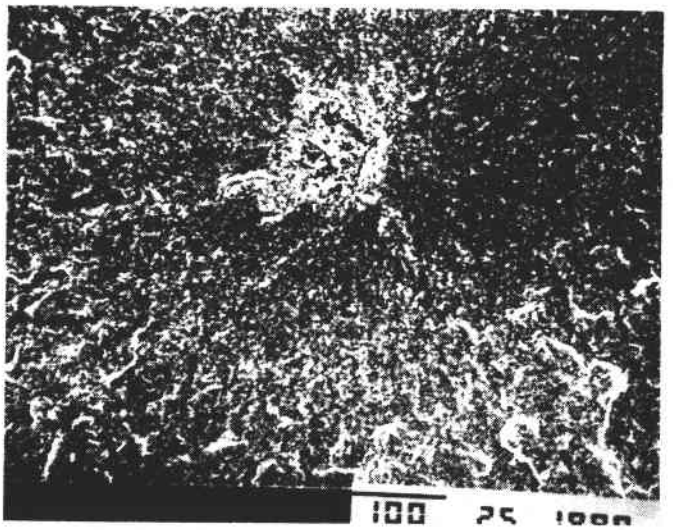

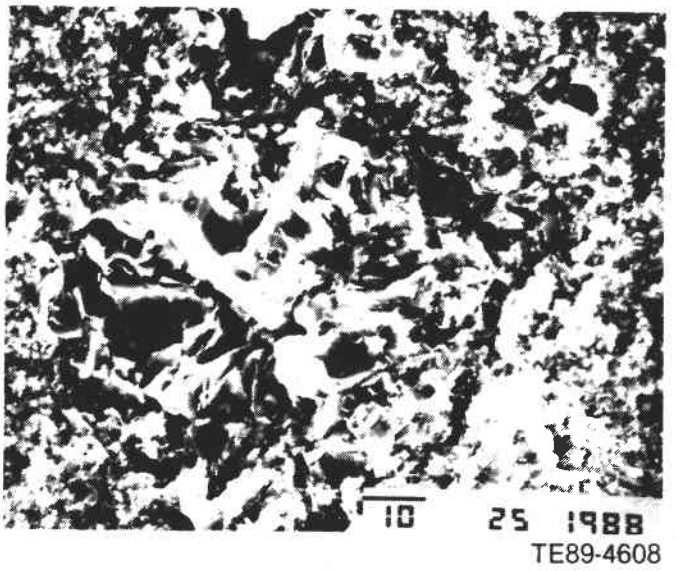

Figure 41. Secondary fracture origin (metallic inclusion) observed in GCCD GN-10 Si_3N_4.

tensile surface condition. The average density measured 3.249 g/cm^3 (99.6% theoretical density).

The flexural strength characteristics of the AY6 Si_3N_4 material are summarized in Table XVI. The primary fracture origins observed in the AY6 Si_3N_4 specimens were small surface flaws, as shown in Figure 42. Several specimens had fractures initiating from small surface and internal pores, as shown in Figure 43. Although the new AY6 Si_3N_4 material produced using Ube powder has the same chemical composition as prior AY6 Si_3N_4 produced using SN502 powder, both the strength characteristics and oxidation behavior of the recent material exhibited dramatic improvements. Earlier AY6 Si_3N_4 demonstrated significant oxidation

Table XVI.
Strength characteristics of GTE Labs injection molded and HIP processed AY6 Si_3N_4 (Ube powder).

Temperature--°C (°F)	Strength--MPa (ksi)
25 (77)	1021.49 (148.15)
1250 (2282)	554.36 (80.40)
1371 (2500)	603.31 (87.50)

Table XVII.
Strength characteristics of GTE Labs injection molded and HIP processed PY6 Si_3N_4 (Ube powder).

Temperature--°C (°F)	Strength--MPa (ksi)
25 (77)	937.65 (135.99)
1000 (1832)	835.33 (121.15)
1250 (2282)	585.80 (84.96)
1371 (2500)	556.29 (80.68)

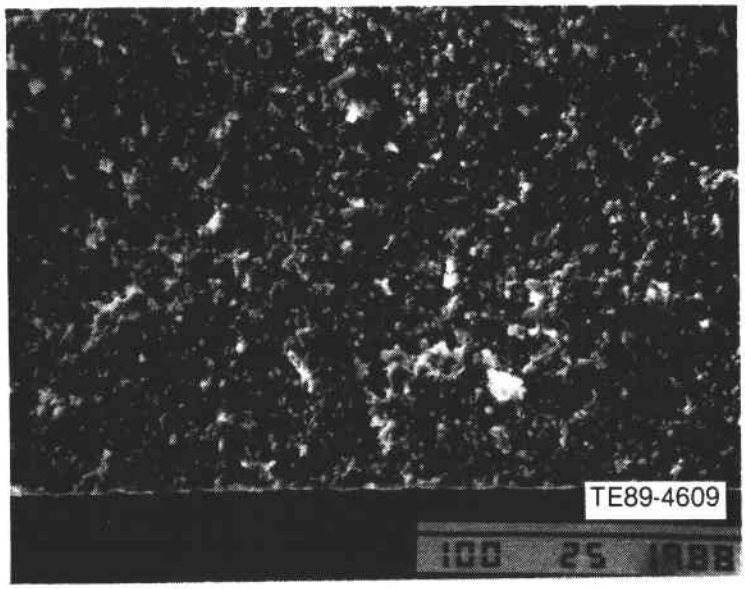

Figure 42. Typical strength-controlling features (surface flaw) observed in GTE Labs AY6 Si_3N_4.

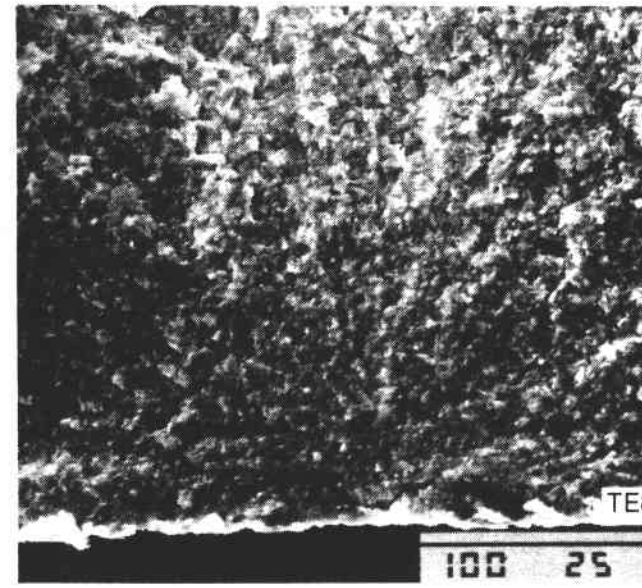

Figure 43. Fracture origin (small internal pore) observed in GTE Labs AY6 Si_3N_4.

and strength degradation when tested in fast fracture at a temperature of 1250°C (2282°F), while the Ube AY6 Si_3N_4 showed little or no oxidation in tests conducted at a temperature of 1371°C (2500°F).

GTE Laboratories PY6 Silicon Nitride. GTE's PY6 Si_3N_4 was produced using Ube Si_3N_4 powder and the new processing facilities at the GTE Labs Prototype Engineering Center. The test bars were fabricated by injection molding and hot isostatic pressing. All specimens were tested with a machined tensile surface condition. The average density measured 3.264 g/cm^3 (99.9% theoretical density).

The flexural strength characteristics of the PY6 Si_3N_4 material are summarized in Table XVII. The typical fracture origins in all specimens were small surface flaws, as shown in Figure 44. Additional testing of this material is planned for 1989, including time-dependen property determination, fracture toughness, and a evaluation of the strength characteristics of the as fired (as-HIP processed) surfaces.

Kyocera SC221 Sintered SiC. Kyocera's SC22 is a sintered beta-SiC, produced using plasma-derive beta-SiC powder. This material is in the developmen tal process at Kyocera and is currently available onl in test bar form. The test specimens were fabricate by isostatic pressing. The average density of thi material was 3.115 g/cm^3 (97% theoretical density).

The strength characteristics of this material are sum marized in Table XVIII. All specimens were tested wit a machined tensile surface condition. The averag room temperature flexure strength measured 425.2 MPa (61.67 ksi) with an associated Weibull modulus c 22.9. This strength level was basically unchanged u

Table XVIII.
Strength characteristics of Kyocera SC221 SiC.

Temperature-- °C (°F)	Strength--MPa (ksi)
25 (77)	425.21 (61.67)
1000 (1832)	404.05 (58.60)
1150 (2102)	419.97 (60.91)
1250 (2282)	402.12 (58.32)
1371 (2500)	423.42 (61.41)

to a test temperature of 1371 °C (2500 °F). In all instances, fracture originated from small internal and surface pores, as shown in Figure 45. The room temperature fracture toughness of the Kyocera SC221 SiC material was 2.6 MPa-$m^{1/2}$, measured using the SENB test method.

Ceramics Process Systems. The material used for initial rotor fabrication was CPS's JW-15 Si_3N_4 composition. The rotors were fabricated using the Quickset injection molding process, a low pressure system developed by CPS with a colloidal solidification mechanism that does not utilize a plastic binder system. As a result of an initial 5-month development

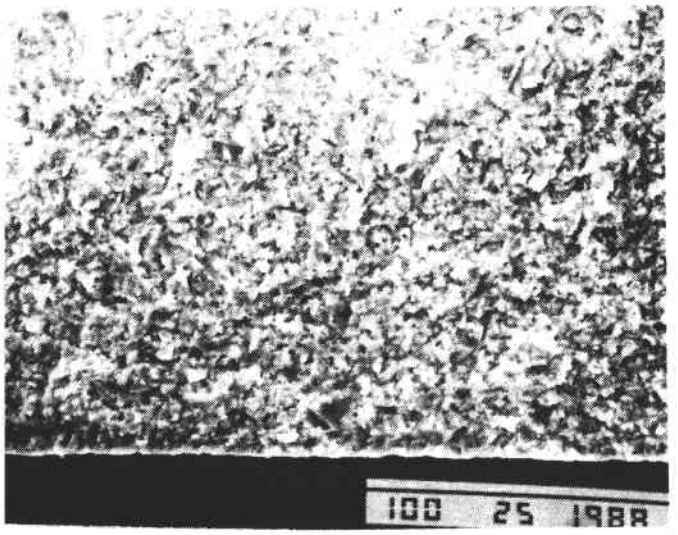

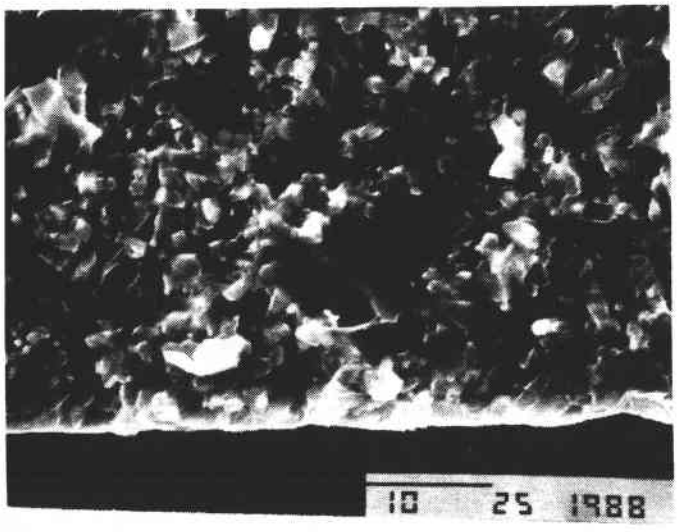

TE89-4611

Figure 44. Typical fracture origin (surface flaw) observed in GTE Labs injection molded and HIP processed PY6 Si_3N_4 test bars.

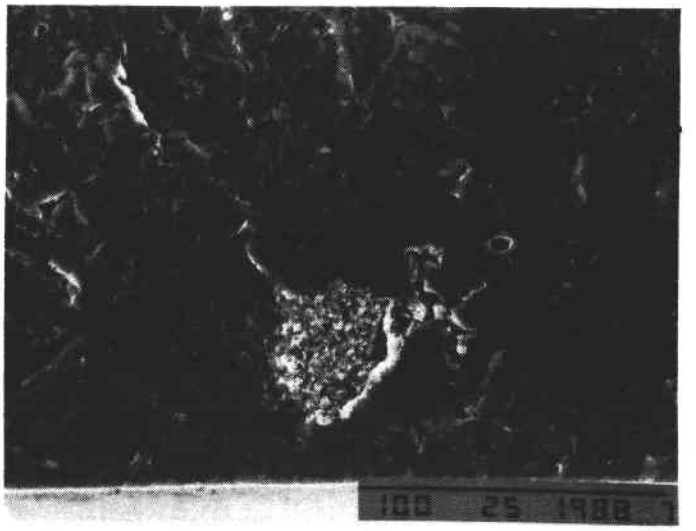

TE89-4612

Figure 45. Typical fracture origins (internal porosity) observed in Kyocera SC221 SiC.

program, six rotors were delivered to Allison for evaluation. Test bars were sectioned from one of the rotors for mechanical property determination. The average density of the rotor measured 3.23 g/cm^3 (96.5% theoretical density).

All of the rotor test bars were evaluated with a machined surface condition. The average room temperature flexural strength was 468.52 MPa (67.95 ksi). With the exception of a single low strength specimen, which failed at a stress of 37.23 MPa (5.4 ksi), the test bars failed at strengths ranging from 420 MPa to 717 MPa (61 to 104 ksi). The typical strength-controlling fracture origins were surface and internal porosity, as shown in Figure 46. The low strength bar fractured from a large surface pore, shown in Figure 47, approximately 2 mm (0.08 in.) in diameter.

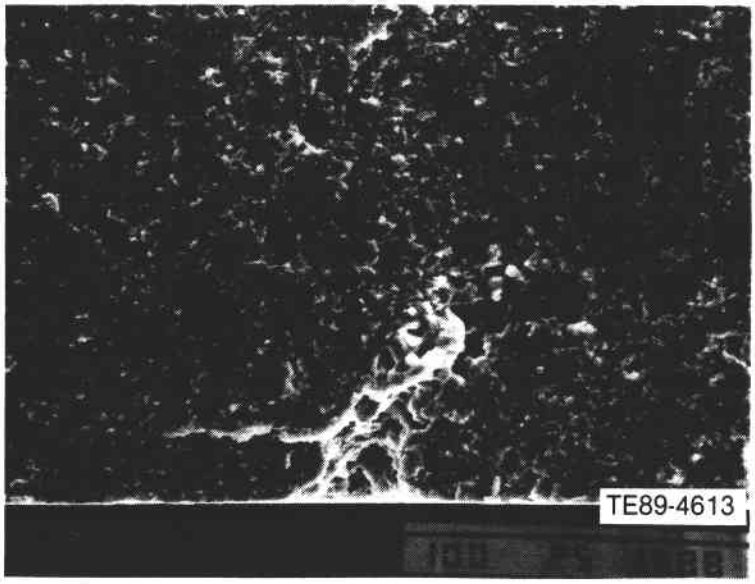

Figure 46. Typical fracture origin (surface pore) observed in CPS JW-15 Si_3N_4 rotor bars.

Kyocera SN251 Rotors. Six AGT100 rotors were on hand from Kyocera; the rotors were fabricated of slip cast SN251 sintered Si_3N_4. These rotors were of the thickened inducer blade design and configured for an interference fit shaft attachment. Each rotor was proof spin tested by Kyocera at room temperature to 112,000 rpm (130% design speed). The SN251 Si_3N_4 material was intended as an improvement/replacement for the SN250M Si_3N_4 components. Previous evaluations at Allison and Garrett had identified deficiencies in elevated temperature strength and time-dependent properties in test bars sectioned from SN250M rotors.

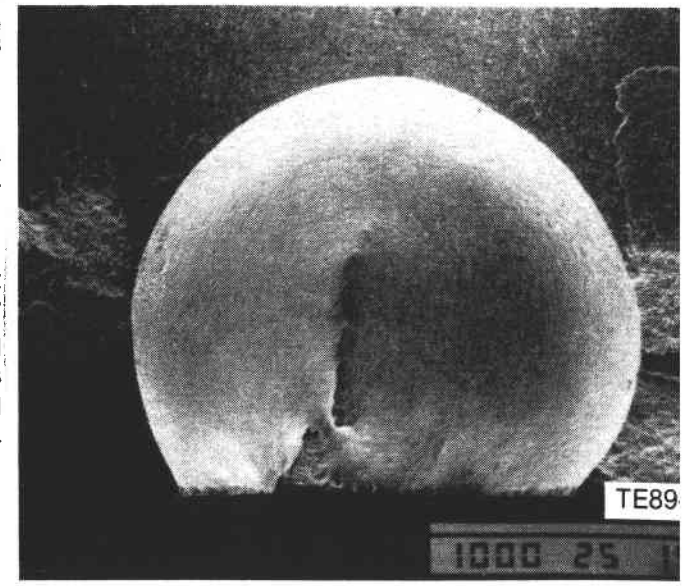

Figure 47. Large surface pore observed as fracture origin in low strength CPS rotor bar. Fracture stress was 37.23 MPa (5.4 ksi).

The microstructure of the SN251 material, shown i Figure 48, consists of relatively equiaxed Si_3N_4 grain interspersed with occasional long grains of bet Si_3N_4, which were 30-300 microns long with aspec ratios of greater than 20 to 1. Chemical analysis of th SN251 material conducted at NASA Lewis indicate that ytterbia (Yb_2O_3) was the primary sintering add tive. The average density of the rotors measure 3.402 g/cm^3 (approximately 97% theoretical density).

The material strength characteristics were evaluate by sectioning test bars from a Kyocera SN251 Si_3N gasifier turbine rotor (S/N 0001-2). The results of th flexural strength testing are summarized in Table XIX Also included are the results obtained from test bar sectioned from prior Kyocera SN250M Si_3N_4 an SN220M Si_3N_4 rotors. All bars were tested with a machined tensile surface condition. The typical roon temperature fracture origins were surface flaws as sociated with the large beta Si_3N_4 grains, as shown i Figure 49. Surface flaws were also observed to be th primary strength-controlling defects at elevated tem peratures (see Figure 50).

The material strength characteristics of test bars sec tioned from the SN251 Si_3N_4 rotors are superio (particularly at elevated temperature) to the strength obtained on SN220M and SN250M Si_3N_4 rotor bars.

Table XIX.
Fracture strength--MPa (ksi)--of test bars cut from Kyocera Si_3N_4 AGT100 gasifier turbine rotors.

Temperature--°C (°F)	SN220M	SN250M	SN251
25 (77)	754.52 (109.43)	622.07 (90.22)	646.27 (93.73)
1000 (1832)	476.10 (69.05)	388.26 (56.31)	523.68 (75.95)
1150 (2102)	369.30 (53.56)	377.16 (54.70)	---
1250 (2282)	---	---	447.90 (64.96)

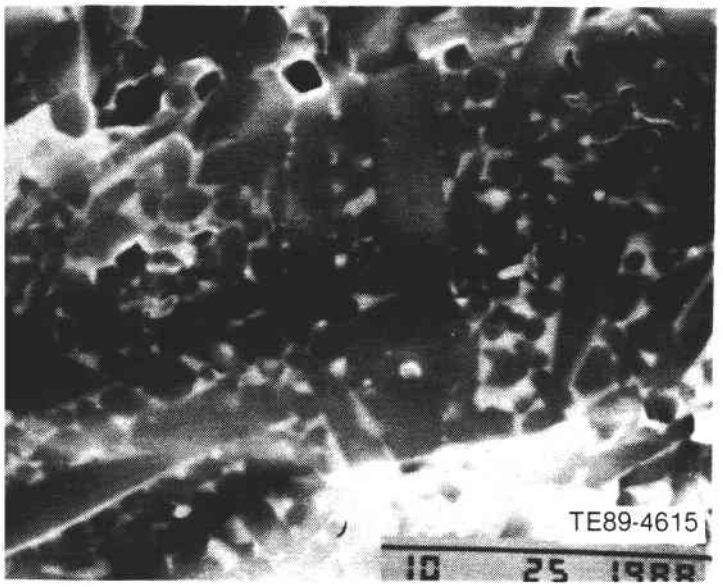

Figure 48. Microstructure of Kyocera SN251 Si_3N_4 gasifier turbine rotor.

Kyocera SN252 Silicon Nitride Rotors. To evaluate component strength characteristics, test bars were sectioned from a Kyocera SN252 Si_3N_4 AGT-5 15-bladed gasifier axial turbine rotor. This rotor (S/N 5K11) was fabricated of slip cast SN252 sintered reaction-bonded Si_3N_4 and had been proof spin tested at room temperature by Kyocera to 80,000 rpm (125% design speed). The average density of the test specimens was 3.329 g/cm^3 (99% theoretical density).

The strength characteristics of the rotor test bars are summarized in Table XX. All bars were tested with a machined tensile surface condition. The average fracture strength of specimens tested at room temperature measured 505.54 MPa (73.32 ksi). Following this testing, all specimens were heat treated using a Kyocera-recommended heat treat cycle of 1400°C (2552°F) in air for 1 hr prior to testing. This heat treat operation is used by Kyocera to form a thin silica layer on the SN252 and SN251 Si_3N_4 materials to prevent subsequent oxidation at lower temperatures and is recommended for all machined surfaces. The average fracture strength of oxidized specimens tested at room temperature was 600.49 MPa (87.09 ksi). Heat treated bars tested at a temperature of 1000°C (1832°F) had an average strength of 512.99 MPa (74.46 ksi), while bars tested at 1250°C (2282°F) had an average strength of 386.60 MPa (56.07 ksi). The typical fracture origins observed in all specimens were long (50-200 micron) needlelike Si_3N_4 grains. These strength-controlling features are shown in Figure 51. Based on the 20% strength increase observed in the heat treated specimens versus the as-machined specimens, all machined surfaces on Kyocera SN252 and SN251 Si_3N_4 will be subjected to the Kyocera-recommended oxidation cycle.

Table XX.
Strength characteristics of Kyocera SN252 Si_3N_4 AGT-5 rotor test bars.

Temperature--°C (°F)	Strength--MPa (ksi)
25 (77)	505.54 (73.32)
25* (77)	600.49 (87.09)
1000* (1832)	512.99 (74.46)
1250* (2282)	386.60 (56.07)

*Oxidized at 1400°C (2552°F) for 1 hr in air.

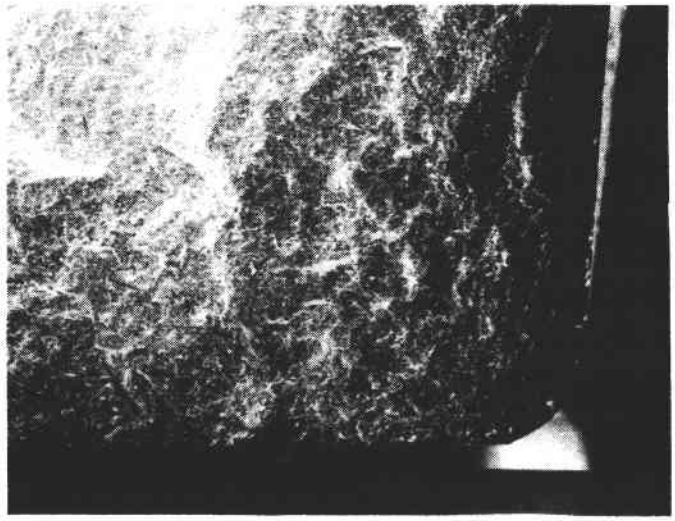

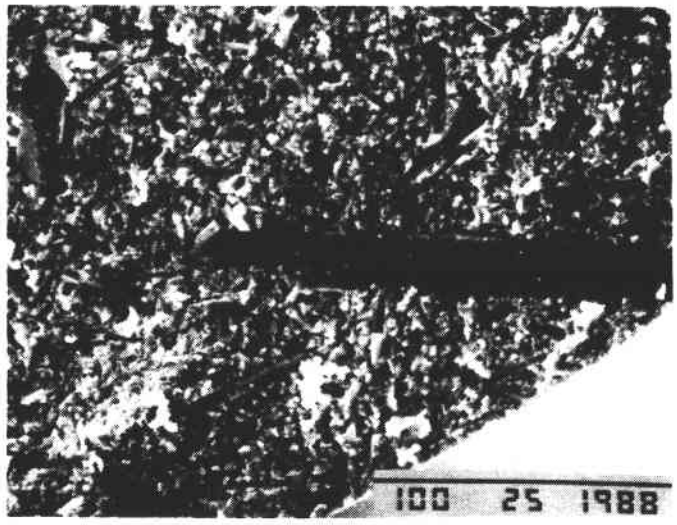

TE89-4616

Figure 49. Typical fracture origin (surface flaw with large beta Si_3N_4 grain) observed in Kyocera SN251 Si_3N_4 rotor bars tested at room temperature.

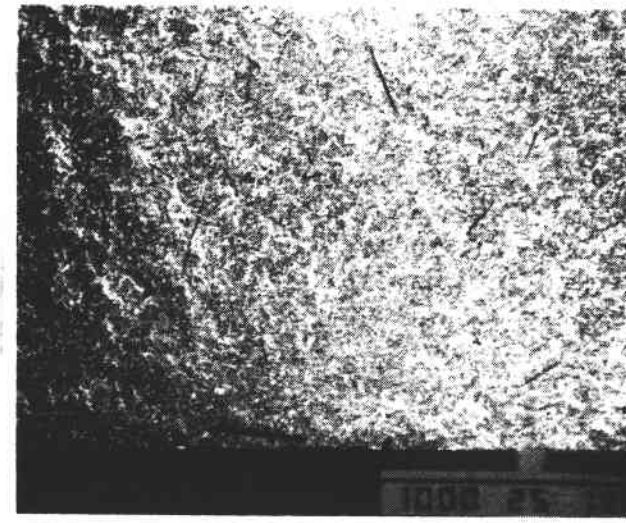

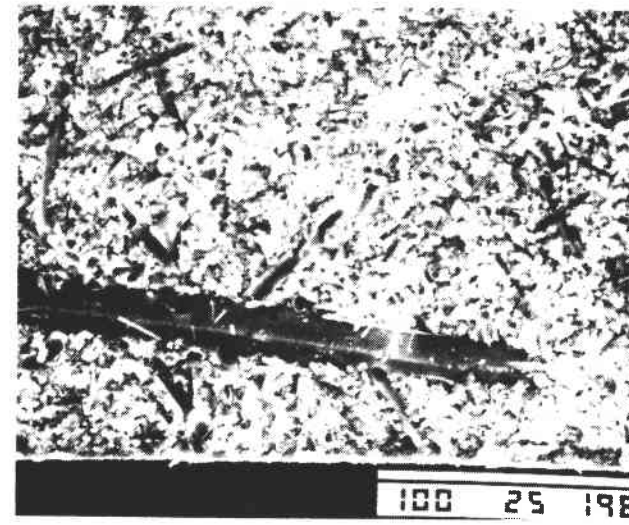

TE89-46

Figure 50. Typical fracture origin (surface flaw with large beta Si_3N_4 grain) observed in Kyocera SN251 Si_3N_4 rotor bars tested at elevated temperature.

3.1.3 Failure Analysis

Objective/Approach

The objective of this effort is to perform a failure analysis on ceramic components that experience damage during rig/engine testing and evaluation. Fractographic analysis is one of the most powerful tools for the failure analysis of an engine or rig tested component. A careful study of the general and detailed features of the topography of a fracture, by visual and by scanning electron microscopy (SEM), provides a wealth of information concerning the failure origin and the failure mode(s). Analysis of hardware failures allows the separation of design features fron material deficiencies, defects, or nonoptimum fabrica tion procedures and suggests the appropriate correc tive measures.

Accomplishments--Fractographic Failure Analysis of AGT100 Test Engine S/N 2, BU22

The all-ceramic gasifier turbine section of the AGT10(test engine (S/N 2, BU22) encountered failure durinç shutdown following the third test cycle at a tempera ture of 982°C (1800°F). For additional details of the engine testing, refer to subsection 1.1.1. Inspection o the engine revealed carbon buildup around the fuel

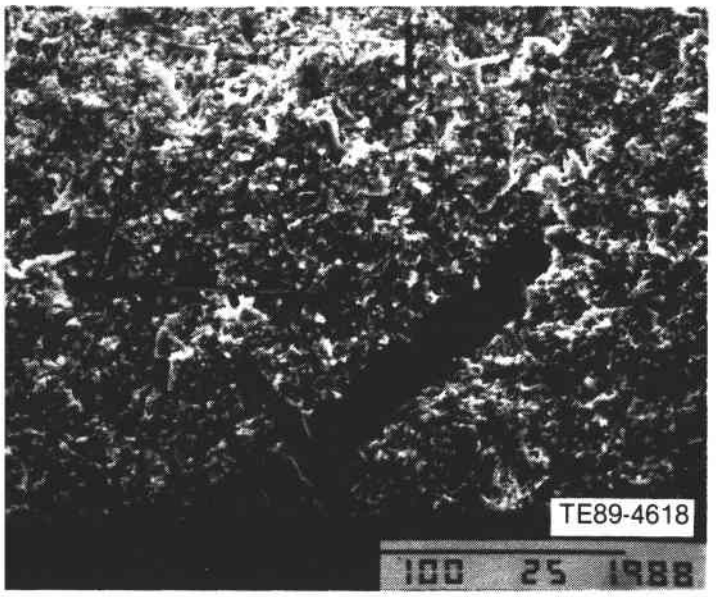

Figure 51. Typical fracture origin (large Si_3N_4 grain) observed in Kyocera SN252 Si_3N_4 rotor bars.

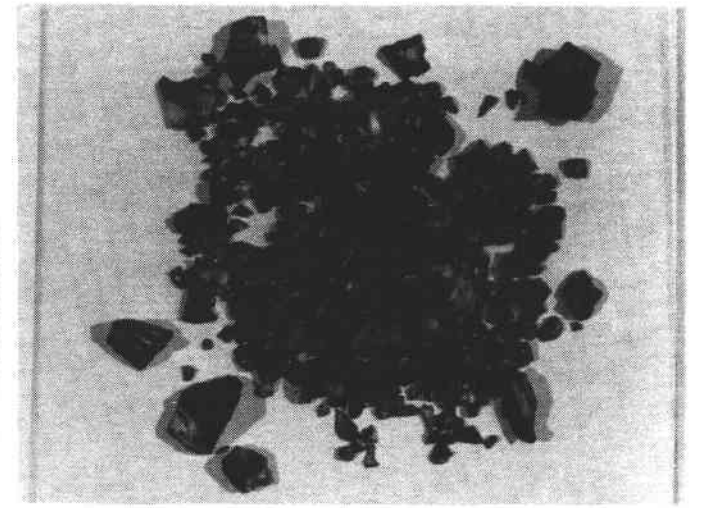

Figure 52. Remnants of S/N 2, BU22 gasifier turbine rotor.

nozzle and fractures occurring in all of the gasifier ceramic components. A fan or butterfly wing of carbon was loosely attached to one side of the nozzle. Located 180 deg across the nozzle from the carbon formation was a light mark indicating the presence of a similar carbon buildup that may have broken away during engine operation. The combustor body and dilution band had very minor damage (small nicks and chips) caused by the impact of fractured segments of the scroll. The regenerator disk suffered minor abrasion. Other ceramic components such as the interturbine coupling, combustor dome, pilot flame tube, and bulkhead showed no distress. Failure analysis was performed on the following failed gasifier section components: rotor, inner and outer backplates, vanes, and scroll.

Gasifier Turbine Rotor (P/N AA101477, S/N FX52308, Carborundum SiC, Total Part Time: 23:43 Hours). The SiC rotor fractured from the stub shaft and was shattered, as shown in Figure 52. A fracture origin could not be identified in these fragments. However, the stub shaft fracture surface was not damaged and a fracture origin was identified, as shown in Figure 53. Moving away from the origin (normal to the surface), the crack front changed direction and headed toward the hub of the rotor, probably branching at the middle of the rotor shaft. Two opposing gouges noted on the zircon insulation ring indicated that the rotor initially fractured at the stub shaft.

Figure 54 shows the details of the fracture origin. No apparent flaw was observed at the origin. The

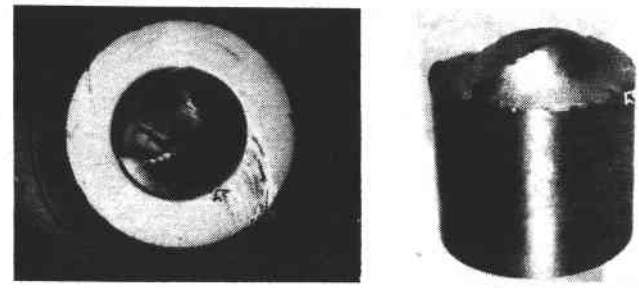

Figure 53. Broken gasifier rotor stub shaft with fracture origin indicated by arrows. Insulator and kennametal rings gouged (left), crack front propagation direction change (right).

smoothness of the fracture surface indicated a low stress type of fracture resulting from shock loading. The 138 MPa (20 ksi) fracture stress, calculated based on the radius of the fracture mirror, was much lower than the material strength of 380 MPa (55 ksi). It is probable that the rotor failure was due to foreign object damage (FOD) resulting from the carbon buildup on the combustor nozzle. When the inducer blade tips of the rotor hit the carbon, the thick airfoils did not fracture. Instead, the shock load was transmitted through the rotor and caused a fracture of the rotor shaft, with the rotor hub subsequently impacting the scroll shroud.

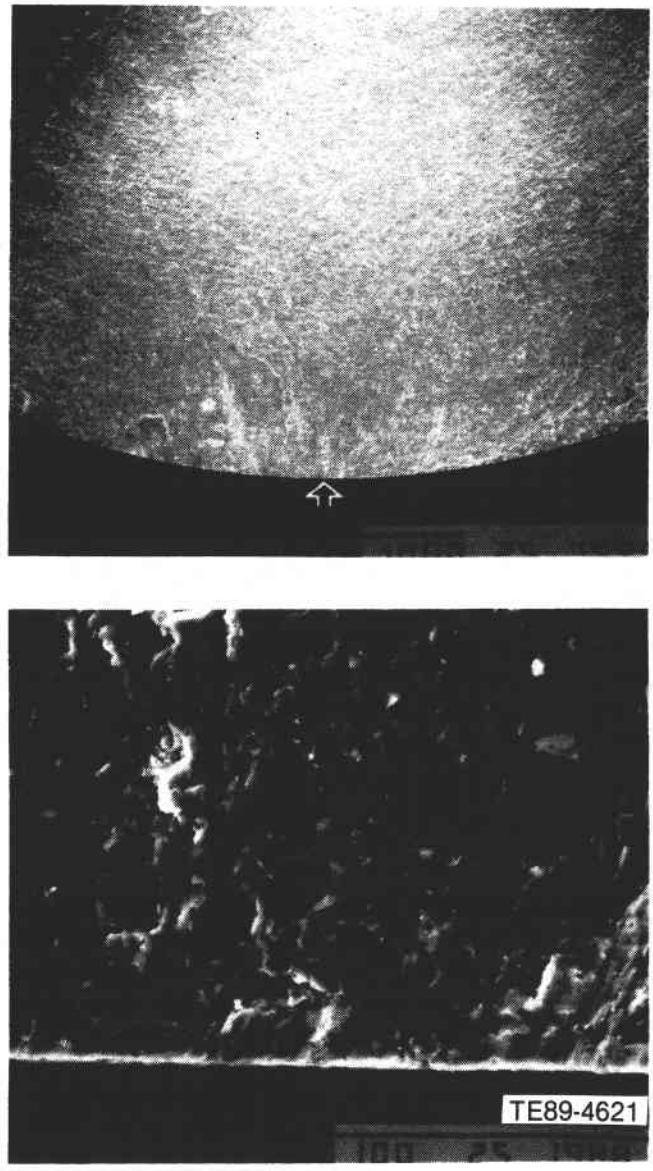

Figure 54. SEM fractographs of the rotor stub shaft.

Gasifier Inner Backplate (P/N AA101485, S/N KX21208, GTE AY6 Si_3N_4, Total Part Time: 23:43 Hours). The front and back surfaces of the reconstructed inner backplate are shown in Figure 55. Figure 56 shows the fracture pattern and crack propagation directions. The inner diameter (i.d.) rim of the backplate experienced large amounts of impact damage. Several rub marks, caused by the rotating rotor, were found on the rim and front face radiating out from the i.d. The fracture pattern indicated that cracks 1, 2, and 3 probably preceded all other cracks. Fractographic analysis indicated that cracks 1 and 2 originated at the i.d. rim from impact damage and crack 3 originated at a deep rub mark on the front face, as shown in Figure 57. Cracks 4 and 5 originated at the edge of the groove and were the result of the rub.

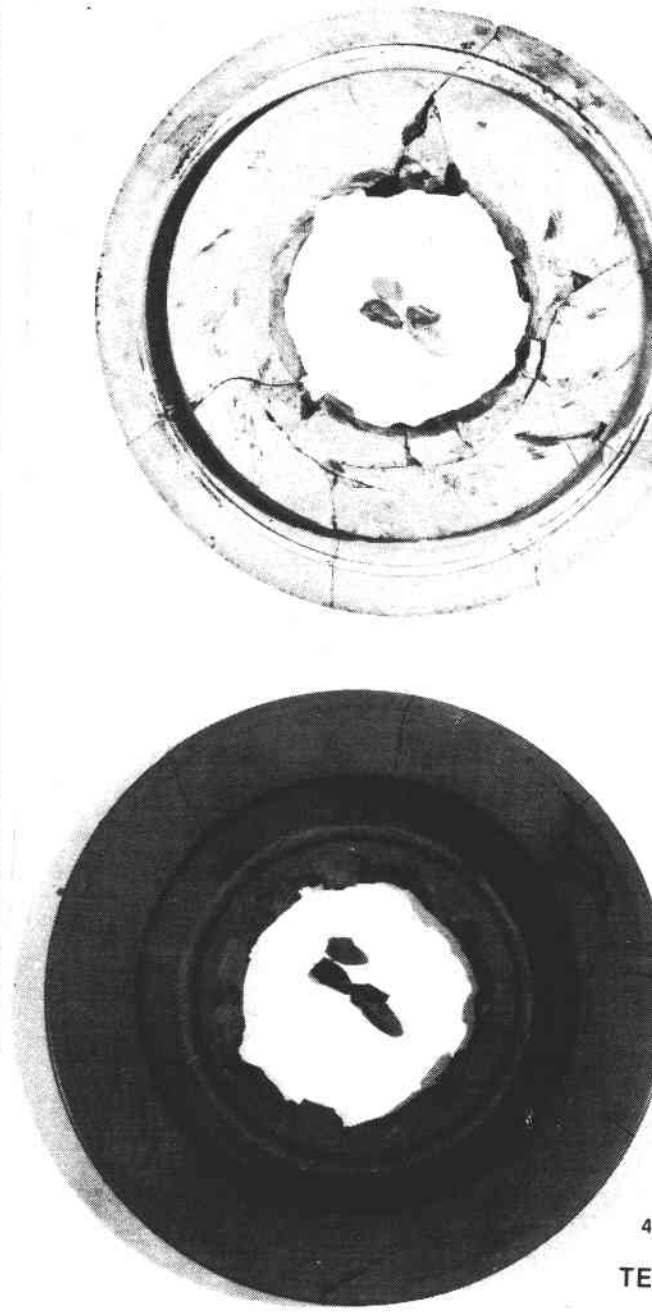

Figure 55. Front (top) and aft (bottom) views of reconstructed gasifier inner backplate.

Gasifier Outer Backplate (P/N AA101165D, S/N FX52944, Carborundum SiC, Total Part Time: 5:5 Hours). The outer backplate shattered into numerou pieces. Figure 58 shows the partially reconstructe backplate. All major cracks initiated at the i.d. Crac origins were not observed at the cross key slots a observed in the previous engine failure (S/N 1, BU26)

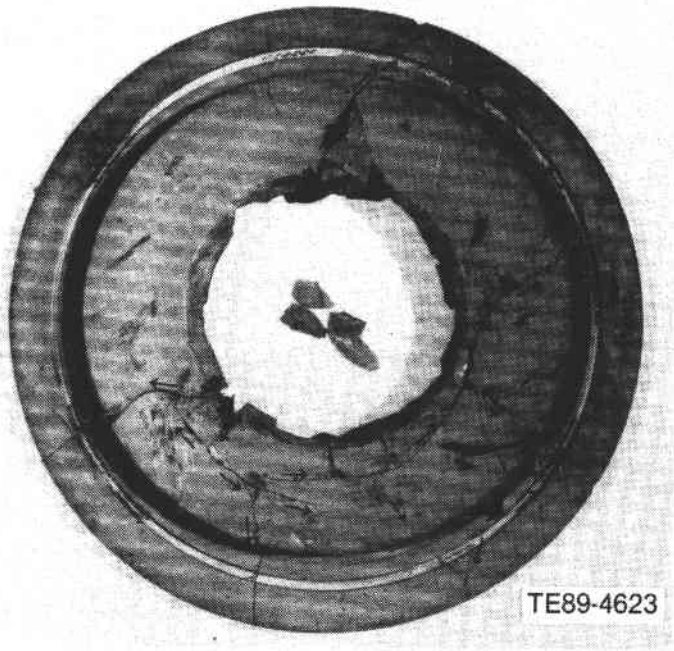

Figure 56. Primary fractures and crack propagation directions of gasifier inner backplate.

Gasifier Vanes (P/N AA101374-4, GTE AY6 Si_3N_4, Total Part Time: 5:54 Hours). Figure 59 shows the remains of 18 gasifier turbine vanes. Deep gouges and rub marks were observed on the suction surface of the vanes.

Gasifier Scroll Assembly (P/N AA101052D, S/N FX38382, Norton NC-430 Siliconized SiC, Total Part Time: 29:24 Hours). Figure 60 shows the reconstructed scroll assembly. The scroll body and the scroll elbow were easily reconstructed. The shroud and the braze joint between the scroll body and shroud could not be put back together due to the extensive damage incurred as illustrated by the large amount of debris. The crack pattern outlined on the scroll indicated multiple origins at the braze joint and o.d. edge. There were several impact fractures, but none were primary failure origins. The crack direction was difficult to determine on the fracture surface of the siliconized SiC, and was therefore not indicated on the crack pattern. A few large remnants of the shroud, shown in Figure 61, showed long circumferential rub marks that probably resulted from contact with the

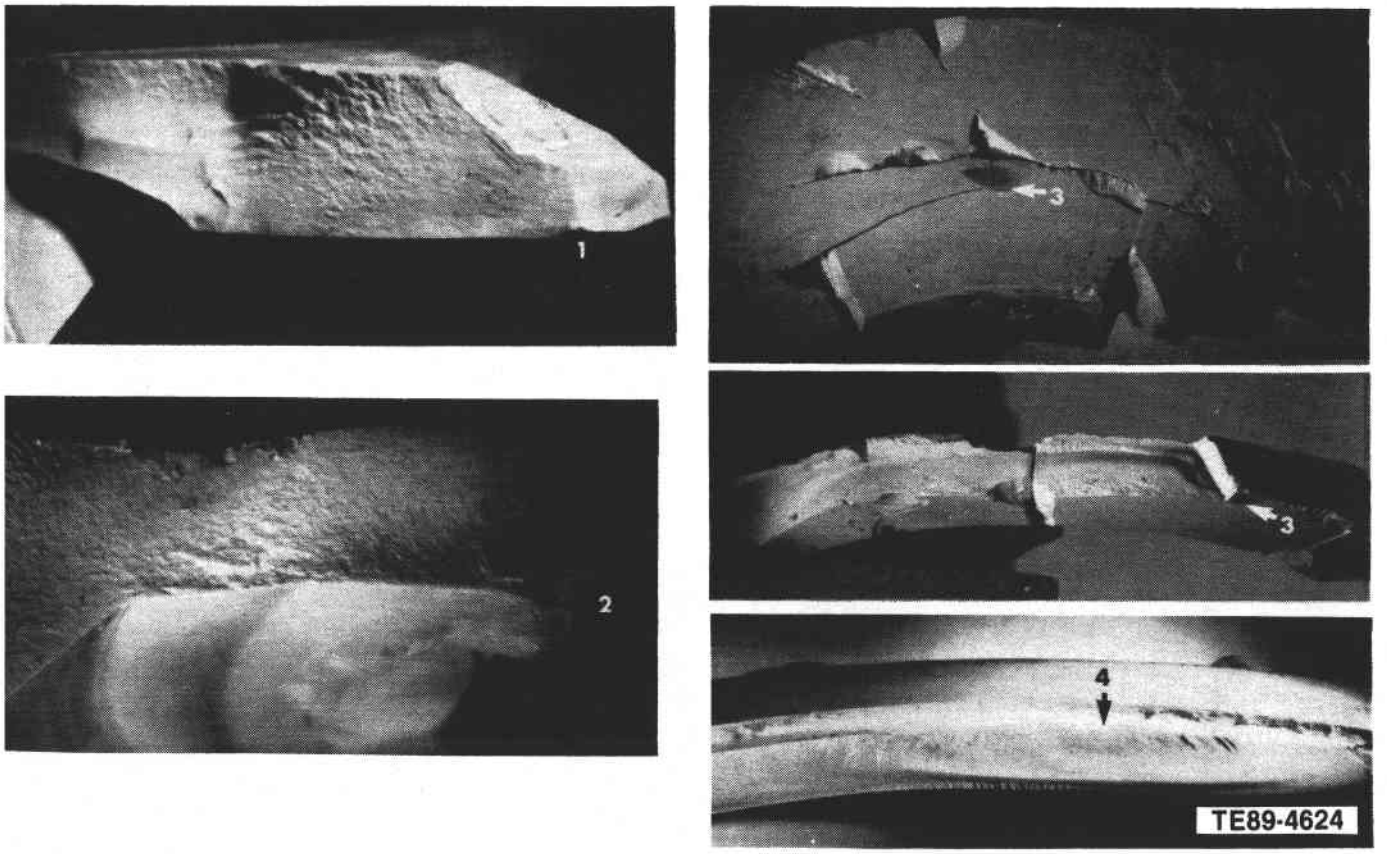

Figure 57. Fractographs of fractures in gasifier inner backplate shown in previous figure.

Figure 58. Partially reconstructed gasifier outer backplate.

rotor airfoils. This indicates that when the rotor started breaking off from the stub shaft, the airfoils were still intact and impacted the shroud. The force from the impact shattered the rotor and initiated the sequential failure of the downstream gasifier ceramic components.

Summary

The following statements summarize the failur analysis:

- The ceramic gasifier section probably faile from FOD. A large piece of carbon buildup o the fuel nozzle apparently broke off during er gine shutdown and was sucked into the ga flow path, striking the rotor.
- The gasifier turbine rotor failed at the stub sha due to shock loading, probably when th thickened inducer airfoil was impacted by th carbon.
- The inner and outer backplates both failed fror impact at their i.d.'s.
- The scroll assembly failed from impact with th turbine rotor. Fracture originated at the braz joint and o.d. edge.

3.2 CERAMIC COMPONENT PROCESS DEVELOPMENT AND FABRICATION

The ceramic component fabrication subsection detail the ongoing ceramic component process develop ment activities at the selected ceramic suppliers, ir cluding Carborundum, Manville, GTE Laboratorie Corning Glass Works, Garrett Ceramic Component Division, Ceramics Process Systems, Drexel Unive sity, and Textron Aerospace Development Cente Allison's approach to ceramic component develop ment continues to be one of subcontracting proces

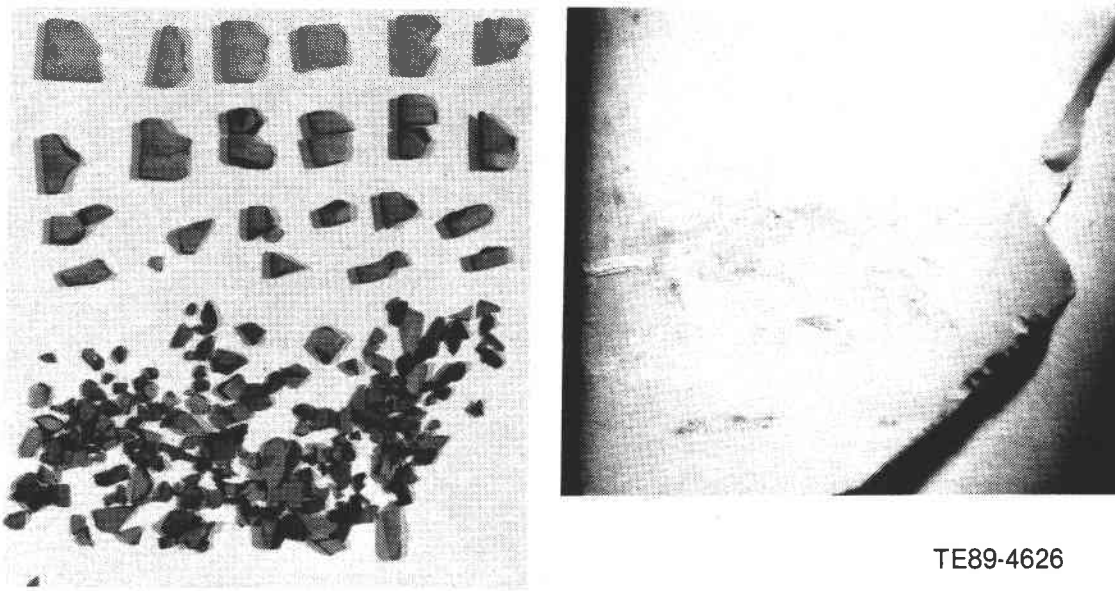

Figure 59. Partially reconstructed gasifier vanes (left) and gouging impact damage on one vane (right).

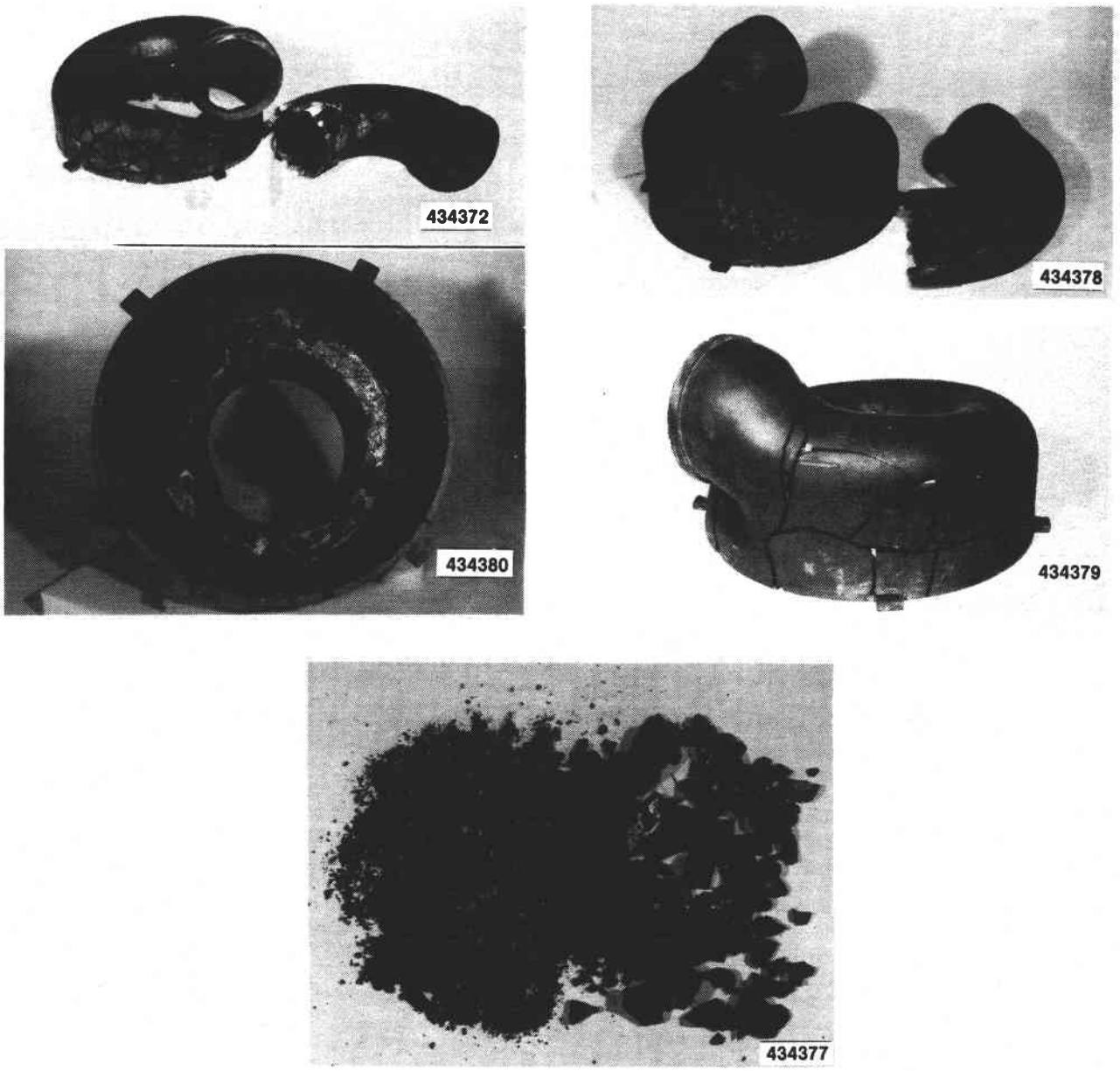

TE89-4627

Figure 60. Reconstructed gasifier scroll assembly and remnants.

development to the domestic ceramic manufacturing community and working in an iterative development loop with those suppliers in areas of component design, characterization, and rig/engine data feedback. The major focus of the component development activities at Carborundum included injection molded SiC gasifier turbine rotors, ceramic/ceramic joining, SiC/TiB_2 characterization, and slip cast SiC scrolls. Manville's efforts concentrated on development and fabrication of ceramic thermal insulation for test rigs and engines. The development activities at GTE Laboratories focused on injection molded Si_3N_4 gasifier turbine rotors, as well as studies addressing toughened Si_3N_4 material systems using both microstructural and SiC whisker reinforcements. Corning Glass Works was involved in extruded alumino-silicate regenerator disk specimens and components. Garrett Ceramic Components Division was focused on the development and fabrication of gasifier turbine rotors using pressure slip cast GN-10 Si_3N_4. The efforts at Ceramics Process Systems addressed Si_3N_4 axial turbine rotor fabrication using its

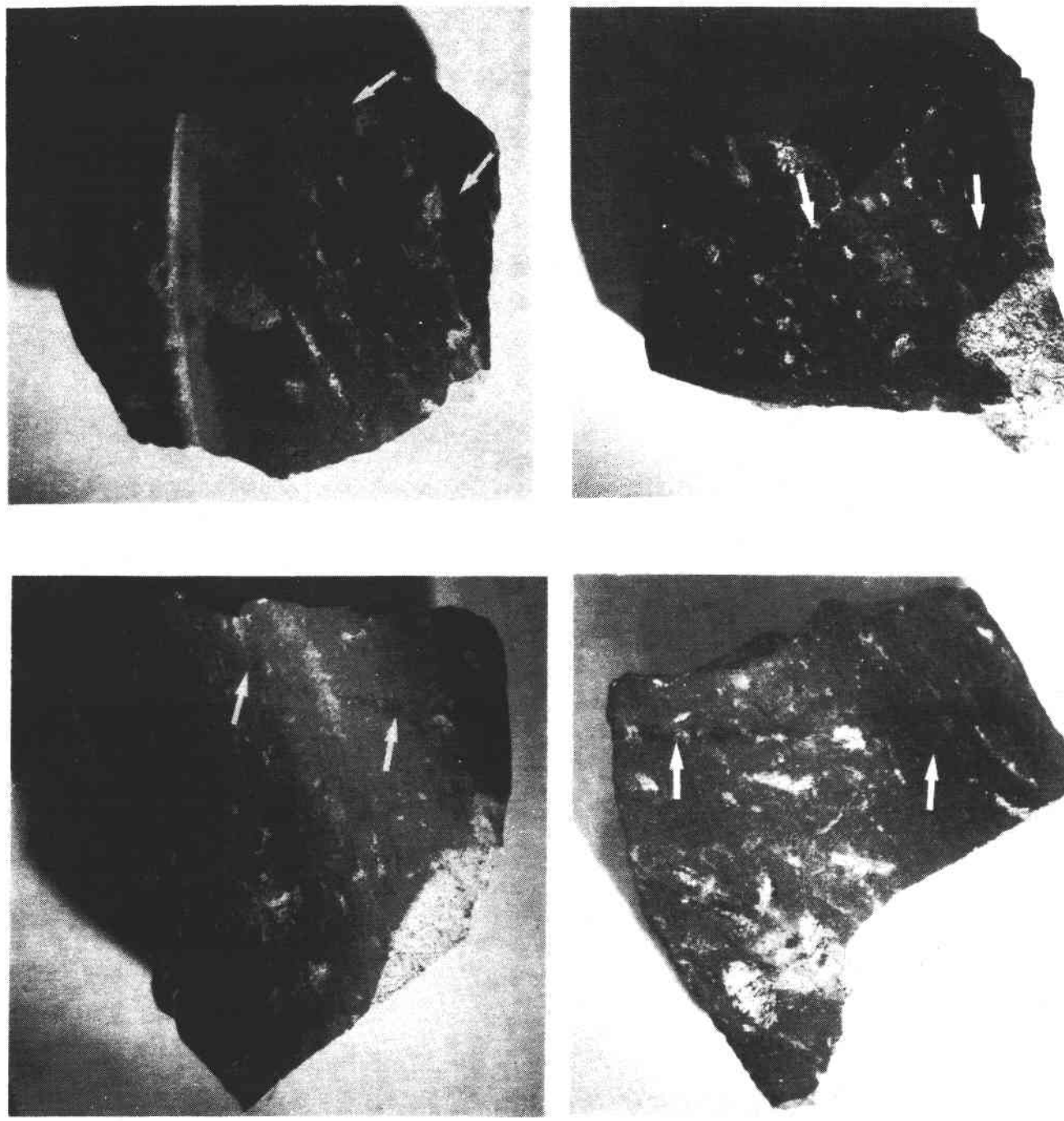

TE89-462

Figure 61. Gasifier scroll shroud pieces showing long curved rub marks left by the rotor airfoils.

Quickset injection molding process. The efforts at both Drexel University and Textron Aerospace Development Center focused on continuous fiber-reinforced ceramic/ceramic composites, with Drexel working on the fabrication of axial turbine rotors and Textron on the fabrication of test specimens for material and process characterization.

3.2.1 Carborundum

The ceramic component development activities a Carborundum (CBO) in 1988 focused on four majo areas: improved rotor processing, ceramic/cerami joining, chemical vapor deposition (CVD) of SiC o SiC/TiB_2, and slip casting. The improved roto processing effort addresses improvements in Si(

material/processes for injection molding axial turbine rotors, generic axial rotor fabrication, and procurement of an engine configuration rotor injection molding tool with subsequent injection molding trials. The joining efforts have focused on various methods of brazing ceramic to ceramic, including characterization of various brazes and siliconized SiC joints. The SiC/TiB_2 development activities focused on the characterization of the mechanical properties of SiC/TiB_2 and the application of CVD SiC for oxidation protection. The slip casting efforts addressed improvements in the slip via chemical modifications in addition to prototype scroll fabrication.

Task I--Improved Rotor Processing

The improved rotor processing activities consist of four areas relating to successful fabrication of injection molded sintered alpha-SiC axial turbine rotors. These include SiC process development, injection molding instrumentation and flow modeling, generic axial rotor fabrication, and engine configuration rotor fabrication.

A SiC dry powder processing matrix was conducted. The goal of this experiment was to evaluate different powder types as well as milling times, mill loading, and processing aids to determine the powder/processing combination providing the highest packing density. The powder responses were evaluated using SEM, particle size distribution, surface area, apparent density, tap density, and compaction density. Modulus of rupture (MOR) strength results were obtained on the as-fired test bars in the SiC process development effort. The average value of 20 bars along with the standard deviation and Weibull modulus are given in Table XXI. The results of testing of SiC test bars with a machined surface condition will be completed in 1989.

The two SX-05 sets provided the highest MOR strengths whereas the experimental powder provided the lowest MOR. It is expected that the Weibull modulus will significantly increase after machining/annealing.

The goal of the injection molding instrumentation effort is to monitor the machine and process control system variables as well as the two pressure transducers within the injection molding tool during each injection molding cycle to provide for increased reproducibility in the molding process. The variables recorded included machine pressure, velocity, position, material pressure in the mold using pressure transducers, and material temperature all as a function of elapsed time in molding. A schematic of the instrumentation is shown in Figure 62. A program was written for the Compaq 286 computer to provide over 200 recorded points during the molding velocity stroke, which usually lasts approximately 1 second. It will also record a suitable number of points between pack pressure and hold pressure to record the influence of pack-hold pressure slope. This system can generate detailed plots of pressure, velocity, temperature, and position as a function of time. The knowledge gained from examination of the actual molding pressures, temperatures, and velocity curves and their relationship to flow lines and green weights of components, in conjunction with designed experiments, has resulted in improved surface quality and final properties as well as minimizing shot-to-shot variability.

Table XXI.
SiC process development test matrix.

Composition	A	B	C	D	E
MOR--MPa (ksi)	339.9 (49.3)	334.4 (48.5)	399.9 (58.0)	384.7 (55.8)	359.9 (52.2)
Standard deviation--MPa (ksi)	52.4 (7.6)	32.4 (4.7)	67.6 (9.8)	53.8 (7.8)	43.4 (6.3)
Weibull modulus	6.6	10.1	5.8	7.5	8.3

Legend:
- A: Experimental powder, standard polymer level
- B: Experimental powder, 2% less polymer
- C: SX-05, molding conditions same as A, B, and E
- D: SX-05 baseline
- E: SX-09 baseline

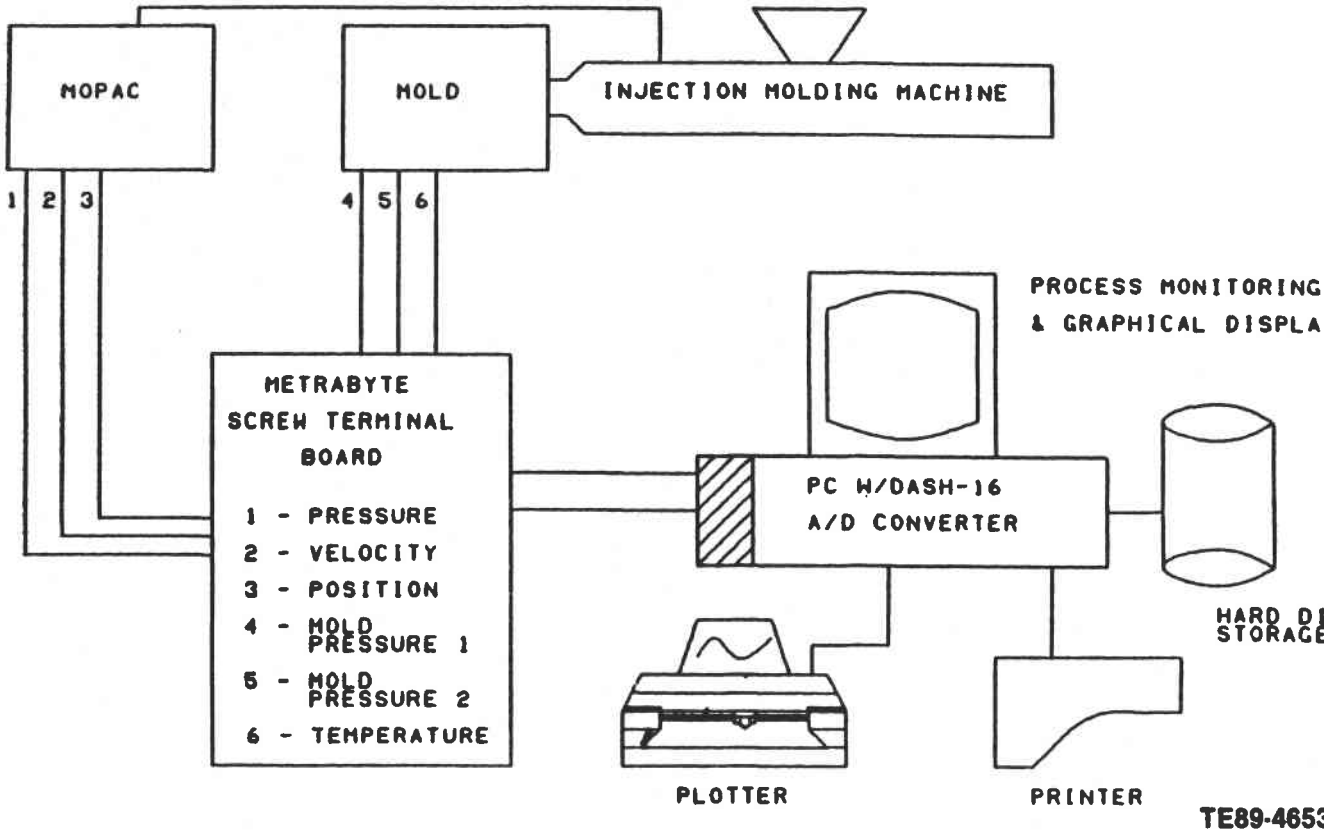

Figure 62. Carborundum injection molding instrumentation schematic.

To determine the effects of various variables in the molding process and to optimize the final engine configuration rotor tool design, activities were conducted on finite element modeling of the injection molding process. Rheological characterization of the injection molding compound was conducted at the University of Lowell Plastic Engineering Department. The data were forwarded, along with the axial rotor model and corresponding drawings, to Moldflow for finite element flow analysis. The main objective of this activity was to determine the optimum flow parameters to minimize the shear rates and shear stresses that occur during the injection molding process.

Two models were created. First, the full flow model was constructed so that the compound would not have to flow through a thickness that required a dimensional approximation. The elements on each surface were assigned the thickness of that surface, as shown in Figure 63. Second, to verify the accuracy of the full model, a Layflat representation of the rotor model was created to facilitate visualization of the flow (see Figure 64). This takes 1/15th of the rotor and makes it planar, except for the rotor shaft, which comes off at 90 deg. This model allows for additional molding variable iterations since this model avoided some of the full rotor model approximations.

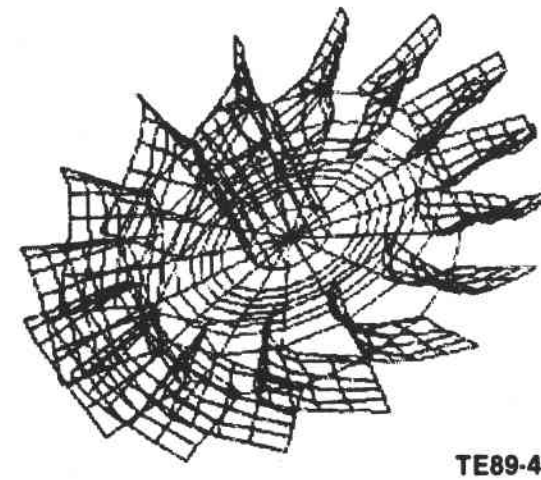

Figure 63. Moldflow rotor FEM model.

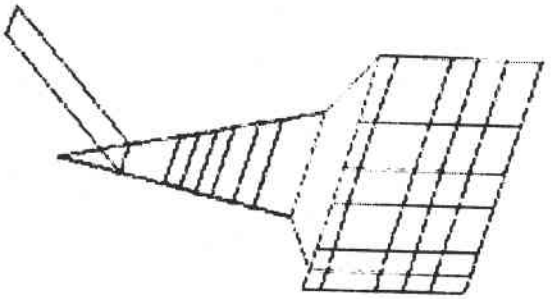

TE89-4655

Figure 64. Layflat rotor model.

The first flow analysis, run at start-up conditions, indicated that flow from the center gate had no problems except for the rapid increase in flow front velocity in the thin outer edges of the blades, which resulted in high shear stresses. Theoretically, high shear stresses may cause separation of polymer from ceramic, which could result in density variations in the molded and baked component resulting in sintering distortion. An optimum set of molding conditions based on standard injection molding guidelines was then determined by comparing the five response variables: fill time injection profiles or isochrones, pressure distribution at instant of fill, flow front temperatures as the material fills part, shear rate during filling, and shear stress during filling.

The isochrones or short shots start-up conditions show a rapid increase in velocity at the end of fill, which causes high shear rates and shear stresses. The isochrones under optimum conditions show a significant change in velocity in the last place to fill (see Figure 65).

The pressure plot start-up conditions show a very high pressure increase required to fill the blade trailing edge due to constant flow rate and rapid increase in flow front velocity. The optimum conditions resulted in a pressure gradient reduction of about 64% (see Figure 66). The flow front temperature stays nearly uniform until it hits the blade, then cools off rapidly and increases slightly at the trailing edge tip. The temperature range under optimized conditions (see Figure 67) was larger than that produced using constant flow rate analysis but was considered a trade-off for shear rate reduction.

The shear rate during filling is a function of section thickness and flow front velocity. The maximum shear rate was reduced by 67% under optimized conditions (see Figure 68).

The thicker the cross section the lower the expected shear stress given the same flow rate. The highest shear stress is in the blade, the last place to fill, resulting from a combination of increased flow front velocity and the fact that this is the thinnest part of the rotor. Note the more uniform shear stress distribution over the blade under optimum conditions (see Figure 69). The maximum shear stress was reduced by 50%.

A summary of the conclusions and recommendations follows:

1. Due to the radial symmetry of the part, the centroid gate location is preferred. Although three other central sprue configurations have been considered, the present location is preferred for two reasons: machining is minimized and flow analysis shows that the shaft fills at the same time as the blade tip.

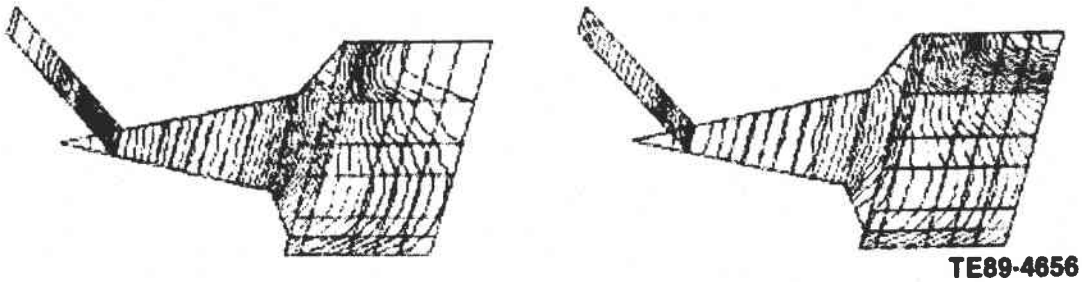

TE89-4656

Figure 65. Isochrones or short shots start-up conditions (left) and optimum conditions (right).

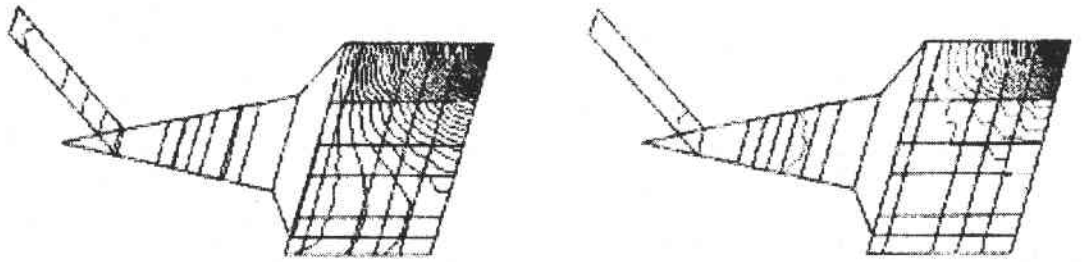

TE89-4658

Figure 66. Pressure plot start-up conditions (left) and optimum conditions (right).

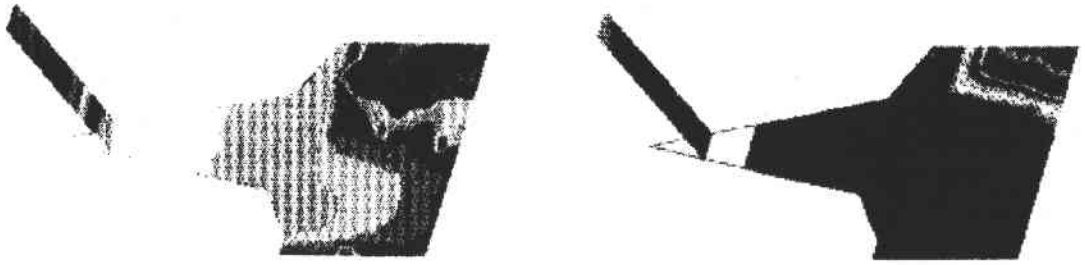

TE89-4659

Figure 67. Flow front temperature start-up conditions (left) and optimum conditions (right).

TE89-4660

Figure 68. Shear rate start-up conditions (left) and optimum conditions (right).

2. The optimum molding conditions will ensure a lower shear rate range as well as shear stress range. Reductions from start-up conditions to optimum conditions for pressure, shear rate, and shear stress were 64%, 67%, and 50% respectively.
3. The isochrones or short shots were also more evenly spaced under optimum conditions.
4. Reducing the shear rates and stresses should help keep the distribution of SiC as even as possible within the polymer carrier. Moldflo has had experience with other fillers and add tives that have shown separation from the bas polymer at higher shear rates and stresses.
5. Due to the desired fast fill time, special con sideration should be taken for liberal ventin The ends of the blades are the most importar areas. This will be addressed in the toc design.

TE89-4661

Figure 69. Shear stress start-up conditions (left) and optimum conditions (right).

In order to accelerate axial rotor development, a generic axial rotor tool was used to assess molding and other processing steps and shrinkage characteristics. To examine the filling pattern of the sprue and part configuration combination, a series of short shots was conducted at 0.25 cm (0.1 in.) stroke increments on the injection molding machine. These results are shown in Figure 70. The reason for the knit line between the sprue and the part on the fully packed-out component is evident from the short shots. The sprue impinges on the rotor back face (shaft end) backfilling the rotor nose end and leaving a depression between the sprue and the part as well as near the outside rim (see Figure 70a). These depressions pack out last, as shown in Figure 70d.

A statistically designed molding matrix was designed and conducted using the generic axial rotor tool to determine the molding variable levels required to reduce knit lines on the surface of the rotor hub prior to receipt of the 15-bladed tool. The design for this Taguchi experimental matrix is shown in Table XXII. Two levels of nine molding variables were selected for the matrix evaluation. The variables included mold temperature, melt temperature, velocity, back pressure, pack pressure, pack time, shot size, hold pressure, and hold time. An L16 orthogonal array was used since this is the smallest two-level design matrix with interaction information that can be used with greater than seven but less than 16 control variables.

Five parts were molded at each condition to establish equilibrium conditions with the exception of mold temperature and melt temperature, which took somewhat longer for stabilization. The last three parts were measured for weight and number of flow lines. The effect of each variable on component weight is shown in Figure 71. In each of the run averages, the lower mold temperature provided the highest weight. The reason is probably due to the fact that the material cooled faster in contact with a cooler mold, thereby shrinking and permitting more material to be packed into the cavity. The total weight difference, however, was only 0.96%. Melt temperature shows the same relationship as mold temperature although much less dramatically. The variability between temperatures is less than the variability within temperature but in the opposite direction. A higher back pressure should have worked the material more thereby increasing its temperature. The slope should have been the same as melt temperature. Both pack pressure and hold pressure show an effect opposite to that expected but the difference is small. Shot size has no effect. Both pack time and hold time show the expected behavior. As the material is held under pressure for a longer time prior to freezing, the component weight should increase. This was particularly evident for hold time where the difference in time is 30 seconds and weight change was second only to mold temperature.

The plots for number of flow lines versus each of the molding variables (see Figure 72) produced the same results as did a previous molding experiment at three levels. The two variables of seven from the previous experiment providing the highest contribution to flow lines were mold temperature and pack time. In this experiment, the mold temperature and pack time slopes were about equal, with the higher values producing fewer flow lines. Higher mold temperatures provided flow time reduction and reduced shear rate and shear stress levels more than in previously designed experiments and flow modeling. However, the statistical significance in this experiment is questionable due to the wide range of responses for mold temperatures and pack times.

Two tooling vendors, Mercury Machine and MDF Tool Corp, were visited by both CBO and Allison in June 1988 to discuss the engine configuration axial rotor design as well as gating, heating and cooling, mold opening, and other tool design options. The 15-bladed tool was ordered from MDF in late June with delivery anticipated in January 1989, with the 20-bladed rotor tool for General Electric (GE) in the

Table XXII.
Rotor molding experimental matrix.

Yates order	TC	Run order	Mold temp	Melt temp	Vel	Back press.	Pack press.	Pack time	Shot size	Hold press.	Hold time
1	(1)	7	1.00	1.00	1.00	1.00	1.00	1.00	1.00	1.00	2.00
2	a	2	1.17	1.00	1.00	1.00	1.25	1.00	1.07	1.25	1.00
3	b	16	1.00	1.10	1.00	1.00	1.25	2.00	1.00	1.25	1.00
4	ab	12	1.17	1.10	1.00	1.00	1.00	2.00	1.07	1.00	2.00
5	c	13	1.00	1.00	1.40	1.00	1.25	2.00	1.07	1.00	1.00
6	ac	1	1.17	1.00	1.40	1.00	1.00	2.00	1.00	1.25	2.00
7	bc	15	1.00	1.10	1.40	1.00	1.00	1.00	1.07	1.25	2.00
8	abc	11	1.17	1.10	1.40	1.00	1.25	1.00	1.00	1.00	1.00
9	d	5	1.00	1.00	1.00	4.00	1.00	2.00	1.07	1.25	1.00
10	ad	3	1.17	1.00	1.00	4.00	1.25	2.00	1.00	1.00	2.00
11	bd	4	1.00	1.10	1.00	4.00	1.25	1.00	1.07	1.00	2.00
12	abd	10	1.17	1.10	1.00	4.00	1.00	1.00	1.00	1.25	1.00
13	cd	9	1.00	1.00	1.40	4.00	1.25	1.00	1.00	1.25	2.00
14	acd	14	1.17	1.00	1.40	4.00	1.00	1.00	1.07	1.00	1.00
15	bcd	8	1.00	1.10	1.40	4.00	1.00	2.00	1.00	1.00	1.00
16	abcd	6	1.17	1.10	1.40	4.00	1.25	2.00	1.07	1.25	2.00

middle of December 1988. Conversations with MDF indicated its confidence in being able to install cooling lines for water in the two mold blocks to permit more flexibility in heating and cooling. Flow modeling results corroborated experimental design findings, and those options required to provide the necessary flexibility were incorporated in the tool.

Task II–Ceramic/Ceramic Joining

Because of the complexity of certain turbine engine components (such as the scroll assembly) and the net shape fabrication limitations of some ceramic forming processes, it is not only necessary to sometimes combine different forming procedures in the subsequent fabrication of a ceramic assembly but to utilize joining methods to maintain the structural integrity of the assembly. The development of ceramic-to-ceramic joining methods, including brazing and siliconized SiC, was investigated in this program.

The initial effort was to evaluate the brazing characteristics of a TiCrV braze composition (54% Ti, 25% Cr, 21% V) developed by Oak Ridge National Laboratory (ORNL) for high temperature refractory braze applications. A coupon brazing test matrix was conducted using isostatic pressed sintered alpha-SiC coupons with a machined braze surface. The brazing test matrix is summarized in Table XXIII. A direct brazing process where the filler metal (TiCrV) is applied as powder in slurry form or as tape was utilized. A fixed braze powder/liquid carrier ratio was formulated and rods 0.25 mm (0.010 in.) in diameter were placed at each end to ensure consistent joint thickness except for No. 11, which used 0.5 mm (0.020 in.) rods, and Nos. 14-16, which used TiCrV tape. Carrier No. 1 (C-1) comprised 15% of the total mixture whereas carrier No. 2 (C-2) comprised a total of 10%. The TiCrV tape was 0.1 mm (0.004 in.) thick. These samples were brazed at 1950°C (3542°F) for 30 minutes. After brazing, the coupons were X-rayed to determine a qualitative measure of braze coverage. Image analysis is being investigated but to date has not proven useful for quantitative measure of braze coverage due to a lack of contrast between the brazed and unbrazed portion on the X-ray. In general, the X-ray results showed the following: a gap of 0.25 mm (0.010 in.) provided better coverage than a gap of 0.5 mm (0.020 in.), and two layers of tape resulted in better coverage than one layer of tape. The total coverage differences between C-1 and C-2 were difficult to measure, although C-2 appeared to provide more uniform dispersion. In all cases except the single tape layer (No. 16), the braze coverage was approximately 60%-75%.

Table XXIII.
Braze experiment test matrix.

Test No.	Description	
169-3-9	$MoSi_2$ + C-1	Standard coupons
169-3-10	TiCrV + C-1	Standard coupons
169-3-11	TiCrV + C-1	Standard coupons
169-3-12	TiCrV + C-1	Alkali-etched coupons
169-3-13	TiCrV + C-2	Standard coupons
169-3-14	TiCrV tape (2 layers) + C-1	Standard coupons
169-3-15	TiCrV tape (2 layers) + C-2	Standard coupons
169-3-16	TiCrV tape (1 layer) + C-2	Standard coupons

To evaluate the temperature and oxidation characteristics of the braze formulations, each sample was sectioned into two pieces. One sample was cycled a total of 10 times between 750°C (1382°F) and 1371°C (2500°F) with a 5 hr hold time at the maximum temperature. Both the virgin and thermally exposed specimens will be submitted to X-ray diffraction, SEM, and transmission electron microscope (TEM) analyses for chemical, mechanical, and microstructural characterization.

Efforts to develop additional joining methods also continued. A successful initial braze joint was accomplished by siliconizing a joint slurry of SiC powder, graphite, and phenolic resin in an induction-heated vacuum furnace. Although the brazed joints appear promising with respect to integrity, difficulties were encountered in furnace operation. Runs have proceeded in both vacuum and Ar atmospheres with the goal of improving furnace operation through improved construction and control, joint uniformity through compositional modification, and reduced braze joint thickness. Mechanical and microstructural examinations of butt-joint sintered alpha-SiC coupons were conducted. After siliconizing in a vacuum furnace, the joint was sectioned into test bars and broken in 4-point flexure at room temperature. The average strength of nine bars was 229.6 MPa (33.3 ksi), with six bars fractured at the siliconized joint. The average strength of these six bars was 252.4 MPa (36.6 ksi). One bar was polished for microstructural evaluation (see Figure 73). The butt joint was only 25 microns thick on average as measured by the silicon with the range being 17-30 microns. In some areas SiC had grown across the joint. A fractional factorial experiment on this siliconized braze system is planned.

Task III--CVD of SiC on SiC/TiB_2

Sintered alpha-SiC was selected as the principal ceramic material of Carborundum for use in ATTAP ceramic component development activities. While offering numerous advantages (superior high temperature properties and lack of degradation in strength with time at temperature), SiC has relatively low values for fracture strength and fracture toughness. Carborundum has recently been developing a new material system, Hexoloy ST, consisting of sintered alpha-SiC with TiB_2 particulate additions. This material exhibits fracture toughness values 50%-100% higher than monolithic sintered alpha-SiC. However, the SiC/TiB_2 material oxidizes significantly at temperatures above 1200°C (2192°F). This oxidation was not observed on specimens previously coated with a thin layer of CVD SiC. The objectives of this task are to determine the baseline mechanical and oxidation behavior of uncoated SiC/TiB_2 and to investigate the procedures involved in using CVD SiC as an oxidation-resistant coating on this material.

A quantity of injection molded and sintered SiC/TiB_2 (20 v/o) test bars was subjected to a MOR test matrix to evaluate the mechanical strength characteristics of both uncoated SiC/TiB_2 material and SiC/TiB_2 with a CVD-applied coating of SiC. The test matrix, summarized in Table XXIV, consisted of room temperature (RT) MOR measurement prior to thermal exposure and after exposure at both 1250°C (2282°F) for 100 hr and 1371°C (2500°F) for 100 hr. The oxidized bars prior to MOR testing are shown in Figure 74. All of the uncoated specimens were completely coated with a layer of TiO_2. The CVD SiC-coated test bars provided higher strength values at room temperature than the uncoated SiC/TiB_2 test bars, although a small reduction in strength of the coated bars was observed after

Table XXIV.
MOR test matrix for coated and uncoated SiC/TiB_2--MPa (ksi).

	As-fired uncoated	As-fired CVD SiC	Machined uncoated	Machine CVD SiC
RT MOR	347.99 (50.5)	415.49 (60.3)	418.39 (60.7)	440.31 (
RT MOR after 100 hr at 1250°C (2282°F)	402.12 (58.3)	374.12 (54.3)	432.39 (62.7)	414.67 (
RT MOR after 100 hr at 1371°C (2500°F)	199.96 (29.0)	304.62 (44.2)	142.17 (20.6)	194.78 (

exposure at 1250°C (2282°F). However, considerable degradation in strength was observed for all specimens after exposure at 1371°C (2500°F) for 100 hr. Although the coated bars exhibited higher strength values, preferential oxidation was observed due to a less than optimum coating. The individual strengths were quite variable and visual observations suggest failures initiating at areas of extensive local oxidation on the low strength bars. Selected bars will be submitted for failure analysis.

A total of 100 SiC/TiB_2 test bars will be supplied to Allison for additional characterization activities in early 1989.

Task IV--Slip Casting

The objectives of this task are twofold: to improve the properties of the slip cast parts based on processing variables, and to fabricate prototype slip cast components to form a data base to provide input for final design of the scroll assembly. The slip development activities were focused on the fundamentals of each processing step, with a goal of improving casting yields and structural integrity by decreasing microstructural and macrostructural flaws. All development work was conducted using an alpha-SiC aqueous slip with a bimodal particle size distribution. The primary factors investigated consisted of binder type and level, dispersants, pH level, and powder cleaning to improve green strength and plasticity in the cast parts. The shape-making development trials initially concentrated on fabrication of prototype scroll bodies. Information resulting from this effort relating to mold design and fabrication, dimensional control, and process yields will be incorporated into the final design of the AGT-5 engine configuration scroll assembly.

The slip development activities have concentrated or (1) binder studies to improve green strength and plas ticity in cast parts; (2) studies to determine the effects of dispersants in an effort to maximize dispersion, min imize viscosity, and minimize the dispersant level; and (3) powder cleaning experiments to minimize the ionic strength in as-received powders and decrease batch to-batch variability. A number of statistically designed experiments have been generated and are currently being conducted to determine the influence of a large quantity of material and processing variables on the final slip quality. Variables that are currently being investigated include dispersant type and level, slurry pH, binder type and level (inorganic and organic), and ionic conductivity. Each variable will first be investigated independently to determine the respective influences and responses, followed by experimentation to evaluate the various combinations of the variables.

An experiment was designed and conducted to determine the optimum solids loading and pH conditions in a slurry for washing soluble materials from the particle surfaces. The results indicate that the lowest solids level at a pH near neutral provides maximum removal of dissolved materials in a reasonable pressing time with high enough solids content (70%) for further processing. An initial test matrix was also conducted in which three organic binders were added to the standard slip casting slurry in 0.05% increments and the viscosity increases measured. The slurry pH was also varied. On the basis of the results of this experiment, binder B was eliminated, with binders A and C being retested using smaller addition increments. Following this effort, the optimum binder system will be determined and test articles will be cast at varying binder content levels and their plasticity and green strength evaluated. Additional efforts are ongoing to identify the optimum dispersant types and levels.

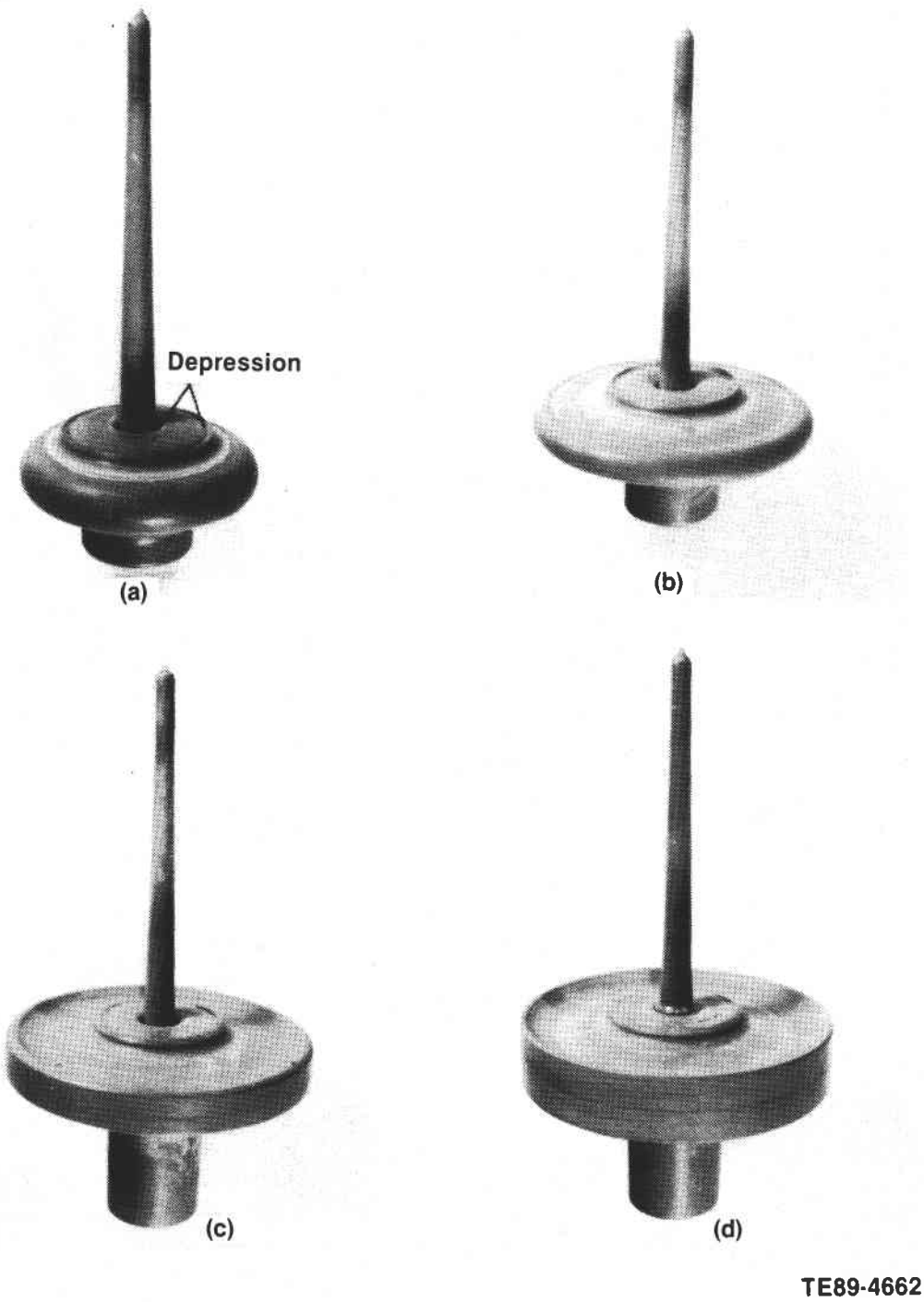

Figure 70. Generic axial rotor hub short shots (CBO).

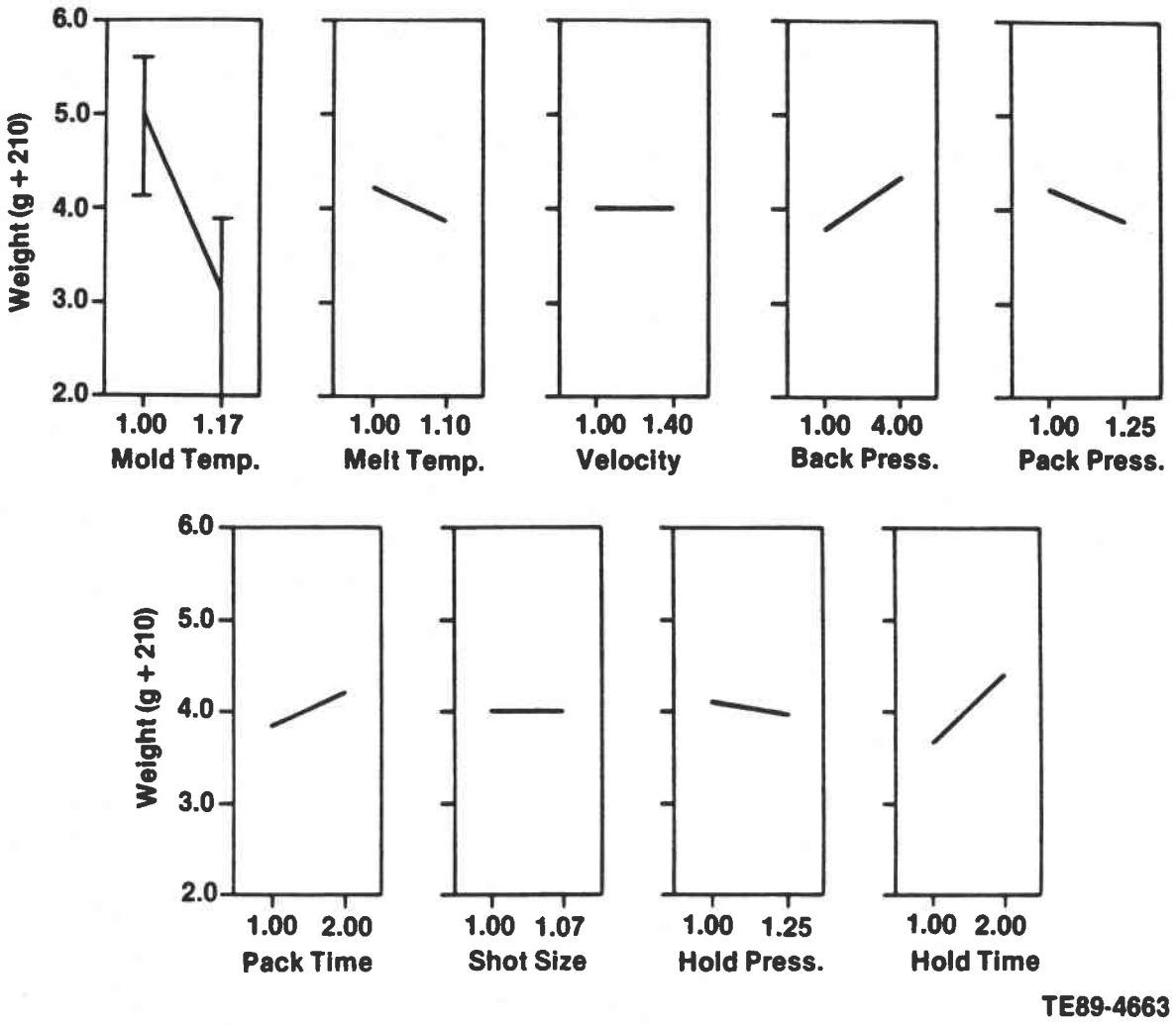

Figure 71. Effect of molding variables on weight.

Based on the results of the initial test matrix in which three organic binders were compared, one was eliminated. The remaining two were retested using smaller increments to discern the differences between them. The important responses were the relative viscosities, slip plasticity imparted to the mix, and increasing plasticity/decreasing brittleness in cast parts. Overall, binder B provided parts with better trim properties and plasticity when green. Methods of green strength evaluation are currently being investigated.

Internal Carborundum development work has identified an additive able to impart some lubrication properties and decrease the brittleness of the nonplastic SiC without increasing slip viscosity. This additive is also effective in improving the surface finish of cast parts. An experiment was carried out in which a cellulose derivative organic binder and a lubricating additive were added to a slip containing the two best dispersing agents. Viscosity passed through a mini mum at about 0.015% binder and increased sharply thereafter at all lubricant concentrations up to 1% The maximum binder content should be less thar 0.05% to maintain low viscosity. This amount may be less than is necessary to increase the green strength.

Because the ceramic scroll assembly final desigr would not be available until late 1988, it was decidec to evaluate an existing AGT-5 metal vortex configura tion for casting purposes by in-house fabrication of a rough model approximately 10% larger to compen sate for shrinkage. From the model, molds were fabri cated and used for initial component fabrication ef forts. Four sintered alpha-SiC parts were cast for evaluation, with two of these sectioned to assess inter nal structural details. The overall quality and castinc characteristics of the cast components (shown ir Figure 75) were acceptable, although sectioning showed that the tongue area of the mold between the

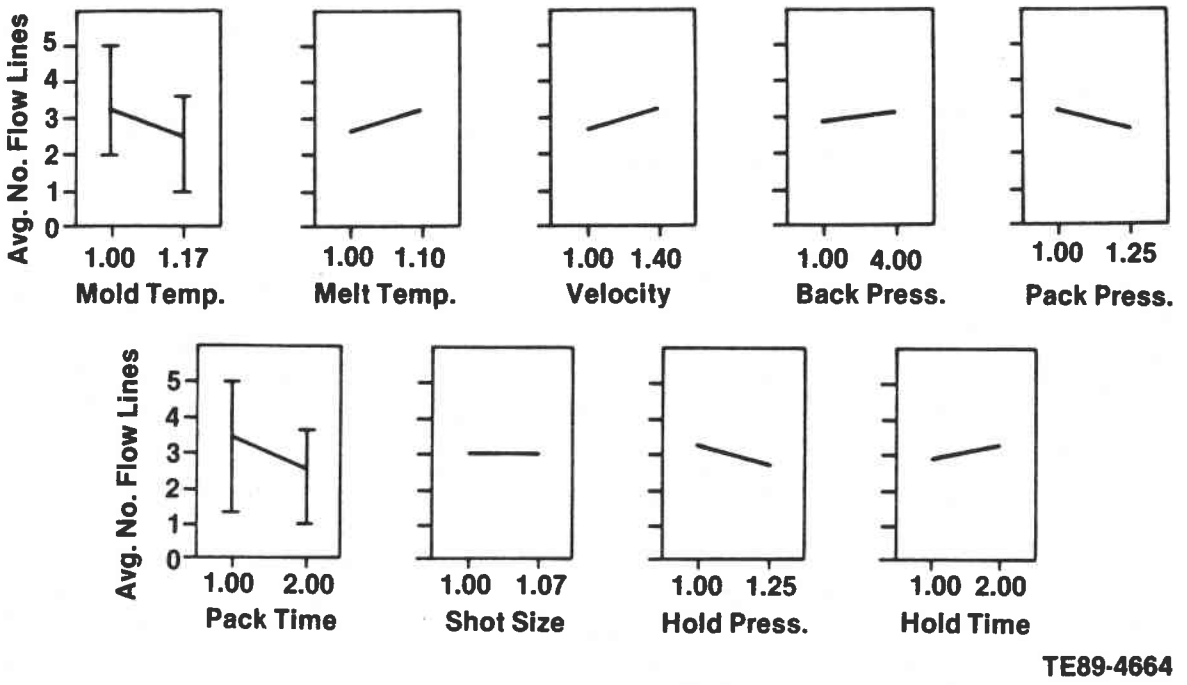

Figure 72. Effect of molding variable on flow lines.

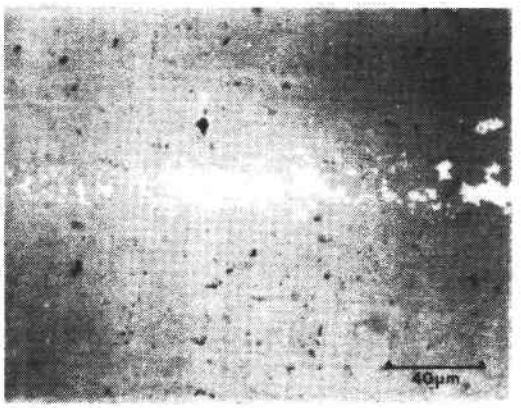

Figure 73. Siliconized braze joint microstructure.

inlet duct and vortex body must be increased in thickness to provide for uniform thickness of the cast part.

A modified plaster model was cast from the first mold. The modifications consisted of removal of stock from the model on both the combustor inlet and vortex body regions to increase the thickness of the tongue area. From this second configuration model, new molds were formed and three parts cast for sectioning and evaluation. These components, shown in Figure 76, demonstrated improvements in wall thickness uniformity and overall part quality.

A third plaster mold configuration was designed and fabricated for casting of SiC scroll bodies. In this model, the throat area was shortened from approximately 60 to 33 mm (2.36 to 1.30 in.). New working molds were fabricated from this model and several parts cast. Two of these parts were deliberately broken in the green state to check for differential thickness in the throat region. A differential was present in one cast but not the other. This represents a borderline state in which conditions such as humidity, mold moisture, viscosity, and time between casts will affect rates of cast and part thickness. Figure 77 shows a sectioned part of this configuration.

A fourth configuration (see Figure 77d) was initiated to provide a buffer against such variable conditions. The throat area was thickened from approximately 10 to 13 mm (0.394 to 0.512 in.) by raising the gas inlet height about 3 mm (0.118 in.) but maintaining the same diameter. Castings trials were made to determine the effect of increasing the thickness of plaster in the throat area. For a 4 mm (0.157 in.) thick part, this iteration has accomplished its goal--to ensure sufficient cast wall thickness in this area and a minimum differential thickness. The minimum diameter or wall separation in this area has been determined to be 15.25 mm (0.6 in.). Figure 78 is a photograph of a fourth configuration as-cast part showing the critical areas. The information generated on scroll slip casting and dimensional control and requirements will be

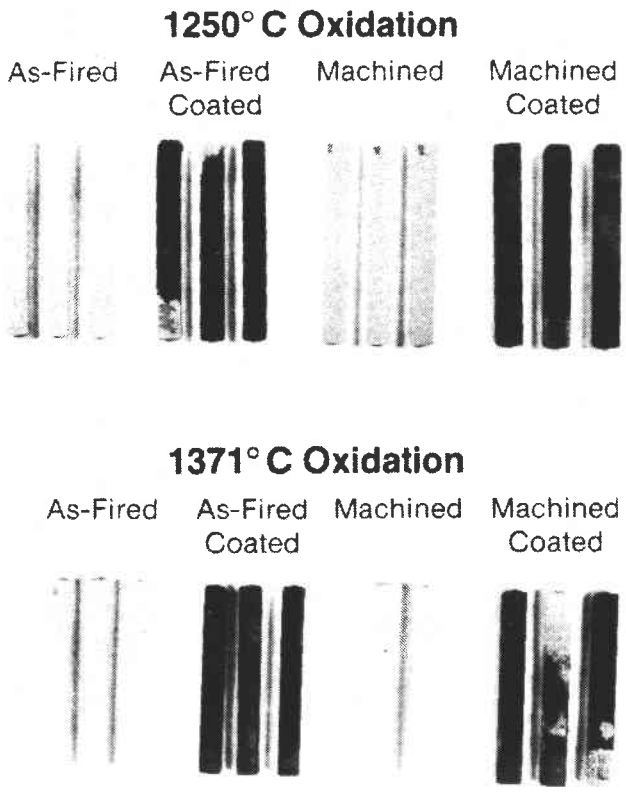

Figure 74. CBO SiC/TiB_2 test bars uncoated and coated with CVD SiC after oxidation at 1250° C (2282° F) for 100 hr (top) and 1371° C (2500° F) for 100 hr (bottom).

utilized to support design of the ATTAP scroll configuration.

Carborundum received preliminary prints for the ceramic scroll assembly in October 1988. In discussions with Allison, recommendations were made for design modifications necessary to facilitate the slip casting process. In response to an initiative to check the feasibility of casting thinner walls and to check variability of wall thickness with thinner walls and variable throat width, parts were cast at 2.5 and 3.0 mm (0.098 and 0.118 in.) wall thickness in the third and fourth configuration molds. These parts were sectioned and showed little variability in wall thickness in the critical areas at a throat width of 12.7 mm (0.5 in.).

3.2.2 Manville

A technical effort was initiated with Manville in Jul 1988 to develop an injection moldable insulation fc automotive gas turbines capable of low cost, hig volume production. The previously utilized insulatio supplied by Manville worked well in place, but re quired a labor-intensive hand lay-up process for insta lation. The technical approach is to modify the insul tion material for injection molding via an iterativ development cycle involving materia development/characterization and injection moldin development. Efforts have primarily focused on two-part binder system study, a shelf life study, the mal characterization, and initial laboratory injectio molding trials on a gasifier housing.

Two-Part Binder System

To produce an injection moldable material, the binde system of the existing standard formula product mu be modified to provide better molding and mol release characteristics. The modifications include the incorporation of (1) a two-part colloidal silica c colloidal silica and colloidal alumina binder syste and (2) methocel gelling agents that stiffen at elevate temperatures. Manville performed the modificatio studies of the binder system as discussed in the fc lowing text.

The first laboratory bench scale two-part binde studies investigated the gelling characteristics of con binations of acid-stabilized colloidal silica or alumir and base-stabilized colloidal silica. The ratio of th acid to base colloids was varied over a wide rang The following response variables were recorded:

- o mixing time--seconds
- o gelling time--seconds
- o pH of combination
- o firmness of gel--subjective evaluation
- o percent of gel--subjective evaluation, 0-100 gel versus free liquid remaining after gelling

Six binder combinations (shown in Table XXV) wer selected from the initial study based on higher percer gel formed and longer gel times, and confirmatio tests of the initial results were performed at room tem perature.

Table XXV.
Binder system combinations.

	Acid	Base	Ratio	Mix time --sec	Gel time --sec	pH	Firmness of gel	Percent gel
I	Nyacol AL20	Nalco 1140	1.33	30	20	6	Firm gel	100
II	Nyacol AL20	Nalco 1050	1.18	30	20	6	Firm gel	100
III	Nalco 1034A	Nyacol 215	15.0	30	15	6.5	Soft gel	100
IV	Nyacol AL20	Nyacol 830	3.33	30	15	5.5	Firm gel	100
V	Nyacol AL20	Nalco 1130	3.33	30	15	6	Firm gel	98
VI	Nyacol AL20	Nalco 1115	2.86	15	15	6	Firm gel	100

The combinations were prepared with the two components at 2°C (35.6°F) to determine if the lower temperature would increase the gel time. Gel time did not increase for any of the six systems.

The six binder systems were incorporated into the complete insulation formula and evaluated for moldability, mold release, dry adhesion to sandblasted metal plates, drying shrinkage, and dry density.

The basic formula for the insulation was the same for all six binder combinations except for the colloidal binders and the total amount of water in the system, as shown in Table XXVI.

The dry components of part A were mixed and the wet components were added and mixed, followed by the addition of the part B materials. The resulting wet mass of insulation was worked into a brass 15 x 2.5 x 1.3 cm (5.9 x 0.98 x 0.51 in.) bar mold placed on a sandblasted 0.6 cm (0.24 in.) thick metal plate. The workability of the material was qualitatively evaluated at this point (see Table XXVII). The ease with which the mold was removed from the wet bar of insulation was noted. The mold release was deemed excellent if the insulation remained on the plate without having to use a top plate to remove the brass mold.

Table XXVI.
Two-part binder systems.

Material	Weight--grams
Part A	
Cleaned cerachrome	60
Cab-o-sil	6
Polyox	1
Sta-lok starch	2
Methocel	1
Polymer	1
Acid colloid	XXX
Water	YYY
Part B	
Base colloid	ZZZ
Water	WWW

Of the three formulas that were easy to mold and demonstrated excellent mold release, only No. III showed acceptable shrinkage and dry density less than 352 kg/m^3. Additional batches of this basic

Table XXVII.
Bar mold binder system evaluation.

	Moldability	Mold release	Dry shrinkage --percent Length	Width	Dry density --kg/m^3
I	Easy to mold	Difficult	0.05	0.00	347
II	Easy but stiff	Difficult	0.2	0.25	355
III	Easy to mold	Excellent	0.2	1.3	341
IV	Easy to mold	Difficult	0.25	3.5	426
V	Easy to mold	Excellent	0.45	2.9	381
VI	Easy to mold	Excellent	3.0	7.6	439

formula were prepared at different water contents to evaluate the effect of water on the desired characteristics of moldability, mold release, shrinkage, and dry density. Results are shown in Table XXVIII.

Increased water content yields excellent moldability and mold release characteristics, acceptable dryer shrinkage, and decreasing density of the dry insulation.

Shelf Life

The initial shelf life study (Table XXIX) showed limited shelf life of several days with good moldability and mold release and acceptable dryer shrinkage but with increasing dry density as the wet insulation ages.

Additional shelf life studies and refinements of the insulation preparation procedures were performed. The first study looked at the premixing of the part A colloidal silica with water and the part B colloidal silica with water (see Table XXX). Insulation prepared using the normal procedure of mixing each individual component sequentially was compared to insulation prepared by the same method except that the two colloidal silicas were premixed with water in the proper proportions before adding to the batch. In addition to premixing the part A and part B colloidal silicas with water before using immediately, sufficient liquids were prepared so that they could be retained for insulation preparation at a later time. This was intended to show that the silica and water mixtures could be held "on the shelf."

The insulation samples prepared with the premixed silicas molded and released from the mold somewhat better than the normally prepared insulation. Insulation made by either procedure was very good in molding, mold release, drying shrinkage and dry density.

Table XXVIII.
Effect of water content (binder system III).

Water to solids content	Age of batch	Moldability	Mold release	Dry shrinkage --percent Length	Width	Dry density --kg/m^3
2.79:1	New	Excellent	Excellent	0.05	1.2	333
2.92:1	New	Excellent	Excellent	0.13	1.0	320
3.04:1	New	Excellent	Excellent	0.05	1.0	312
3.06:1	New	Excellent	Excellent	0.00	1.0	303
3.06:1	2 days	Good	Good	0.18	1.0	347
3.06:1	2 days	Good	Good	0.20	2.2	328

Table XXIX.
Shelf life study.

Water to solids content	Age of batch	Moldability	Mold release	Dry shrinkage --percent Length	Width	Dry density --kg/m^3
3.06:1	New	Excellent	Excellent	0.30	1.0	298
	1 day	Excellent	Excellent	0.33	0.3	307
	4 days	Good	Good	0.20	3.5	317

Table XXX.
Premixing shelf life study.

Age of silica water mixtures	Moldability	Mold release	Dry shrinkage --percent Length	Width	Dry density --kg/m^3
Normal unmixed	Excellent	Excellent	0.1	1.9	315
Premixed 1 hr	Excellent	Excellent	0.1	-0.7	320
Premixed 7 days	Excellent	Excellent	0.4	1.3	315
Premixed 14 days	Excellent	Excellent	0.1	0.0	311

The wet mass of insulation prepared by using premixed silica and water mixtures was "creamier" or "smoother" than that prepared by the "normal" procedure. This premixing procedure was adopted for all batches following the insulation shelf life study described in the following text. Two batches of insulation were prepared by the "normal" procedure of batching the components sequentially (i.e., no premixing of the silicas and water) and the prepared wet insulation was stored in plastic bags. One bag was kept in the laboratory at room temperature. The other bag was kept in a refrigerator at about 2°C (35.6°F). Molded samples were prepared and tested for moldability, mold release, drying shrinkage, and dry density. The totally prepared wet insulation seems to degrade when maintained at room temperature. The moldability and mold release were excellent at the start and became poor by the third week of storage. The drying shrinkage and dry density started out within normal limits and reached a maximum at three and seven days. At longer storage times the shrinkage was less than this maximum but was higher than desired. The dry density remained 16 to 32 kg/m^3 higher than at the start. Storage in the 2°C (35.6°F) refrigerator appears to keep the prepared insulation in better working condition. The moldability was excellent initially and remained very good after the third day. The mold release was excellent and progressively worsened to fair by the third week of storage. The drying shrinkage and dry density was acceptable throughout the life of the storage study. The slight degradation in the moldability and the progressive worsening of the mold release leads to the preliminary conclusion that the prepared insulation can be retained and used for post-molding patching and in-service repairs if the material is kept in cool storage.

The next shelf life study looked at using premixed silica and water and premixing of the dry solids and the Nalco 2332 polymer. Three batches of wet insulation were prepared. The first was a control batch prepared by the "normal" procedure but with premixed water and silicas stored at room temperature. This involved dry blending the solids and then adding the Nalco 2332 polymer. The second batch involved dry blending the solids, adding and blending in the polymer, and then storing the "dry" mix in a plastic bag for one day before adding the premixed silicas and water. The third batch was the same as the second except that the "dry" mix, including the polymer, was stored in a plastic bag for one week before adding the premixed silicas and water. All three insulation batches were stored at 2°C (35.6°F) in the refrigerator between moldings. All three batches of insulation maintained excellent molding and mold release characteristics.

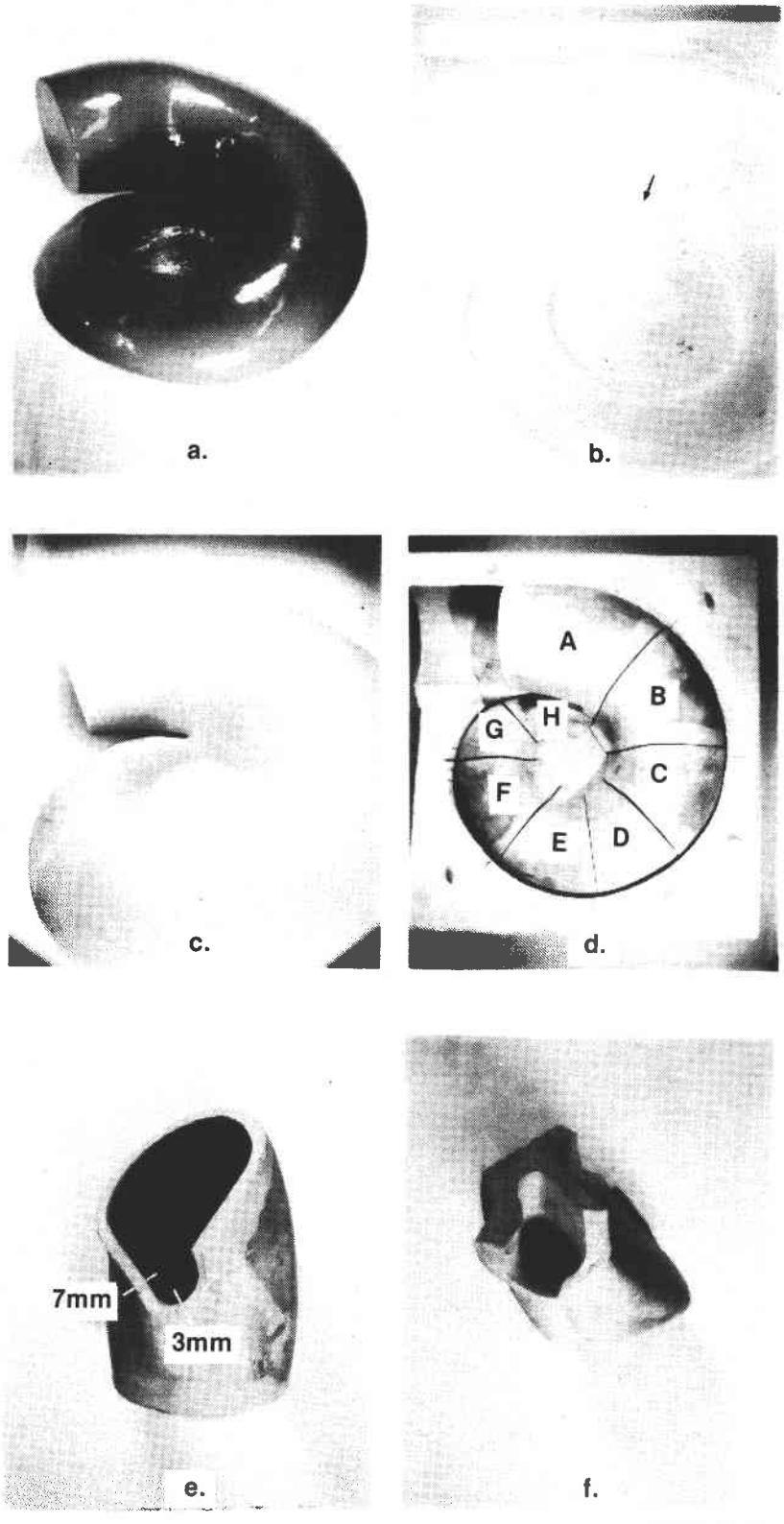

Figure 75. Metal vortex design Mod I: (a) model, (b) mold showing narrow tongue, (c) cast part, (d) part cut into sections, (e) section A showing wall thickness differences, and (f) section H.

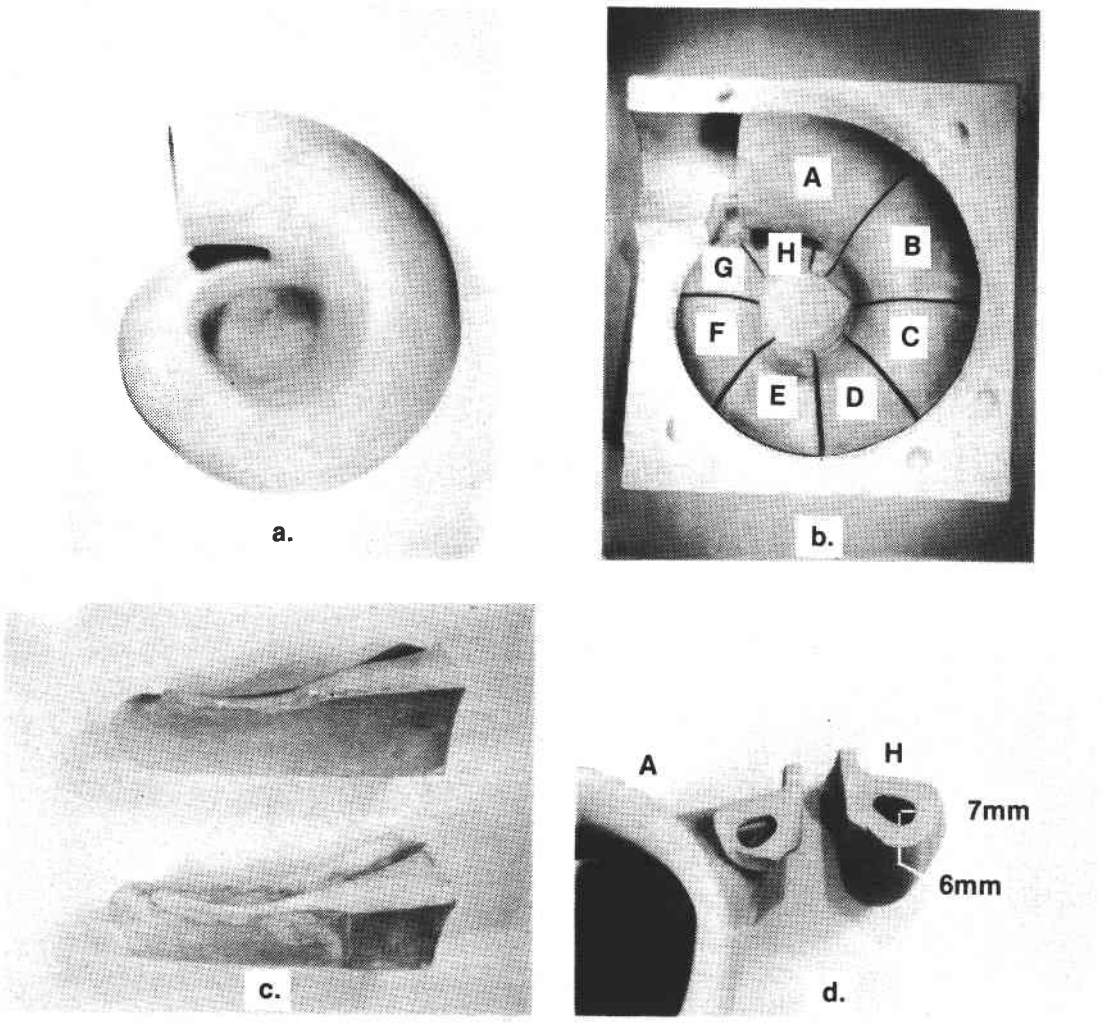

Figure 76. Metal vortex design Mod II: (a) part showing increased throat radius, (b) part cut into sections, (c) mold inserts showing expanded tongue (top) and original narrow tongue (bottom), and (d) sections A and H showing improved wall thickness uniformity.

The drying shrinkage was well within the desired range and the dry density was consistent at 320 kg/m^3 except for the newly mixed insulation, which was 16 kg/m^3 less dense.

The shelf life studies conducted to date show that:

- o Insulation to be stored for later use should be refrigerated.
- o The polymer can be preblended with the fiber and other dry components.
- o The colloidal silicas can be premixed with the makeup water. The resulting insulation is "creamier" and the molding and mold release characteristics are better than obtained by the previous mixing procedures.

Additional shelf life studies are planned to verify these observations. These will include revising the insulation preparation procedure to include both preblending the polymer and solids for long-term storage before wet batching and also premixing the colloidal silicas and water for long-term storage before addition to the dry solids and polymer. The wet insulation will be stored in the refrigerator between moldings. A control batch prepared by this improved procedure will be kept at room temperature.

Thermal Characterization

Following the two-part binder and shelf life studies, flat plate samples of the best formulation of the insulation were prepared for thermal conductivity testing. Two

sets of samples were prepared (see Table XXXI). One set was prepared with cleaned cerachrome fiber as in previously formulated materials. The second was prepared with uncleaned as-received (raw) fiber. The thermal conductivity samples were molded in a 25 x 25 x 1.3 cm (9.84 x 9.84 x 0.51 in.) strip mold. Companion samples for density and drying shrinkage measurements were molded in the 15 x 2.5 x 1.3 cm (5.91 x 0.98 x 0.51 in.) mold.

Thermal conductivity test results are reported in Table XXXII for one cleaned fiber sample and for part of the testing for one raw fiber sample.

The cleaned fiber sample after exposure to the hot face temperature of 1161°C (2122°F) in the high temperature calorimeter showed less than 1% linear shrinkage in the plane of the sample and less than 2% linear shrinkage in the thickness. The sample lost 5.95% of the initial dry cured weight. The thermal conductivity of the raw fiber sample was slightly lower than the cleaned fiber sample. This may be a result of the slightly higher density of the raw fiber sample and radiation blocking by the shot particles from the uncleaned fiber. Additional testing is planned in the high temperature calorimeter on clean and raw fiber samples molded on 0.6 cm (0.24 in.) thick metal plates to simulate actual engine mounting of the insulation.

Injection Molding Development

Initial laboratory-scale injection molding trials were conducted. These trials were conducted in late October and were the first attempts at non-hand-molding of the insulation. The small-scale trials included the following:

1. Successfully loaded insulation into the injection cylinder through a 3-way valve from an air-pressurized storage hopper. Air pressure needed to move the insulation from the hopper to the cylinder ranged from 140 to 350 kPa (20 to 50 psi).
2. Successfully expelled the insulation from the injection cylinder with no back pressure into a catch bucket using a pneumatic drive cylinder. Subsequent injection of the insulation into the mold cavity of an AGT-5 gasifier housing was difficult. The pressure apparently was not enough to force the insulation into the entire mold cavity.
3. Successfully converted the pneumatic drive cylinder to hydraulic activation. Injection of the insulation into the mold cavity of the AGT-5 gasifier housing improved. The insulation filled all but two small areas of the mold cavity. The insulation had been worked fairly hard and had expressed some of the liquid, so it may not be totally representative of "as mixed" insulation. The mold released from the material poorly, leaving some of the insulation on the housing as desired but retaining a significant amount of material on the mold.

Further trials are planned with modified injection equipment and female molds. The drive cylinder will be replaced with a higher pressure capacity cylinder with a longer stroke so that the total capacity of the injection cylinder can be utilized. This should allow the injection of the AGT-5 housing in one shot. The female mold surface will be cleaned and polished for mold release studies, including the application of mold release agents.

Table XXXI.
Thermal conductivity test samples.

Fiber clean/ raw	Mold size--cm	Moldability	Mold release	Dry shrinkage --percent Length	Dry shrinkage --percent Width	Dry density --kg/m^3
Clean	15x2.5x1.3	Excellent	Excellent	0.3	1.9	325
		Excellent	Excellent	-0.2	0.0	315
	25x25x1.3	Excellent	Excellent			304
Raw	15x2.5x1.3	Excellent	Excellent	0.5	1.9	328
		Excellent	Excellent	0.0	0.0	320
	25x25x1.3	Excellent	Excellent			307

Table XXXII.
Thermal conductivity test results.

Sample	Hot face temp-- °C (°F)	Cold face temp-- °C (°F)	Mean temp-- °C (°F)	Apparent thermal conductivity --W/m-K	Test density --kg/m^3
Tested in high temperature heat meter--ASTM C-518					
6195-42-1	371 (700)	260 (500)	316 (600)	0.075	355
Clean	482 (900)	371 (700)	427 (800)	0.088	
Fiber	593 (1100)	482 (900)	538 (1000)	0.102	
Tested in high temperature calorimeter--ASTM C-201					
6195-42-1	741 (1366)	62 (144)	401 (754)	0.084	341
Clean	856 (1573)	75 (167)	466 (871)	0.095	
Fiber	936 (1717)	84 (183)	510 (950)	0.105	
	1062 (1944)	101 (214)	582 (1080)	0.121	
	1161 (2122)	118 (244)	639 (1182)	0.136	
Tested in high temperature heat meter--ASTM C-518					
6195-42-2	371 (700)	260 (500)	316 (600)	0.069	370
Raw	482 (900)	371 (700)	427 (800)	0.087	
Fiber	593 (1100)	482 (900)	538 (1000)	0.101	

3.2.3 GTE Laboratories

The objectives of GTE Laboratories ATTAP ceramic development efforts are to supply turbine rotors with state-of-the-art material properties to support AGT-5 engine test activities and to improve current materials and processes to enhance the resistance of the ceramic rotors to damage/failure in the engine environment. To accomplish these objectives, a 3-phase technical effort is being conducted. In Task I, the process technology will be developed for fabrication of AY6 and PY6 Si_3N_4 axial turbine rotors. The remaining two technical efforts address the requirement for improved impact resistance in turbine rotors. In Task II, the fracture toughness of monolithic PY6 Si_3N_4 will be increased by microstructural modifications. Task III will address toughness improvements of PY6 Si_3N_4 by the incorporation of SiC whisker reinforcement.

Task I--Rotor Shape-making Development

The objective of this task is to establish and demonstrate reliable AY6 and PY6 Si_3N_4 rotor fabrication processing methodology. The specific goals for 1988 were the following:

- o demonstrate shape-making fabrication capabilities and state-of-the-art material properties in complex large cross-section components
- o design and fabricate the ATTAP rotor injection molding tool

All component fabrication activities in the ATTAP program were performed using Ube silicon nitride powder. The switch to Ube starting material is based on a business decision at GTE to end production of GTE SN502 Si_3N_4 powder and on a proprietary survey of material produced using commercially available high purity Si_3N_4 powders. The internal GTE study, completed prior to the start of the ATTAP program, demonstrated that Ube silicon nitride compositions produced properties that equaled or exceeded those representative of GTE SN502 powder.

The Ube-based material was easily compoundable using GTE's injection molding binder system and standard compounding equipment. The binder, compounding, and molding processes were similar to those developed for the AGT100 turbine rotor. However, these processes have been scaled up and improved and are now performed in the clean room

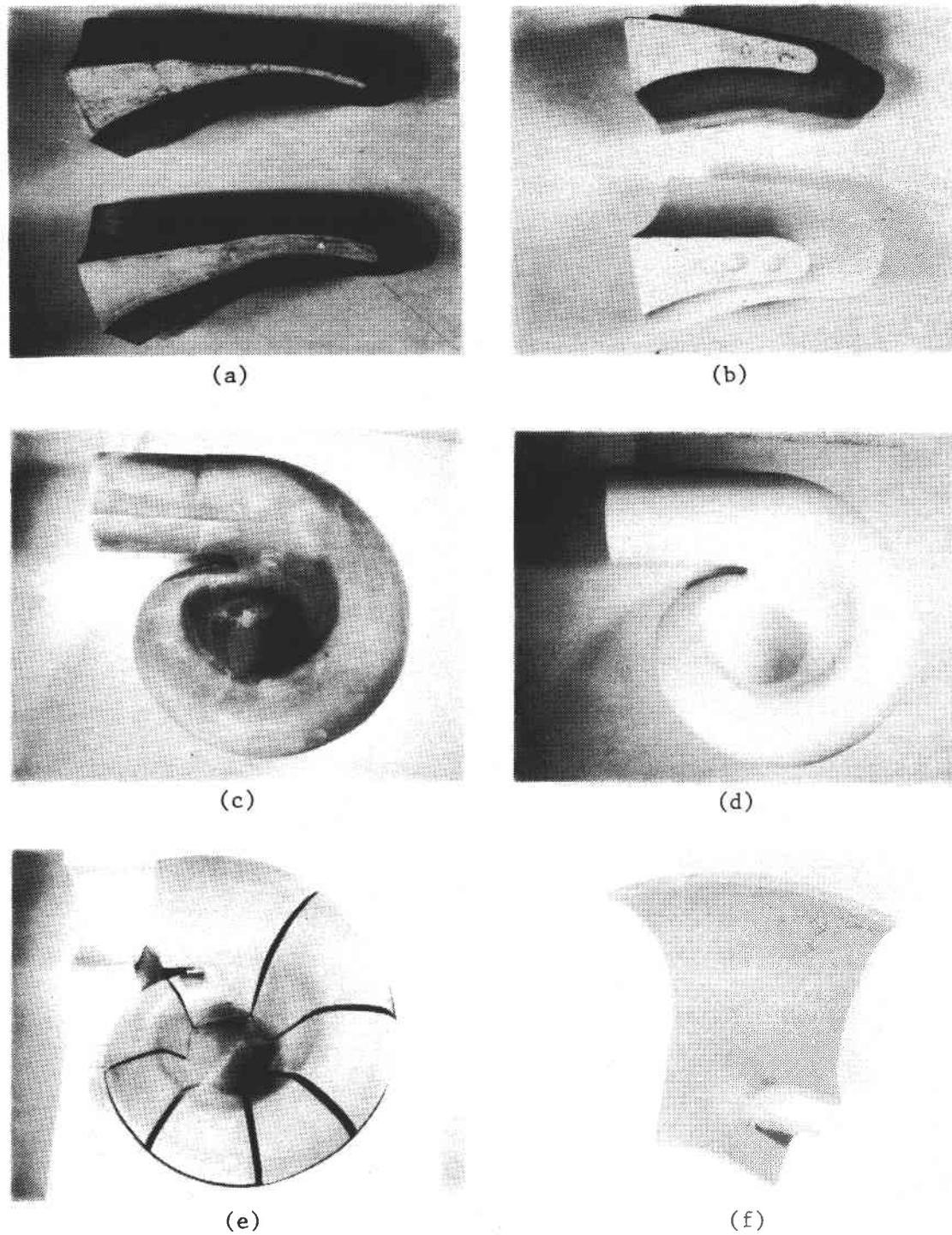

Figure 77. Views showing (a) mold insert configurations 1 and 2, (b) mold insert configurations 3 and 4, (c) No. 3 configuration cast part, (d) No. 4 configuration model, (e) No. 3 configuration cast part cut into sections, and (f) section through throat area of No. 3 configuration cast part.

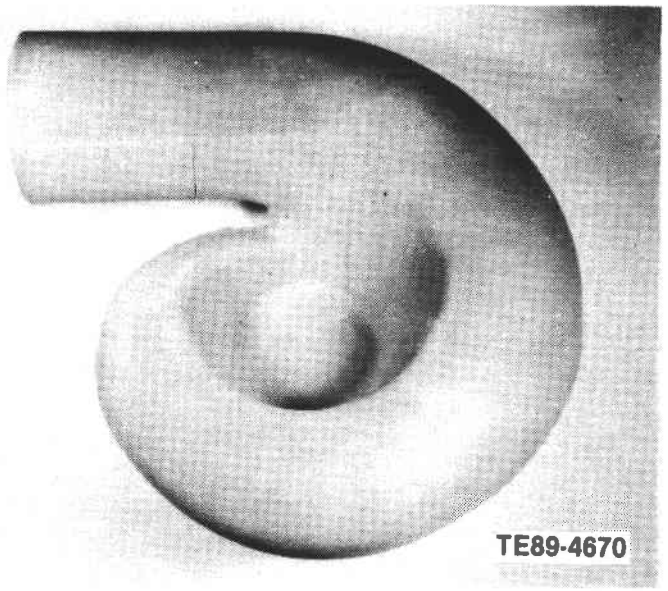

Figure 78. Fourth configuration as-cast part, AGT-5 metal scroll pattern.

environment of the GTE Labs Prototype Engineering Center. The room temperature and high temperature properties of the HIP processed Ube AY6 and PY6 Si_3N_4 materials are summarized in Table XXXIII. For comparison, similar properties from GTE SN502 material are also shown. These results demonstrate the recent materials properties improvements observed in numerous silicon nitride components fabricated in GTEL's Prototype Engineering Center.

Despite the demonstration of excellent material properties in Ube test bars, difficulties were initially encountered in attempts to fabricate large cross-section complex geometry components from the Ube mix. Component surface cracking occurred due to excessive shrinkage of the molded components during solidification in the mold. Occasionally, the cracking did not appear until the parts went through binder burnout and densification. A comparison of the cracking behavior with components fabricated from SN502 starting material clearly demonstrated that the Ube mix is more prone to cracking and therefore required a change in starting morphology in order to reduce/eliminate molding-related shrinkage.

Two modifications to the standard Ube material are under evaluation and have been processed through molding and HIP using tensile bar samples. Mechanical property qualification is in process and, based on the results, one of the modified Ube-based systems will be selected for use in initial AGT-5 rotor fabrication efforts.

Although excellent properties have been obtained for both AY6 and PY6 Si_3N_4 material with machined surfaces, concerns remain with the characteristics of the as-fired surface properties. Initial data on properties of as-fired AY6 Si_3N_4 (see Table XXXIV) show a significant degradation in strength relative to machined surfaces. A systematic study has been initiated to evaluate and improve the properties of the as-fired surfaces.

The 15-bladed gasifier rotor injection molding tool has been designed based on extensive discussions among Allison, GTE, and the tool houses. Two machining houses were evaluated and MDF Corporation was selected for tool fabrication. A purchase order was issued in August 1988 with anticipated delivery in March 1989. The tool design incorporates several features based on GTE's experience with injection molding of large cross-section components. This experience drew heavily on rotor fabrication activities conducted on the AGT100 program. The tool design also includes an appropriate amount of machining stock in the rotor for finish machining the high stress regions of the rotor and detailed balancing prior to spin testing. The initial rotors will be molded with a solid shaft that will be green machined to the final configuration.

Task II–Toughened Monolithic Rotors

The objective of this task for 1988 was to identify initial process conditions for increasing the fracture toughness of monolithic PY6 Si_3N_4. The basic mechanism for achieving improved fracture toughness involved microstructural modifications, specifically focusing on increasing the average grain size. By increasing the grain size of Si_3N_4, resistance to crack growth increases because the crack is deflected more by propagation around the grains. There may be an upper limit to increasing the fracture toughness of monolithic Si_3N_4 by grain growth, however. If the grains become too large, less energy will be required to propagate a crack through a grain (transgranularly) than around the grain (intergranularly), which will limit the degree of crack deflection and thus limit the fracture toughness. The objective of this task is to identify the upper limit of fracture toughness for monolithic Si_3N_4 and then bring the PY6 ATTAP rotors to this level.

Enhancement of material fracture toughness during densification was initially examined by hot pressing. Although hot pressing is not a viable method for producing ATTAP components, the equipment setup

Table XXXIII.
Properties of GTE Prototype Engineering Center-processed AY6 and PY6 Si_3N_4.

Material	Strength--MPa (ksi) 25°C (77°F)	1000°C (1832°F)	1200°C (2192°F)	1400°C (2252°F)
SN502 PY6	717 (104)	---	572 (83)	469 (68)
Ube PY6	917 (133)	---	696 (101)	510 (74)
Ube AY6	1055 (153)	814 (118)	662 (96)	---

Table XXXIV.
Comparison of machined and as-fired AY6 Si_3N_4strengths.

Material	Surface	Strength--MPa (ksi) 25°C (77°F)	1000°C (1832°F)	1200°C (2192°F)
SN502 AY6	Machined	807 (117)	710 (103)	503 (73)
SN502 AY6	As-fired	427 (62)	441 (64)	324 (47)
Ube AY6	Machined	944 (137)	814 (118)	662 (96)
Ube AY6	As-fired	414 (60)	365 (53)	255 (37)

allowed for analysis of the densification kinetics and microstructure development of Si_3N_4 under simulated HIP conditions. In addition, results gathered from the hot pressing study provided information necessary to design experimental HIP cycles to evaluate the effects of different HIP conditions on the properties of monolithic PY6 Si_3N_4.

To study the effect of different densification times and temperatures on microstructure and material properties, a test matrix was established for hot pressing PY6 silicon nitride. Ube-based PY6 billets were hot pressed at 1750°C (3182°F) and 1800°C (3272°F) for three different lengths of time: 150, 325, and 500 minutes. In the first test, 150 minutes was the shortest time for attaining full density. Longer hot pressing times allowed for continued alpha-to-beta Si_3N_4 transformation and grain growth to occur. It was not useful to hot press below 1750°C because the alpha-to-beta Si_3N_4 transformation is quite slow below this temperature; hot pressing above 1800°C leads to dissociation of the silicon nitride. Hot pressing was conducted with 35 MPa (5 ksi) pressure in a nitrogen atmosphere using boron nitride-coated graphite dies. The effects of different densification conditions were evaluated in terms of microstructural characteristics (alpha-to-beta Si_3N_4 ratio, grain size, grain size distribution, aspect ratio) and material properties (fracture toughness, strength).

All of the PY6 billets were hot pressed to near theoretical density. Samples were polished and subsequently etched by a process that removed the grain boundary (glassy) phase to reveal the grain structure. The grain structures produced under each densification condition are shown in Figure 79. The average grain size increases with hot pressing time and temperature from 1750°C (3182°F) at 150 minutes to 1800°C (3272°F) at 500 minutes.

The fracture toughness of each billet was measured by the controlled surface flaw technique with an average of five samples. The results are shown in Figure 80. At both temperatures, fracture toughness increased approximately 20% with an increase in time from 150 to 500 minutes. The limit to which fracture toughness can be increased by grain growth is uncertain. Figure 80 shows that at 1750°C (3182°F), fracture toughness values still appear to be increasing after the 500 minute hot press cycle. To determine if the fracture toughness could be increased further by growing Si_3N_4 grains, a billet was hot pressed at 1750°C for 1500 minutes (25 hr). The results are plotted in Figure 81 and show that the extended hot

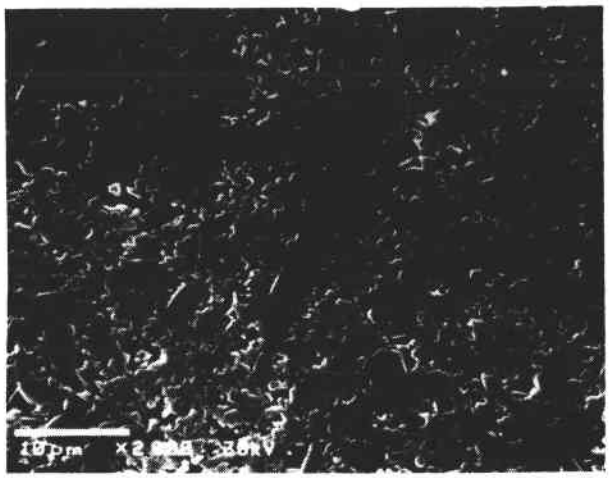

1750°C, 150 min

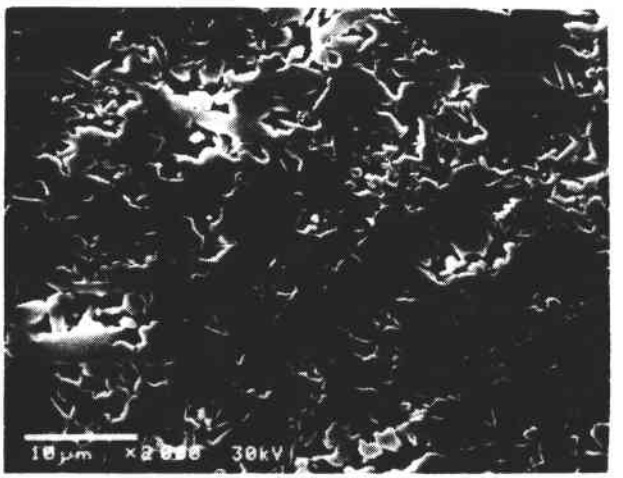

1800°C, 150 min

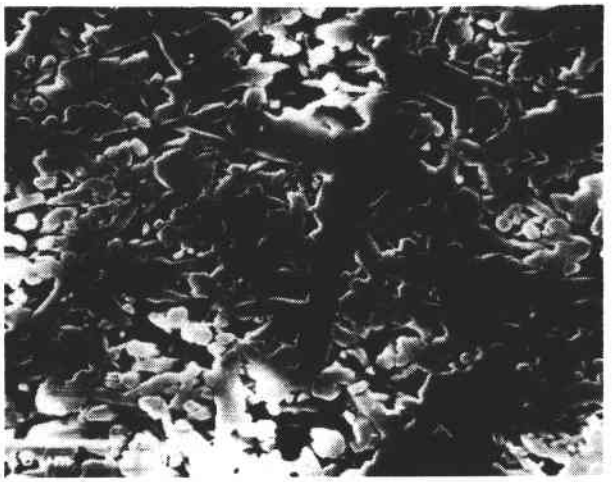

1750°C, 325 min

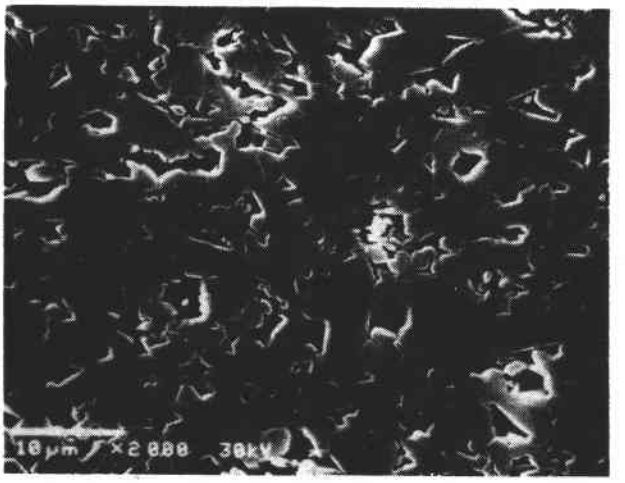

1800°C, 325 min

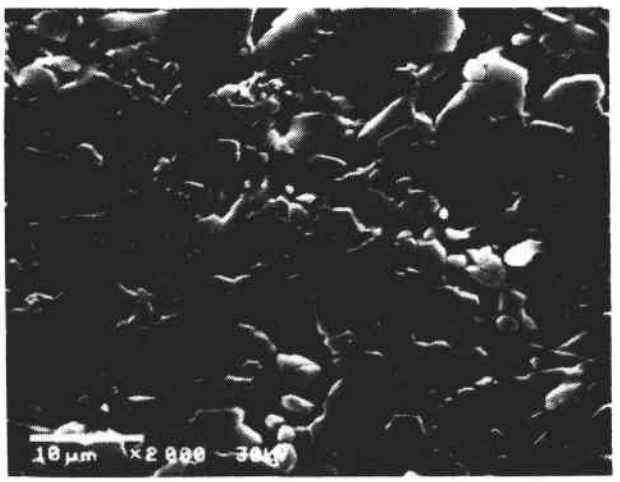

1750°C, 500 min

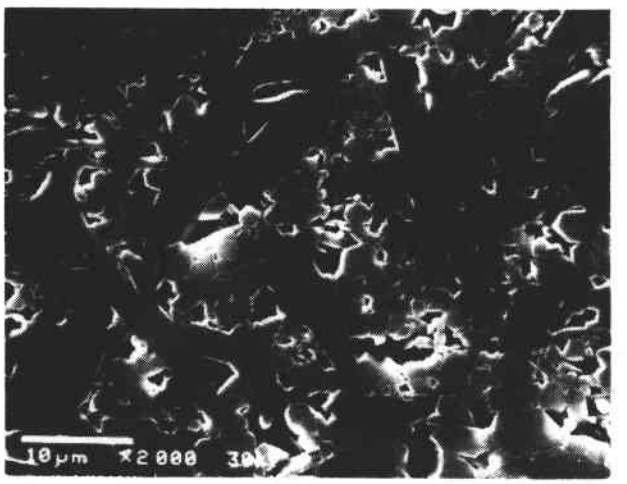

1800°C, 500 min

TE89-4629

Figure 79. Microstructures of hot pressed PY6 samples.

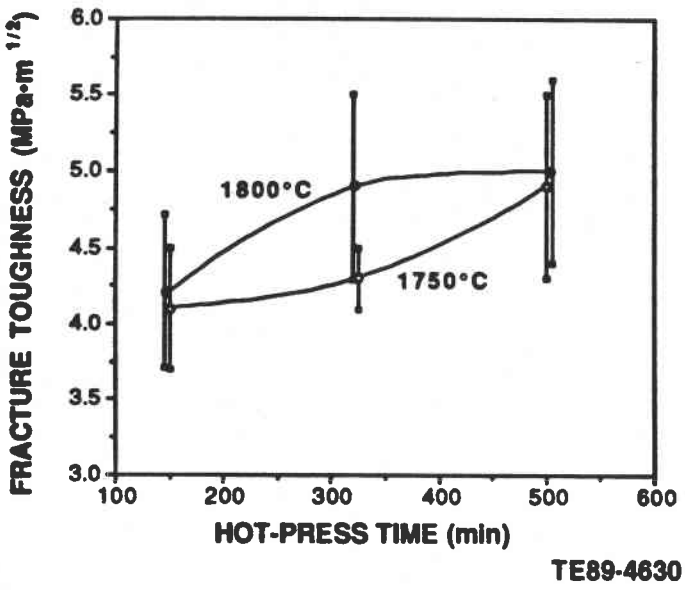

Figure 80. Improved fracture toughness of monolithic PY6 material.

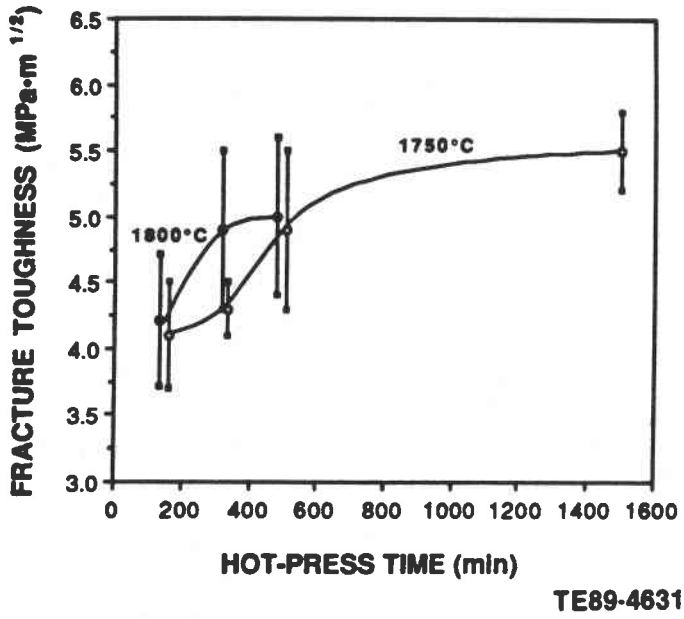

Figure 81. Continued grain growth increases fracture toughness.

pressing time increased the fracture toughness to 5.5 MPa-$m^{1/2}$, 34% higher than the fracture toughness of the 150 minute hot press cycle. It is also evident that the fracture toughness appears to be approaching a limit.

The flexure strength of material produced under each densification condition was also measured, with the results summarized in Figure 82. All billets displayed high strength and high Weibull moduli indicative of excellent reliability. However, the anticipated increase in strength expected from the increase in fracture toughness with longer hot pressing times was not observed. According to fracture mechanics theory, higher fracture toughness should lead directly to higher fracture strength if the critical flaw population remains unchanged. The lack of increase in strength in the PY6 material indicates that as the fracture toughness increases with hot pressing time, the critical flaw population also changes.

Several possible reasons have been identified for the change in critical flaw population: material compositional changes, grain sizes exceeding the critical flaw size of the material from exaggerated grain growth, changes in the grain morphology, or changes in the distribution of the grain boundary phase. At the longer hot pressing times, significantly larger weight losses in the hot pressed billets were measured compared to billets hot pressed for shorter times. Because hot pressing is an open system and high temperatures are necessary to achieve full density, some decomposition may have occurred in the PY6 material. Billets that lost considerable weight during hot pressing were analyzed by X-ray diffraction to detect the presence of free silicon (a by-product of silicon nitride decomposition), but no evidence of this type of decomposition was found. The possibility of compositional changes in the grain boundary phase is also being investigated.

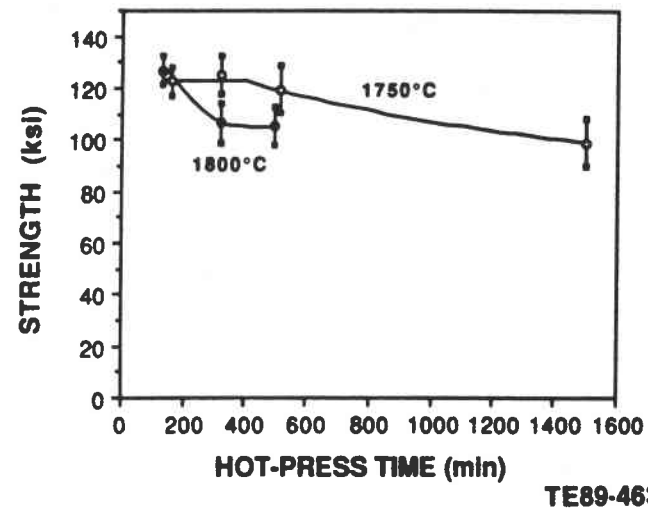

Figure 82. Room temperature strength of hot pressed Ube PY6 material.

No evidence of exaggerated grain growth was observed in any of the hot pressed billets. However, quantitative analysis of the grain size distributions in the billets showed that a percentage of grains larger than the calculated flaw sizes was evident in billets hot pressed at the longer times. The larger grains might have become critical flaw origins, resulting in decreased strength. It is important to note that while efforts are being made to determine the origin of changes in the flaw population, any decomposition problems resulting from long densification times in an open system such as hot pressing will not present any difficulties in developing processes for ATTAP rotors since the rotors will be densified in a closed HIP system.

The knowledge gained from the hot pressing study in understanding the microstructural development during densification must be translated to complex shapes via the HIP cycle. The wider range of process conditions possible in the HIP system also provides a greater range of flexibility to develop an optimal densification cycle for producing a large-grained, high aspect ratio microstructure to increase fracture toughness.

The micrograph of Ube PY6 Si_3N_4 powder densified under HIP conditions initially used in the ATTAP program is shown in Figure 83a, along with the microstructure developed in the hot pressing study. The two microstructures are significantly different and result in different fracture toughness. The much larger grained hot pressed microstructure has a fracture toughness of 4.9 MPa-$m^{1/2}$, while the finer grained HIP processed microstructure has a fracture toughness of 3.3 MPa-$m^{1/2}$.

Initial experiments to evaluate different HIP conditions focused on modifying the HIP cycle to produce a microstructure more closely resembling the hot pressed microstructure shown in Figure 83b. X-ray diffraction analysis of the initial HIP processed Ube PY6 specimens (see Figure 83a) revealed incomplete conversion to beta-Si_3N_4 during densification. To produce complete conversion, the HIP cycle was modified by increasing both the densification time and temperature. A modified cycle allowing for full conversion to beta-Si_3N_4 resulted in a microstructure consisting of acicular, high aspect ratio beta-Si_3N_4 grains (see Figure 83c), with an increase in fracture toughness from 3.3 to 4.6 MPa-$m^{1/2}$.

Efforts in 1989 will concentrate on optimizing the microstructure of large cross-section samples

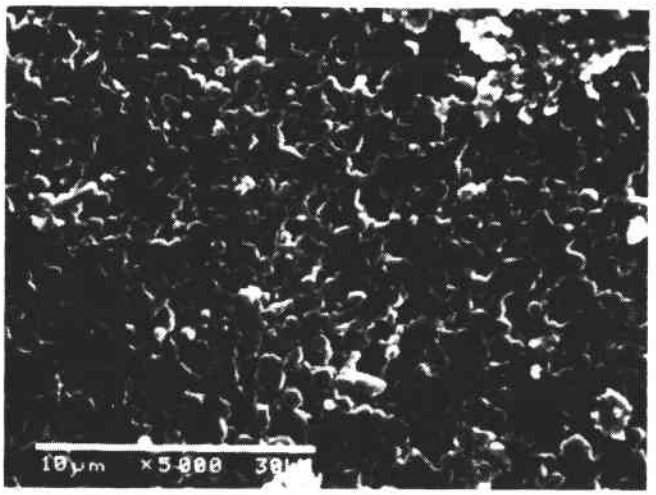

a) Baseline HIP process

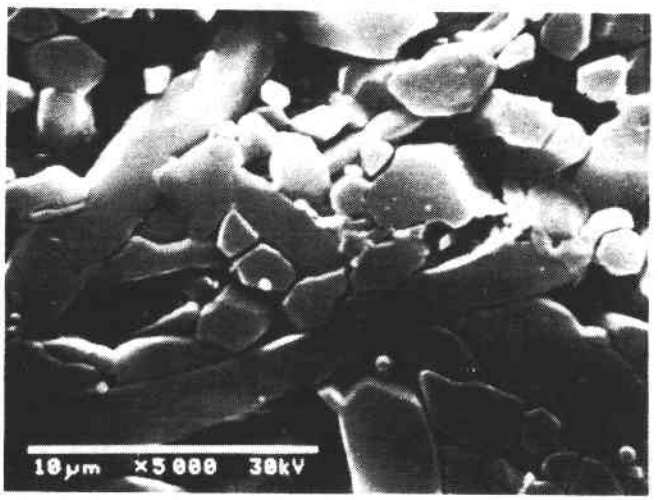

b) Desirable hot-pressed microstructure

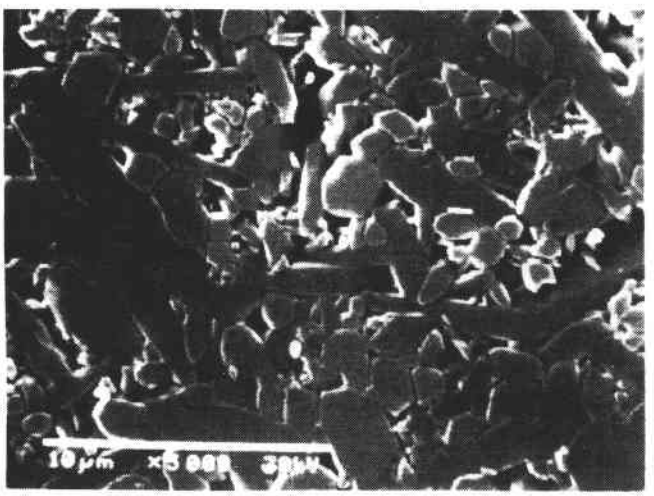

c) Modified HIP cycle microstructure

TE89-4633

Figure 83. Microstructures of PY6 samples.

processed through the HIP method. The results will be used to establish a modified process for hot isostatic pressing AGT-5 rotors with improved fracture toughness.

Task III--Toughened Composite Rotors

The objective of this task in 1988 was to evaluate the densification kinetics and material properties of PY6 Si_3N_4 containing 30 v/o SiC whiskers. Improvements in fracture toughness, strength, and creep resistance were demonstrated in the CTAHE project for additions of SiC whiskers in an AY6 Si_3N_4 matrix. At 30 v/o whisker additions, a 40% increase in fracture toughness and a 25% increase in fracture strength were observed. However, whisker reinforcement also decreased the densification rate of the composite material by limiting particle rearrangement. To extend the concept of whisker reinforcement of the PY6 Si_3N_4 matrix containing less densification additives than the AY6 Si_3N_4, the feasibility of attaining near-theoretical density must first be demonstrated. If densification is possible, notable improvements in material properties must then be determined to establish the benefit of utilizing whisker-reinforced PY6 material for ATTAP rotors.

As in Task II, hot pressing provided the best opportunity for evaluating the feasibility of densifying PY6/SiC_w composite material and generating samples quickly for material property measurements. Results from whisker reinforcement of AY6 Si_3N_4 showed that significant improvements in material properties were not attained until a 30% volume loading of SiC whiskers was attained. Based on these results, Ube-based PY6 Si_3N_4 powder was blended with 30 v/o SiC whiskers from Advanced Composite Materials Corporation (ACMC) for hot pressing experiments.

Initial hot pressing of the whisker-reinforced PY6 material revealed that higher temperatures and longer densification times were necessary to attain full density compared to the monolithic PY6 material. Figure 84 shows the decrease in densification rate during hot pressing of PY6 material with 30 v/o SiC_w additions. However, a hot pressing temperature of 1825°C (3317°F) allowed fully dense composite billets to be produced.

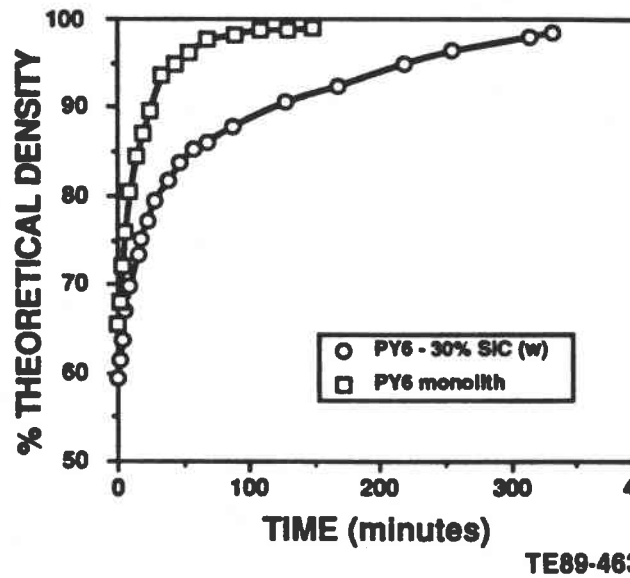

Figure 84. Hot pressing densification behavior of PY6 and PY6-30 v/o SiC whisker composite.

To evaluate the effect of whisker reinforcement in the PY6 Si_3N_4 matrix, the material properties of monolithic and composite billets hot pressed to near-theoretical density under similar densification conditions were compared. Table XXXV gives the material properties of a monolithic PY6 billet and a composite PY6-30 v/o SiC_w billet hot pressed for 325 minutes. The composite billet was hot pressed at a slightly higher temperature (1825°C [3317°F]) than the monolithic billet (1800°C [3272°F]) to achieve full density.

As shown in Table XXXV, the potential for toughening PY6 Si_3N_4 with whisker reinforcement is indicated by improvements in fracture toughness, hardness, and fracture strength. The significantly higher strength of the composite material at 1400°C (2552°F) is believed to be a result of retardation of grain boundary sliding by the SiC whiskers. The high temperature required to densify the composite material in conjunction with the difficulty associated with uniformly distributing the whiskers increases the probability of occurrence of processing-related flaws. Two types of processing defects characteristic of hot pressed PY6-30 v/o SiC whisker billets are shown in Figure 85. The metallic inclusion is silicon metal resulting from local decomposition of Si_3N_4 at high temperature. The low density region is probably the result of inhomogeneous dispersion of the SiC whiskers.

Table XXXV.
Properties of hot pressed monolithic and composite PY6 Si_3N_4 materials.

Material	Strength--MPa (ksi) 25°C (77°F)	1400°C (2552°F)	K_{IC}--MPa-$m^{1/2}$	Hardness--GPa
Monolithic PY6	783 (114)	462 (67)	4.9	14.2
PY6-30% SiC_w	807 (117)	552 (80)	5.3	16.2
Difference	+9%	+19%	+8%	+14%

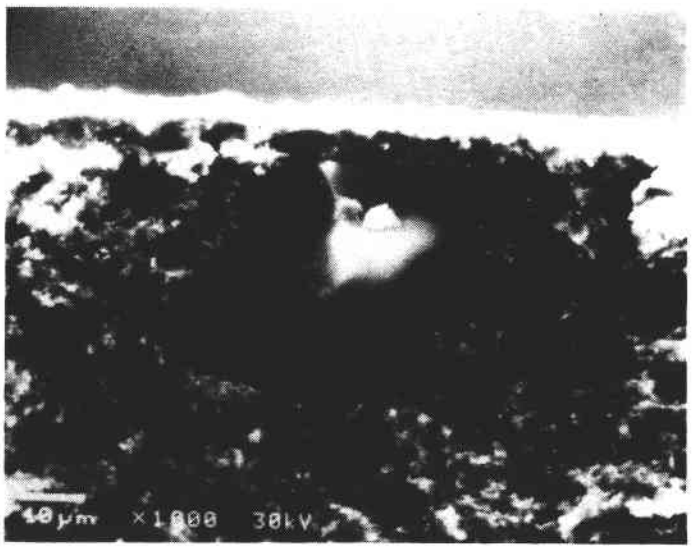

a) Silicon metal inclusion

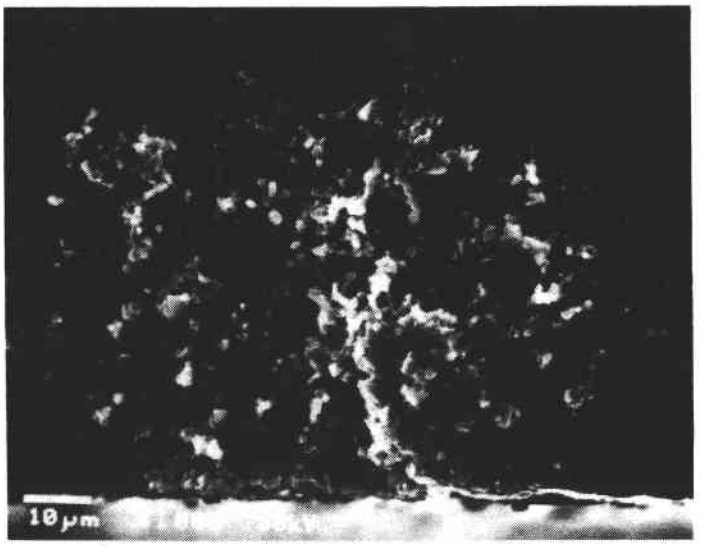

b) Low density region

TE89-4636

Figure 85. Processing defects in hot pressed PY6-30 v/o SiC whisker composites.

Efforts in the second year of the program will focus on developing process conditions for hot isostatic pressing whisker-reinforced PY6 material and shape-making activities using thick cross-section parts. The shape-making effort will draw heavily on experience gained in an ongoing CTAHE program at GTE that has defined some of the molding parameters required for distortion-free thin cross-section components. Evaluation of material properties and dimensional control of HIP processed material will lead to a feasibility decision for producing large cross-section AGT-5 rotors with PY6 Si_3N_4 composite material.

3.2.4 Corning Glass Works

Corning was placed under contract at midyear for the first phase of a program aimed at 1-piece regenerator disk extrusions. The extrusion process is sought for improved quality and reduced cost over the spiral-wrap process. Inability to control thin walls and resultant low strength is inherent to the wrap process. The first phase effort is to produce 39 x 60 x 76 mm (1.55 x 2.38 x 3.0 in.) samples for material characterization and cyclic temperature tests. Cell geometry is to be as follows:

- 2 to 1 aspect ratio rectangles
- 202 cells/cm^2 (1300 cells/$in.^2$)
- 0.11 mm (4.4 mil) wall thickness

The material is to be the proven low expansion aluminum silicate (AS).

Corning defined the following tests for material characterization and proof of acceptable quality:

- coefficient of thermal expansion
- bulk chemistry
- X-ray diffraction
- flexural strength
- compressive strength
- porosity

Batch rheology work was done to establish particle size, binders, extrusion aids, and quality assurance methods for optimum extrusion. An available die with slightly fewer cells than the new goal was used for the rheology work. Die design and process definition were completed and the manufacture of two dies was initiated. Ion exchange equipment was refurbished and operation was checked for use in converting extruded lithium aluminum silicate (LAS) to AS.

3.2.5 Garrett Ceramic Components Division (GCCD)

A 2-phase technical effort with GCCD was initiated in December 1988. The schedule for this development program is shown in Figure 86. The objective of this activity is to develop and deliver engine quality silicon nitride AGT-5 gasifier turbine rotors for test and evaluation. GCCD will tailor its pressure slip casting techniques and proprietary mold technology to develop and fabricate GN-10 Si_3N_4 rotors. In Phase I, subscale GN-10 Si_3N_4 rotors will be produced to establish a processing and properties baseline for axial turbine rotors. In Phase II, the techniques developed in Phase I will be scaled up to produce full-scale engine quality GN-10 Si_3N_4 AGT-5 rotors.

Phase I–Subscale 15-Bladed AGT-5 Rotor

Initial activities for GN-10 Si_3N_4 axial turbine rotor fabrication will be conducted using molds fabricated from an existing plastic AGT-5 rotor. These rotors will be undersize due to shrinkage. Tooling for the slip cast configuration B (primary shaft up) was completed and molds prepared. To date, five molds for this configuration have been fabricated. The statistical process control (SPC) charts for slip specific gravity, viscosity, pH, and zeta potential have been established.

Tooling for configuration A (primary shaft down) should be completed by March 1989. Evaluation of this casting geometry will begin immediately once the tooling is complete.

Specific nondestructive evaluation (NDE) procedures applicable to the axial turbine rotor (part orientation, handling) have been completed. The NDE inspection/characterization steps have been incorporated into the in-process documentation sheets. Visual, microfocus X-ray, fluorescent penetrant, and dimensional inspections will be utilized for rotor evaluation, in addition to weight, density, and strength determinations.

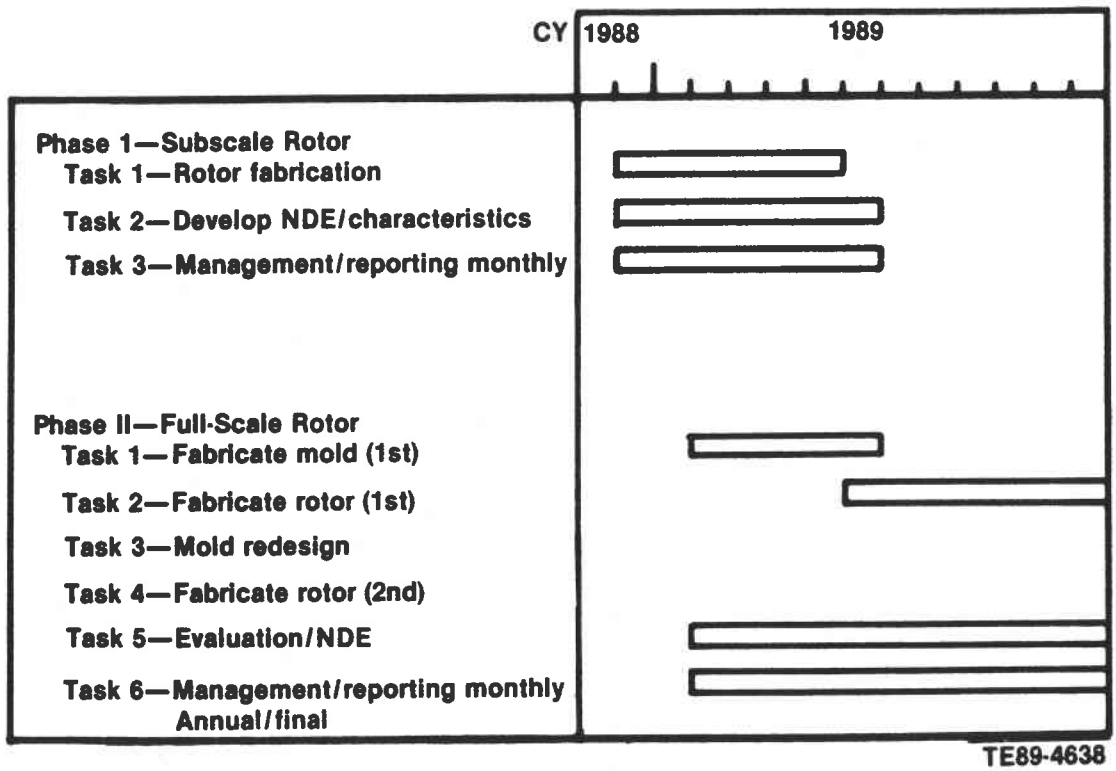

Figure 86. GCCD rotor development program schedule.

Phase II--Full-Scale AGT-5 Rotor

The processing procedures and NDE techniques established in Phase I will be expanded to fabricate full-scale, engine quality AGT-5 gasifier turbine rotors. No work will be done on the design of the full-scale AGT-5 rotor tooling and mold until the optimum casting configuration (A or B) has been determined. Allison has provided the blade book and prints for the 20-bladed AGT-5 rotor. Discussions have been held with GCCD concerning oversize patterns that will be required for mold fabrication for the full-scale rotor. Both stereo lithography and aluminum male masters will be explored for mold fabrication.

3.2.6 Ceramics Process Systems

A 5-month program was conducted with Ceramics Process Systems (CPS) to fabricate AGT-5 axial gasifier turbine rotors. The program schedule is summarized in Figure 87. The material used for this initial activity was JW-15 Si_3N_4. The objective of this effort was to demonstrate the applicability of the CPS Quickset injection molding process to the fabrication of complex geometry turbine components. The Quickset process is a low pressure (<0.7 MPa [199 psi]) aqueous-based system with a colloidal solidification mechanism that does not utilize a binder system. The process flowchart is summarized in Figure 88. As a result of binderless processing, CPS Quickset-molded ceramic materials have demonstrated isotropic shrinkages with tolerances of 0.0008 cm/cm and as-fired surface finishes of less than 0.4 microns. This process has the potential for significant reductions in cost and improved yields over conventional thermoplastic injection molding processes.

The initial rotor fabrication trials were conducted utilizing two silicone rubber molds. The rotors produced with these molds exhibited numerous surface defects from poor mold wetting and air bubbles as a result of insufficient deairing of the slip prior to injection. Concurrent with this activity, an aluminum-silicone rubber tool was designed and fabricated. This tool, shown in Figure 89, had silicone rubber blade inserts with aluminum hub features. Although metal vane inserts were designed and costed, their fabrication was not within the program timing and cost constraints. A total of 150 Si_3N_4 rotors were manually injected to optimize the mold filling, venting, gating, and demolding parameters. The overall quality of the molded parts was significantly improved relative to the initial rotors molded with the rubber tool. The rotor surfaces (hub and shaft) that contacted the metal tool surfaces were smooth and texture-free. The rotor blades, however, were rough and textured due to the poor wear characteristics of the silicone rubber blade inserts. No problems related to mold filling or part solidification were encountered once the tool had been properly modified. The sintering development work for the AGT-5 rotor was carried out during the fourth month of the program. The packing, settering, furnace placement, and sintering times and temperatures were the primary source of variation in the fired densities of the rotors, which ranged from 2.80 to 3.24 g/cm^3. The rotors were sintered in a boron nitride-based packing powder, which produced fired densities that were strongly a function of packing powder aging.

Both molded and sintered rotors were sectioned and analyzed at CPS on the scanning electron microscope and chemically analyzed using energy-dispersive X-ray analysis. A majority of the porosity was of uniform size of 5 microns with some deairing pores in the range of 30 microns. Quickset injection molded billets of the same thickness as the AGT-5 rotors were fabricated to simulate rotor molding and firing conditions for the JW-15 Si_3N_4 composition. Mechanical property evaluation was conducted on these test bars, which gave an average room temperature flexure strength of 617.1 MPa (89.5 ksi) with a Weibull modulus of 8. The fracture toughness as measured by indentation strength in bending was 5.6 MPa-m$^{1/2}$.

A total of six Si_3N_4 rotors were received by Allison for the program deliverables. One of the rotors is shown in Figure 90. The densities of these rotors are summarized in Table XXXVI. Nondestructive evaluation of the rotors revealed flow lines present in the rotor hub and shaft region, with the blades having a rough surface texture and poor dimensional conformance due to the silicone rubber blade tool inserts. Microfocus X-ray and computed tomography inspections detected small internal voids in the rotors, primarily in the blade and shaft areas.

Table XXXVI.
Densities of CPS Si_3N_4 axial turbine rotors.

Rotor No.	Density--g/cm^3	% theoretical
CPS-1	3.24	97.0
CPS-2	3.23	96.5
CPS-3	3.23	96.5
CPS-4	3.14	94.0
CPS-5	3.09	92.0
CPS-6	3.08	92.0

While the initial rotors received from this development activity with CPS were not engine quality, CPS has demonstrated the feasibility of fabricating complex geometry turbine components using its Quickset injection molding process. The Quickset process has the potential for significant improvements in yield, microstructural uniformity, dimensional control, and product cost. A follow-on program with CPS for fabrication of AGT-5 turbine components is being evaluated.

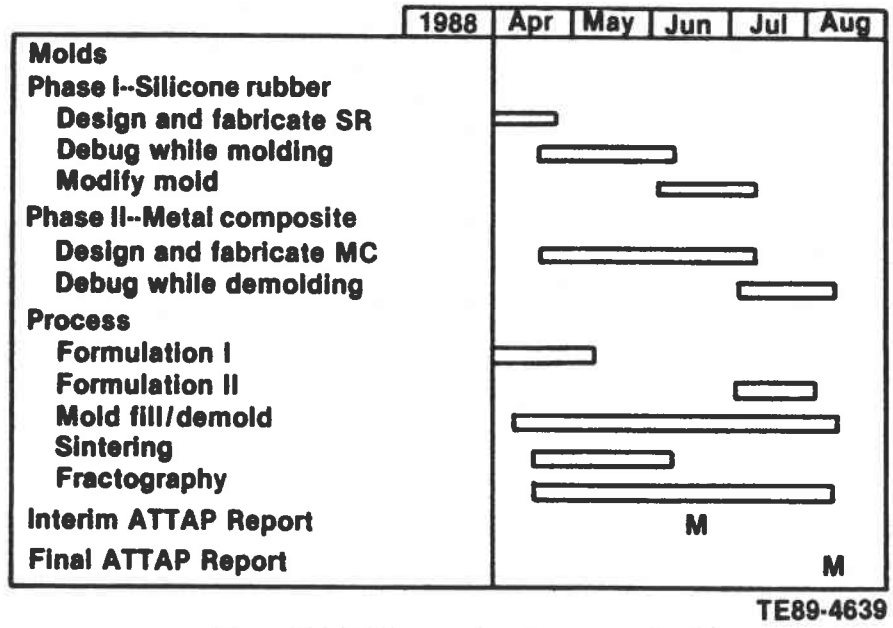

Figure 87. CPS rotor development schedule.

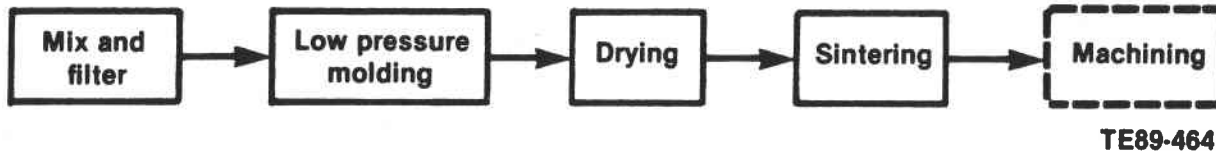

Figure 88. Quickset molding process flowchart.

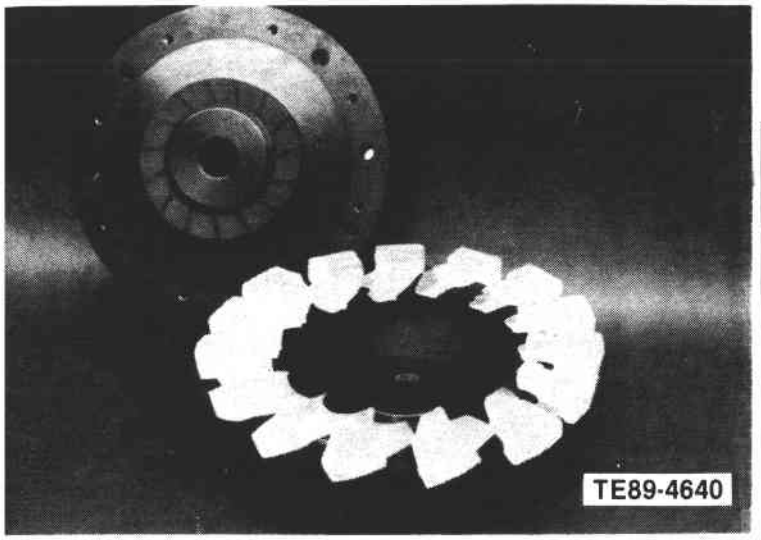

Figure 89. CPS rotor molding tool.

Figure 90. CPS Si_3N_4 gasifier turbine rotor.

IV. COMPONENT RIG DEVELOPMENT AND TEST

4.1 COMPONENT RIG DEVELOPMENT

4.1.1 Combustor Rig Development

Objective/Approach

The objective of this effort is to upgrade the present AGT-5 combustor evaluation/development capabilities to meet the requirements of the RPD. This will be via either increasing the temperature capabilities of an existing rig or the design/development of a new combustor rig. Combustor rig utilization will include evaluation of combustor ceramitization efforts, and combustor technology design and development aimed at the reduction of carbon as a source of FOD as well as reduced emissions.

Accomplishments

The following combustor rig goals were achieved:

- o completed preliminary design of existing rig upgrade
- o began conceptual design efforts for new rig

An existing rig (see Figures 91 and 92) incorporates a modified AGT-5 engine block utilizing only one of the regenerator disks. The second regenerator disk was replaced by a blank-off plate with quartz viewing windows (for the burner inlet and regenerator inlet cavities) and additional instrumentation required for regenerator performance evaluation. A dummy gasifier section is employed incorporating only the housing and scroll necessary for correct flow distribution and delivery to the power turbine section. Compressor discharge pressure is supplied from a remote, dynamometer-driven, AGT-5 engine compressor and enters the rig at the compressor diffuser plane.

Flow exiting the gasifier scroll (nozzle) enters a simulated power turbine nozzle (see Figure 93) and temporarily is diverted outside of the rig where it passes through a back pressure valve. The flow is then returned to the rig at the regenerator inlet plane.

To upgrade the rig's temperature capabilities, the preliminary design concept mainly consisted of a redesign of the back pressure valve and its associated plumbing. Both regenerator disks were included in the design to attain the proper burner inlet temperatures. Cooling air manifolds from the hot gasifier rig design were incorporated to control the regenerator

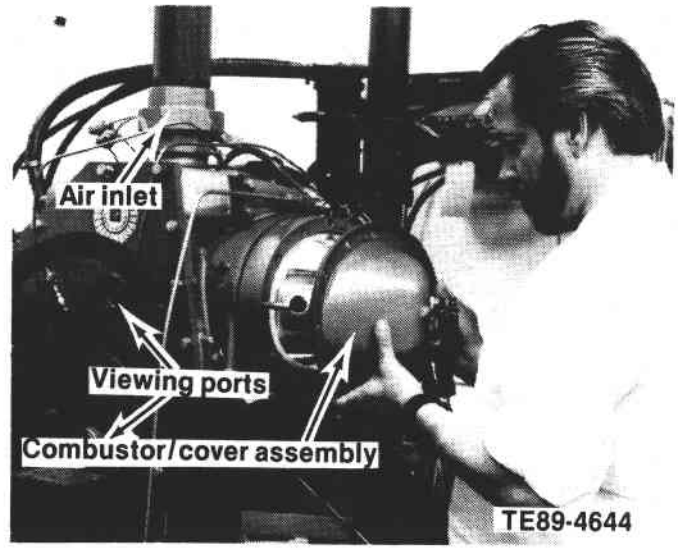

Figure 91. Existing AGT-5 combustor rig.

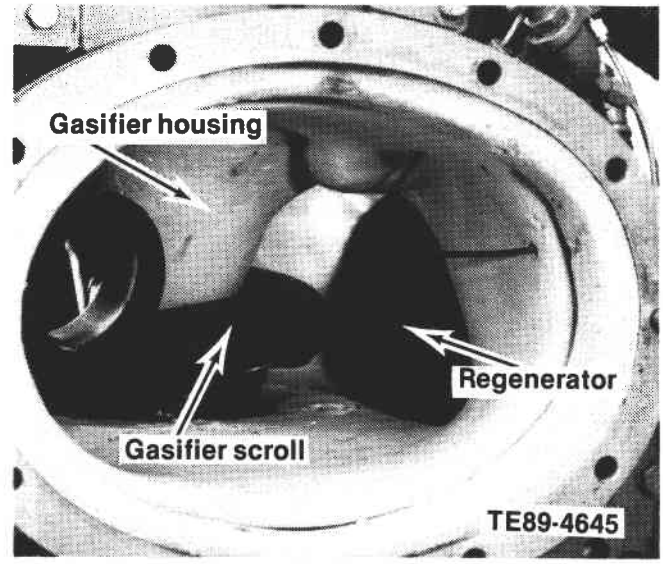

Figure 92. Existing AGT-5 combustor rig (cover removed).

inlet temperature. A design review meeting was held to evaluate the preliminary design and the following items were addressed and resolved:

- o vortex view port orientation
- o hot side airflow orifice material--ceramic
- o piping material downstream of gasifier section--Hastelloy
- o cooling air admission--downstream of emissions probe

The preliminary design is ready to be released. However, before the initiation of the final design effort, preliminary designs of a completely new rig must be completed. Discussions have taken place concerning a new rig, which might be a combined combustor/hot gasifier/regenerator rig. The potential benefits (i.e., maximization of rig and facility utilization and hardware dollars, etc) are being weighed against the trade-offs necessary to combine any or all of these rigs into one. One of the motivations in combining the combustor rig with a gasifier rig is that the combustor could be evaluated under real-time engine transient conditions.

4.1.3 Turbine Rotor Rig Development

4.1.3.3 Hot Gasifier Rig Development

Objective/Approach. The objective of this activity is the design and fabrication of a hot gasifier rig to be utilized in the testing of AGT-5 ceramic gasifier components and assemblies. The rig will be capable of operating at RPD conditions and will have an increased instrumentation capability as compared to an engine. Rig design will focus on simulating actual engine operating conditions as closely as possible where practical and reasonable.

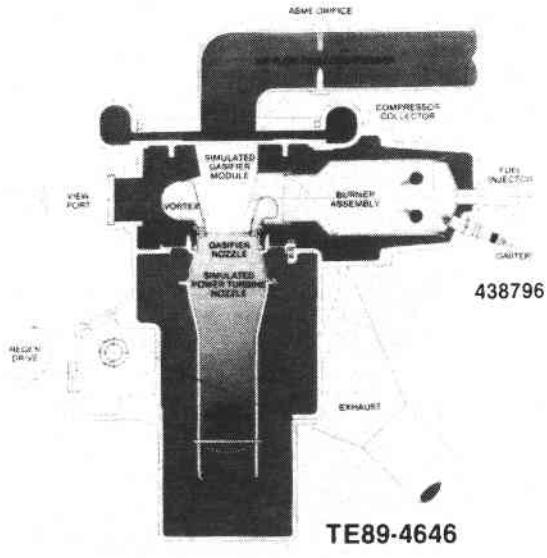

Figure 93. Schematic of existing AGT-5 combustor rig.

Accomplishments. The following hot gasifier goals were achieved:

- o applied design data acquired through t operation of an existing GM-owned gasifier t rig to the AGT-5 hot gasifier rig design
- o completed the design and procurement of a h gasifier rig
- o completed gasifier rig installation in a test c facility

Valuable AGT-5 rig design data were obtained throu the operation of a similar (AGT-5 family member) G owned hot gasifier rig. Over 60 hr of test time was a cumulated on an existing (background data to ATTA Kyocera ceramic gasifier rotor. Information obtair was directly applied to the AGT-5 hot gasifier design in areas such as airflow throttle control, burn inlet air preheating, optical pyrometer location a data handling techniques, and quartz viewing wind design.

The rig design is based on the AGT-5 engine with power turbine removed. Figure 94 is a schematic the AGT-5 hot gasifier rig. Filtered air enters the s tion containing a throttle valve, exits into a 90 deg bow, and enters a flow-straightening section. T throttle valve is used to control pressure ratio acr the turbine. The air exits the straightening secti enters the compressor, and discharges at high pr sure into the collector. From the collector, air ent the regenerators where it is preheated before enter the combustor. The hot gas exits the combus scroll and enters the gasifier section. The ceramic t gasifier rotor can be seen through the quartz view window at the rear of the test rig. This quartz wind also provides an unobstructed view for a high f qu ency optical pyrometer that will provide surfa temperature profiles of the blade and disk. T pyrometer response is fast enough to obtain seve single-blade surface temperature measurements 100% design speed.

At the rear of the rig a particle containment assem prevents large ceramic fragments from damaging regenerator cores should a failure occur. Shoul failure occur, the electrically driven regenerators st rotation. This will prevent small fragments of mater if present, from becoming lodged between the s and disk.

With the absence of the power turbine section, gas temperature entering the regenerator (hot side much higher than would be normally experienced

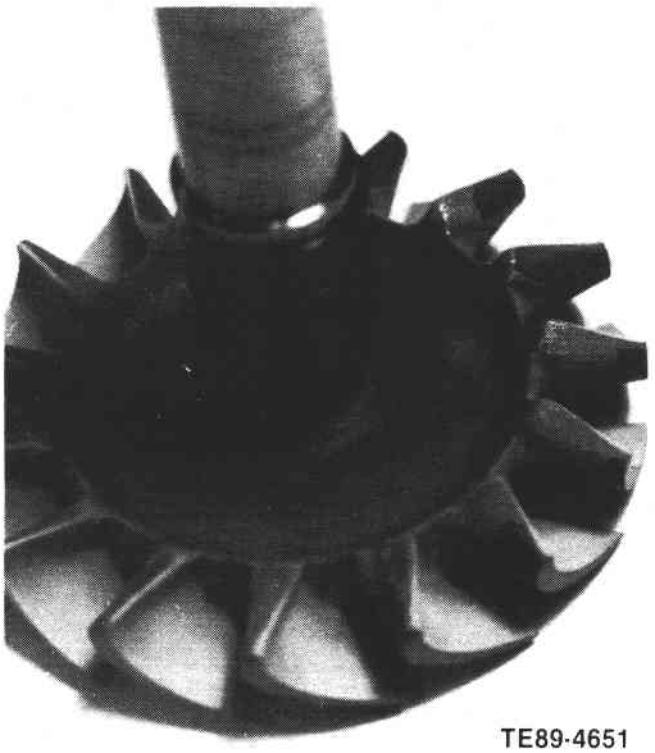

TE89-4651

Figure 98. Ceramic gasifier rotor after molten metal impact.

ment of mechanical integrity at early development temperature levels. Additional development may be required as turbine inlet operating temperatures are progressively raised to 1371°C (2500°F). The rig demonstrated a sound mechanical system other than marginal oil drain-back from the regenerator drive system. Due to the limited running time, maximum temperatures during initial running of the hot rig were only about 1030°C (1886°F).

4.2.4 Regenerator Rig Test

Objective/Approach

The objective of this activity is to conduct cyclic temperature testing of candidate regenerator material samples. Primarily, the focus of ATTAP's regenerator activity is the development of an extruded ceramic disk. The unique operating characteristics, however, of the AGT-5 engine (resulting in reduced time at high regenerator inlet temperatures) and improved cyclic oxidation resistance of new metal alloys make evaluation of metal candidates worthwhile. The approach is to perform cyclic temperature testing for both ceramic and metal to examine the most life-threatening exposure for each:

- o cyclic crack growth for ceramic
- o cyclic oxidation for metal

Accomplishments

The following regenerator rig test goals were achieved:

- o initiated overhaul of cyclic rig for adaptation to AGT-5 engine cycles
- o prepared two metal samples for test

Efforts were initiated on the cyclic temperature gas burner rig to simulate AGT-5 engine accel-decel cycles. A quench airflow circuit for temperature control with solenoid valves was designed and a controller programmed to simulate the AGT-5 engine cycles. Cooling water leaks in the rig were delaying testing at year's end.

Metal foil samples of Haynes 214 (Ni16Cr3Fe5Al-Y) and a catalytic converter alloy (Fe20Cr5Al-Ce) were formed and diffusion-bonded. Good bonds were confirmed by pull test and metallographic examination. A preoxidation treatment was utilized to enhance oxidation resistance of the 214 material. Extruded aluminum silicate ceramic samples are on order (see subsection 3.2.4).

V. PERFORMANCE AND DURABILITY TESTING--TEST-BED ENGINES

5.2 DURABILITY TESTING

5.2.3 Test-bed Engine Fabrication and Test

5.2.3.1 Test-bed Engine Fabrication

Objective/Approach. The objective of this activity is to fabricate an all-new AGT-5 durability test-bed engine and to support all engine test activities through instrumentation/build/repair activities. This activity also includes fabrication of new engine components when required to evolve the AGT-5 to a high temperature durability test-bed engine.

Accomplishments. The following test-bed goals were achieved:

- o completed fabrication of new AGT-5 durability test-bed engine
- o modified test facility to accept new durability engine (GM funding)
- o instrumented test-bed engines for regenerator spike and soak-back temperature testing
- o initiated reinsulation of the durability test-bed engine with Manville's injection moldable material via hand lay-up

Hardware procurement and fabrication of an all-new AGT-5 durability test-bed engine was initiated and completed. The engine is presently configured as a 1038°C (1900°F) metal engine. Operation on the General Motors' gas turbine durability schedule (see subsection 1.4.4) for extended periods of time will accomplish the following:

- o prove the mechanical reliability of the test-bed
- o reduce the "mixing" of mechanical problems with ceramic problems
- o reduce ceramic component test time through elimination of potential mechanical problems
- o allow preparation and checkout of test facility instrumentation, data acquisition, and safety interlock systems prior to ceramic component testing

The test-bed engine durability test facility was modified to accommodate the extra instrumentation required for the durability engine safety and control routines. A conditioned air supply system was installed and utilized in testing. The air system supplies clean, controlled, and consistent engine air inlet conditions that will provide consistent test conditions for data comparison.

After initial durability engine testing, the engine was removed from the stand due to low engine oil pressure. The engine was disassembled and corrective measures were taken. The engine was then assembled for test with additional thermocouples for acquisition of engine soak-back temperature data. Following this test, the engine was removed from the stand and reinsulation with the new Manville material was initiated.

Another test-bed engine was instrumented for temperature spike measurement at the regenerator inlet during engine acceleration and deceleration. These data were useful and necessary to the establishment of the regenerator cyclic temperature rig test cycle and control algorithm.

5.2.3.2 Test-bed Engine Testing

Objective/Approach. The objective of this activity is to perform shakedown durability testing of the AGT-5 durability test-bed engine, high temperature durability verification of the test-bed, and evaluation of ceramic hot flow path components and engine insulation. This will be accomplished through operation on the General Motors' gas turbine durability schedule and steady-state tests at idle, cruise, and full-power conditions.

Accomplishments. The following test-bed engine test goals were achieved:

- o performed an engine test to shake down the durability engine control algorithm
- o completed initial shakedown testing of a new durability test-bed engine
- o began test-bed operation on a durability cycle
- o performed a soak-back temperature test
- o performed a regenerator inlet temperature spike test during engine accelerations and decelerations
- o performed initial testing of a ceramic gasifier rotor in a test-bed engine

During the fabrication of the new durability test-bed engine, another AGT-5 test-bed engine was installed in the durability test facility to allow the checkout and shakedown of the new durability controller program.

Minor corrections and modifications to the program were implemented and verified prior to installation of the new durability test-bed engine.

Following completion of the durability test-bed engine's fabrication, the engine was installed in the test facility. Initial running was done to establish the baseline engine performance. This consisted of warming up the engine and recording data at the peak power point of set gasifier speeds. This engine was then run on the controlled durability cycle a total of 14 times accumulating 31.4 hr. The engine was operated a total of 50 hr before being removed from the test stand due to low oil pressure. The engine was operated on the durability schedule at this time to begin durability verification and to test the computer control system and schedule algorithm under extended test conditions. The engine output speed controller was calibrated during this testing and all the engine shutdown routines were checked. The conditioned air inlet system was initially used and verified during this testing.

This durability engine was also instrumented with additional thermocouples to test engine soak-back temperatures at the following locations:

- o gasifier and power turbine shaft bearings
- o gasifier nozzle ring groove

Strip chart recorders were used to record the temperatures at these locations as well as turbine speeds, gasifier turbine inlet temperature, and regenerator inlet temperature. The engine was run on the durability cycle for two tests of one cycle (1 hr) duration each. One test started with a warm engine and the other with a cold engine (18 hr soak). This test was also useful in providing initial data on temperature spikes at the thermocouple locations during gasifier accelerations.

Another test-bed engine was installed in the test facility and run for 12.1 hr with an all-metal configuration to establish baseline engine performance. The gasifier rotor was then replaced with a rotor containing a Kyocera 15-blade Si_3N_4 gasifier wheel (background data to ATTAP) to obtain initial experience in running an engine with a ceramic component. Peak power data were also obtained for the ceramic rotor engine. Radial tip clearances at running temperatures were 109% higher with a ceramic wheel and a metal shroud as compared with a metal wheel. The drop in gasifier turbine efficiency due to the tip clearance increase limited the engine to 78% gasifier speed (1028°C [1882°F] turbine inlet temperature) while staying within the metal regenerator temperature limit of 880°C (1616°F). Metal regenerators were used for this testing because the ceramic regenerator cores were not yet available. After accumulating 41.7 hr of running over 8 days, with the vast majority of the time spent at or near 75% gasifier speed, the engine failed to restart. Inspection of the burner cavity revealed that large amounts of hard carbon had formed around the fuel nozzle due to restricted fuel nozzle airflow passages resulting from incomplete machining during fabrication. Hard carbon particles were found in the regenerator inlet cavity indicating that the particles had passed through the ceramic gasifier rotor. Flaking of the metal burner liner was also noticed at a point where the liner had been modified for assembly purposes. Metal particles from this point may have also passed through the gasifier rotor. Inspection of the gasifier rotor revealed that only minimal damage had been suffered: a slight chip on the trailing edge tip of a blade (see Figure 99). Regenerator damage on a subsequent start attempt required the removal of this engine from the test stand.

This engine was returned to the test facility after repairs in an all-metal configuration, and baseline engine performance was recorded after the regenerator break-in schedule was run. The Kyocera 15-blade rotor was then reinstalled into the engine. Again the engine was limited to 75% gasifier speed to stay within the metal regenerator temperature limit. Running time accumulated was 280.5 hr, the majority of the time spent at or near 75% gasifier speed, bringing the total time for this rotor running in the engine to 322.2 hr. The engine was removed from the test stand and inspection of the rotor revealed no additional damage. Engine testing of this rotor was discontinued and the rotor was installed in the new hot gasifier rig to allow shakedown running of that rig (see subsection 4.2.3.3).

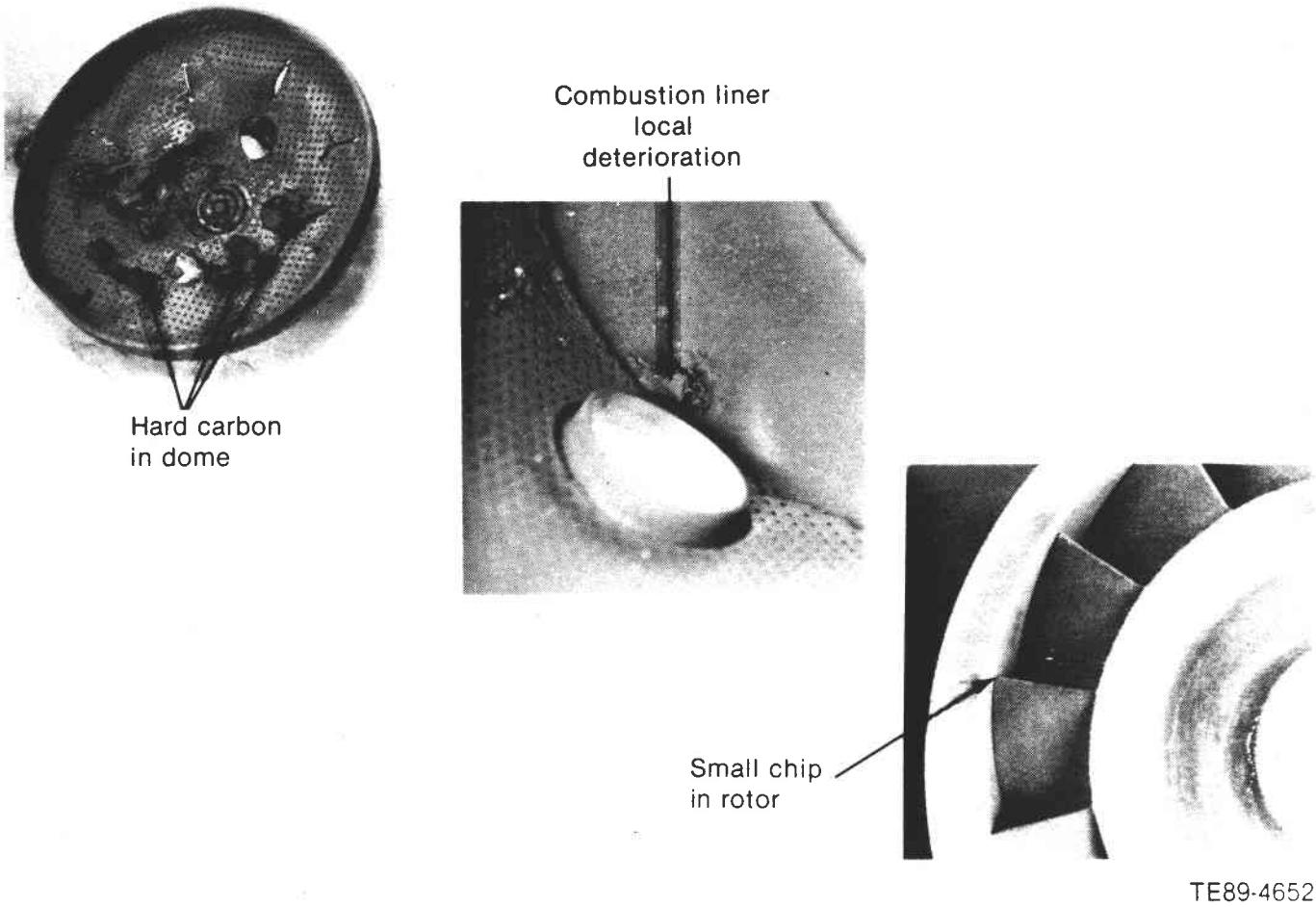

Figure 99. Foreign object survivability--ceramic turbine rotor.

APPENDIX. TERMS AND DEFINITIONS

α	alpha
ACMC	Advanced Composite Materials Corporation
AES	Advanced Engineering Staff
AGT	automotive gas turbine/Advanced Gas Turbine
AS	aluminum silicate
ATTAP	Advanced Turbine Technology Applications Project
AVG	active variable geometry
BIT	burner inlet temperature
BOC	Buick, Oldsmobile, Cadillac
BOT	burner outlet temperature
BSFC	brake specific fuel consumption
BU	build
BVG	burner variable geometry
°C	degree centigrade
CBO	Carborundum
CCM	Contractors Coordination Meeting
cm	centimeter
CMC	ceramic matrix composite
CPS	Ceramics Process Systems
CTAHE	Ceramic Technology for Advanced Heat Engines
CVD	chemical vapor deposition
CVI	chemical vapor infiltration
DOE	Department of Energy
ext	extruded
°F	degree Fahrenheit
FCM	function control module
FE	fuel economy
FEM	finite element method
FOD	foreign object damage
FPI	fluorescent penetrant inspection
gal	gallon
GCCD	Garrett Ceramic Components Division of Allied-Signal Aerospace Company
GE	General Electric Company
gm	gram
GM	General Motors
GT	gasifier turbine
GTE	GTE Laboratories Inc
HIP	hot isostatic pressed
hp	horsepower
i.d.	inner diameter
$in.^2$	square inch
$in.^3$	cubic inch
IWC	inertia weight class
kg	kilogram
K_{IC}	fracture toughness
km	kilometer
kPa	kilopascal
ksi	kilopounds per square inch
kW	kilowatt
ℓ/L	liter
LAS	lithium aluminum silicate
LeRC	Lewis Research Center
MOR	modulus of rupture
NDE	nondestructive evaluation
OCC	outer combustor case
o.d.	outer diameter
POS	probability of survival
psi	pounds per square inch
RB	reaction bonded
RPD	reference powertrain design
rpm	revolutions per minute
SEM	scanning electron microscopy
SENB	single edge notched beam
SiC	silicon carbide
Si_3N_4	silicon nitride
SL	sea level
S/N	serial number
SPC	statistical process control
SS	steady-state
TEM	transmission electron microscope
THM125C	GM production automatic transmission
TIT	turbine inlet temperature
TVG	thermally actuated variable geometry
2-D	two-dimensional
v/o	volume fraction, percent
WOT	wide open throttle

1. Report No.	2. Government Accession No.	3. Recipient's Catalog No.
NASA CR-185133		

4. Title and Subtitle	5. Report Date
Advanced Turbine Technology Applications Project (ATTAP) --1988 Annual Report	June 1989
	6. Performing Organization Code
7. Author(s)	8. Performing Organization Report No.
Engineering Department, Allison Gas Turbine Division	EDR 14232
	10. Work Unit No.
9. Performing Organization Name and Address	
Allison Gas Turbine Division of General Motors Corporation P.O. Box 420 Indianapolis, IN 46206-0420	11. Contract or Grant No. DEN 3-336
	13. Type of Report and Period Covered Contractor Report November 1987-December 1988
12. Sponsoring Agency Name and Address	14. Sponsoring Agency Code
U.S. Department of Energy Office of Conservation and Renewable Energy Washington, DC 20545	DOE/NASA

15. Supplementary Notes

Annual report, prepared under Interagency Agreement DE-A101-85CE50111.
Project Manager P. T. Kerwin, Propulsion Systems Division,
NASA Lewis Research Center, Cleveland, OH 44135

16. Abstract

ATTAP activities during the past year were highlighted by an extensive materials assessment, execution of a reference powertrain design, test-bed engine design and development, ceramic component design, materials and component characterization, ceramic component process development and fabrication, component rig design and fabrication, test-bed engine fabrication, and hot gasifier rig and engine testing. Although significant technical challenges remain, all areas experienced progress. Materials assessment activities entailed engine environment evaluation of domestically supplied radial gasifier turbine rotors that were available at the conclusion of the Advanced Gas Turbine (AGT) Technology Development Project as well as an extensive survey of both domestic and foreign ceramic suppliers and Government laboratories performing ceramic materials research applicable to advanced heat engines. A reference powertrain design was executed to reflect the selection of the AGT-5 as the ceramic component test-bed engine for the ATTAP. Test-bed engine development activity focused on upgrading the AGT-5 from a 1038°C (1900°F) metal engine to a durable 1371°C (2500°F) structural ceramic component test-bed engine. Ceramic component design activities included the combustor, gasifier turbine static structure, and gasifier turbine rotor. The materials and component characterization efforts have included the testing and evaluation of several candidate ceramic materials and components being developed for use in the ATTAP. Ceramic component process development and fabrication activities were initiated for the gasifier turbine rotor, gasifier turbine vanes, gasifier turbine scroll, extruded regenerator disks, and thermal insulation. Plans for 1989 include delivery of gasifier turbine rotors, vanes and scrolls, injection moldable thermal insulation, and extruded regenerator matrix samples. Component rig development activities included combustor, hot gasifier, and regenerator rigs. Test-bed engine fabrication activities consisted of the fabrication of an all-new AGT-5 durability test-bed engine and support of all engine test activities through instrumentation/build/repair. Hot gasifier rig and test-bed engine testing activities were performed.

17. Key Words (Suggested by Author(s))		18. Distribution Statement
Automotive gas turbine Ceramic components Structural ceramics Engine configuration rotors Alternate propulsion systems Vehicular propulsion	Alternate fuels Emissions Improved fuel economy	Unclassified, unlimited

19. Security Classif. (of this report)	20. Security Classif. (of this page)	21. No. of Pages	22. Price*
Unclassified	Unclassified	103	

* For sale by the National Technical Information Service, Springfield, Virginia 22151